



SAPIENZA
UNIVERSITÀ DI ROMA

FACULTY OF ENGINEERING

Department of Chemical Engineering, Materials and Environment

Degree of Doctor of philosophy in

CHEMICAL PROCESSES FOR INDUSTRY AND ENVIRONMENT XXXV CYCLE

Dissertation

WASTE MATERIALS AS ADSORBENTS FOR WATER TREATMENT:

From material characterization to applications in
continuous operation systems

by

Leone Mazzeo

Supervisor

Prof. Luca Di Palma

November 2022

TABLE OF CONTENTS

SYNOPSIS	9
CHAPTER I.....	11
1. Introduction.....	11
1.1 Freshwater Management.....	11
1.2 Wastewater treatment.....	12
1.2.1 Pre-treatment	12
1.2.2 Primary Treatment.....	13
1.2.3 Secondary Treatment.....	13
1.2.4 Tertiary Treatment	13
1.3 Pollutants.....	15
1.3.1 Dyes.....	15
1.3.2 Heavy Metals	16
CHAPTER II.....	17
2. Adsorption theory and modelling	17
2.1 Theoretical background.....	17
2.1.1 The adsorption fundamentals	17
2.1.2 Solid-gas Isotherms.....	20
2.1.3 Solid-Liquid adsorption	23
2.1.4 Batch kinetic modelling.....	27
2.1.5 Column kinetic modelling	35
CHAPTER III	41
3. Adsorbent materials for water treatment.....	41
3.1 Activated Carbons.....	41
3.1.1 Physical activation	42
3.1.2 Chemical activation	42
3.1.3 AC production and Market	43
3.2 Zeolites.....	44
3.2.1 Zeolite synthesis.....	44

3.2.2	Zeolites production and Market	45
3.3	Low-cost agro-waste adsorbents.....	46
3.3.1	Yerba Mate Tea.....	46
3.3.2	Aloe Vera.....	46
3.3.3	Pteris vittata Fern	47
3.4	Material Analysis.....	48
3.4.1	BET analysis	48
CHAPTER IV		50
4.	Yerba Mate (<i>Ilex paraguarensis</i>) as Bio-Adsorbent for the Removal of Methylene Blue, Remazol Brilliant Blue and Chromium Hexavalent: Thermodynamic and Kinetic Studies	50
4.1	Materials preparation and characterization	50
4.1.1	Bio-adsorbent preparation	50
4.1.2	Chemicals	51
4.1.3	Analysis	51
4.1.4	YM Characterization.....	52
4.2	Adsorption tests.....	54
4.3	MB adsorption batch tests using YM.....	55
4.3.1	Isotherm and thermodynamic studies	55
4.3.2	Kinetic studies	56
4.4	Isotherm and Thermodynamic studies	57
4.5	Kinetics experiments and fitting of model parameters.....	59
4.5.1	Model validation	63
4.6	Adsorption of RBB and Cr(VI) using YM and CYM	65
CHAPTER V		68
5.	Effect of Water–Ethanol Extraction as Pre-Treatment on the Adsorption Properties of Aloe vera Waste.....	68
5.1	Chemicals.....	69
5.2	Bio-adsorbent preparation	69
5.3	Bio-adsorbent characterization.....	69
5.4	Batch Tests	70
5.4.1	Equilibrium tests	70
5.4.2	Kinetic tests	70

5.5	Bio-adsorbent pre-treatment.....	71
5.6	Equilibrium	74
5.7	Kinetic tests	81
CHAPTER VI.....		87
6.	Characterization of waste roots from the As-hyperaccumulator <i>Pteris vittata</i> as low-cost adsorbent for methylene blue removal.....	87
6.1	Chemicals.....	87
6.2	Bio-adsorbent preparation	87
6.3	Bio-adsorbent characterization.....	88
6.4	Batch Tests	89
6.4.1	Equilibrium tests	89
6.4.2	Kinetic tests	90
6.5	Equilibrium	91
6.6	Kinetic tests	94
CHAPTER VII.....		100
7.	Fixed-bed adsorption of Methylene Blue on <i>Pteris Vittata</i> bio-adsorbent.....	100
7.1	Chemicals.....	100
7.2	Bio-adsorbent	101
7.3	Experimental set-up and column tests	101
7.4	Bed void fraction and solid apparent density estimation	102
Conclusions.....		111
References.....		112

LIST OF FIGURES

Figure 1-1 Freshwater withdrawal in 2017, aggregated by continent and by water sector use (km ³ /year)[3].	11
Figure 1-2 Percentage of water bodies in Europe not in good ecological status ¹ in2021.....	12
Figure 1-3 (a) MBR with sidestream membrane and (b) MBR with submerged membrane [6].	14
Figure 2-1 Schematic representation of the Gibbs modelling of adsorption between two bulk phases α and β .	18
Figure 2-2 Graphical representation of the Langmuir isotherm.	21
Figure 2-3 Classification of the isotherms into five types.	23
Figure 2-4 Individual and composite isotherms. Full line: composite isotherm. Broken line: A “solute, B “solvent”. For dilute conditions, the two curves overlap (for the solute) or are specular (for the solvent) [25].	25
Figure 2-5 Schematic representation of a batch adsorption system that changes over time (from a coloured solution to a transparent one) with a focus on the external mass transfer resistance a) and the resistance due to the diffusion through macro-pores b) and micro-pores c).	28
Figure 2-6 Schematic representation of the Linear Driving Force Model.....	34
Figure 2-7 Schematic description of the typical operation cycle of a fixed-bed adsorption column. <i>Top</i> advancement of the mass transfer zone (MTZ) through the column. <i>Bottom</i> breakthrough curve [29].	36
Figure 2-8 Differences between dispersive and compressive behavior.....	38
Figure 2-9 Linearity parameter of a Langmuir isotherm: relation with isotherm shape.	40
Figure 3-1 Direct-fired rotary kiln (a); Indirect-fired rotary kiln (b). Configuration: air, steam and CO ₂ inlet (1); Gas exit (2) for the indirect configuration are just the gas resulting from the combustion of a fuel while for the direct one are included the product of activation (mainly H ₂ , CO); Char inlet (3); Activated carbon exit (4).	43
Figure 3-2 Zeolite A (a) and faujasite-type zeolites X and Y (b) formed by sodalite cages.	44
Figure 3-3 Hydrothermal synthesis process. The crystallization occurs in an autoclave (a). Then, the product is filtered and oven dried (b). The remaining solid is the zeolite (c) [33].	45
Figure 3-4 Yerba mate plant and Tea.	46
Figure 3-5 Focus on the <i>Aloe Vera</i> structure (left); example of an industrial rind and gel separation unit.	47
Figure 3-6 <i>Pteris Vittata</i> fern hydroponic culture with a focus on fronds (a) and roots (b) [52].	48
Figure 4-1. Infrared spectra of the YM (a) and CYM (b) samples [54].	52
Figure 4-2. FE-SEM micrographs of the YM (a-b) and CYM (c-d) samples [54].	53

Figure 4-3. Zero Charge point (pH_{pzc}) of YM, determined by the pH drift method. The Zero Charge point is represented by the intersection of the two curves: the black dotted (\bullet) curve shows the final pH (pH_f) of the suspension respect to the initial one (pH_i); the white dotted curve (\circ) represents the condition $pH_i=pH_f$ [54].	54
Figure 4-4. MB adsorption removal efficiency after 72h of equilibrium tests at different YM dosage. Conditions: 20 mg/L of MB, 50 mL of volume, $pH=6$ and $25\text{ }^\circ\text{C}$ [54].	55
Figure 4-5. Langmuir and Freundlich Isotherms obtained by a non-linear fitting of the adsorption data of MB using Yerba Mate at 298 K. The error bars represent the standard deviation [54].	58
Figure 4-6. MB adsorption on Yerba Mate at different R (100, 200, 300 for each graph) and temperatures 283 K (a), 293 K (b) and 313 K (c) [54].	61
Figure 4-7. Variation of the parameters of fitting bq_{max} (a) and $kLDFa$ (b) with temperature and the ratio between the solid dosage and the initial concentration of MB respectively. The points reported are the mean of the fitting values [54].	62
Figure 4-8 Adsorption kinetics of Methylene Blue on Yerba Mate at 298 K for $R=200$ and $R=400$. The dashed lines represent how the model (with $bq_{max} = 0.44$ [L/g] and $kLDFa = 0.02$ and $kLDFa = 0.04$ [1/min] for $R = 200$ and $R = 400$ respectively) predicts the trend of adsorption [54].	64
Figure 4-9. Variation of the characteristic time of adsorption of Methylene Blue using Yerba Mate versus R . The points reported are the mean of the fitting values. Moreover, the error bars represent the maximum and minimum difference between the values of fitting and the mean [54].	65
Figure 5-1. Equivalent Gallic Acid concentration (C GAE) along three pre-treatment cycles using water, water-ethanol (25% v/v) and water-ethanol (50% v/v) solutions as solvents [73].	72
Figure 5-2. Zero-point charge ($pHZC$) determination for AV0, AV25 and AV50. The zero-point charge is represented by the intersection of the characteristic lines for all the samples with the bisector of the graph [73].	73
Figure 5-3. a) TG-DTG curves of as-received Aloe vera; b) DTG curves of AV0, AV25 and AV50 [73].	74
Figure 5-4. Isotherms at 20°C for AV0, AV25 and AV50 fitted with Langmuir model. Only for AV50 it was provided the fitting with Freundlich model [73].	75
Figure 5-5. Relation between pore volume and diameter for AV0, AV25 and AV50 [73].	77
Figure 5-6. a) Plot of the removal percentage at equilibrium of MB (R) versus the initial concentration for AV0, AV25 and AV50; b) plot of the ratio $RAV25/RAV0$ versus the initial concentration; c) plot of the ratio $RAV25/RAV50$ versus the initial concentration; d) plot of the ratio $RAV0/RAV50$ versus the initial concentration [73].	79
Figure 5-7. Isotherms of AV0 at $10\text{ }^\circ\text{C}$, $20\text{ }^\circ\text{C}$ and $40\text{ }^\circ\text{C}$ fitted by Langmuir model [73].	80

Figure 5-8. Natural logarithm of the Langmuir constant b versus the reciprocal of temperature. The dotted line represents the result of the linear regression which equation is reported in the graph together with the value of R^2 [73].	81
Figure 5-9. Experimental kinetic data for a) AV0, b) AV25 and c) AV50 reported as the ratio between the concentration of Methylene Blue in water and its initial concentration (C/C_{in}) versus time. The solid line represents the model prediction while the dotted line the expected equilibrium threshold [73].	84
Figure 6-1. Scanning Electron Microscope (SEM) micrographs of pre-treated PV. A) Top view of the root; B) Root section [75].	88
Figure 6-2. Zero-point charge (pH_{ZC}) determination for PV. The zero-point charge is represented by the intersection between the characteristic lines for PV and the bisector of the graph [75].	89
Figure 6-3. Isotherms of <i>Pteris vittata</i> (PV) for the adsorption of Methylene Blue at 20°C and 40°C [75].	91
Figure 6-4. Preliminary experimental results (solid concentration q , percentage of MB removed $R\%$) for batch tests at 20°C, initial concentration of MB 4.5 mg/L and duration of the test 110 min for different solid dosages. The dotted lines represent the expected values at equilibrium [75].	94
Figure 6-5. Kinetic test results for different solid dosages at 20°C a) and 40°C b). The initial concentration of MB used was 4.5 mg/L [75].	96
Figure 6-6. Values of kLa and their standard deviation obtained from each estimation at 20°C and 40°C. The dotted lines represent the result of the linear regression together with the linear expression obtained and the correspondent value of R^2 [75].	97
Figure 7-1 Aloe Vera Particle size distribution in dry and wet status.	100
Figure 7-2 Column experimental set-up: (1) Vessel for the storage of the inlet solution; (2) Peristaltic pump; (3) glass column provided of thermostatic jacket; (4) outlet solution drum	102
Figure 7-3 MB experimental and predicted breakthrough curves at 20°C for <i>Pteris Vittata</i> roots of 0.8 cm (a) and 0.4 cm (b) of length.	106
Figure 7-4 Plot of the estimated parameter $kLDFa$ versus the Reynolds number Re . The error bars correspond to the confidence interval with a significance level of $\alpha = 0.02$.	107
Figure 7-5 MB experimental and predicted breakthrough curve at 20°C for <i>Pteris Vittata</i> roots of 0.8 cm of length (test V1).	109
Figure 7-6 Reynolds number vs dimensionless flowrate and column cross sectional area.	109

LIST OF TABLES

Table 1-1 Properties of Methylene Blue and Remazol Brilliant Blue.....	15
Table 3-1 Commonly adopted compounds for BET analysis together with their isotherm temperature and cross-sectional area[53].	49
Table 4-1. Specific surface area (SSA) of YM samples.....	53
Table 4-2. Bio-adsorbent concentrations in batch tests	56
Table 4-3. Comparison of the Langmuir and Freundlich constants for different types of food waste bio-adsorbents.	58
Table 4-4. Removal efficiency of MB, RBB and Cr(VI) on YM and CYM samples.	66
Table 5-1. Langmuir and Freundlich isotherm parameters at 20 °C for AV0, AV25 and AV50.....	75
Table 5-2. Langmuir isotherm parameters for agro-waste adsorbents.....	76
Table 5-3. BET-BJH data for treated <i>Aloe vera</i> samples.	77
Table 5-4. Langmuir isotherm parameters at 10 °C, 20 °C and 40 °C for AV0.....	80
Table 5-5. kinetic fitting parameters at 20 °C for AV0, AV25 and AV50.....	85
Table 6-1. Preliminary kinetic tests dosage (g/L) according to the amount of solid and liquid used.....	90
Table 6-2. Langmuir isotherm parameters for PV at 20°C and 40°C.	91
Table 6-3. Langmuir isotherm parameters for agro-waste adsorbents.....	93
Table 6-4. Estimated values for the effective diffusion coefficient at 20°C and 40°C.....	97
Table 6-5. Estimated values of the dimensionless Biot number (<i>Bi</i>) at 20°C and 40°C.....	98
Table 7-1 Operating conditions of experimental runs. ($T = 20 \pm 0.1 \text{ } ^\circ\text{C}$, $M_s = 0.232 \text{ g}$) .	102
Table 7-2 Evaluation of the solid intrinsic density of <i>Pteris Vittata</i> based on the bed void fraction estimation for each test. ($M_s = 0.232 \text{ g}$).....	103
Table 7-3 Empirical expression for the evaluation of <i>Pé</i> in liquid-solid fixed bed columns.	104
Table 7-4 Values of the common parameters to all the kinetic tests used in theoretical model	104
Table 7-5 Empirical expression for the evaluation of <i>Sh</i> in liquid-solid fixed bed columns for low Reynold's numbers.	107
Table 7-6 Operating conditions of the test V1.	108

SYNOPSIS

Wastewater treatment is a crucial activity that prevents soils and water bodies pollution avoiding the decrease of freshwater availability. Industrial and agricultural sectors are the main responsible for the generation of contaminated water and standard primary or secondary treatments are usually not enough to deal with such effluents. As a matter of fact, a specific tertiary treatment is often required for the removal of recalcitrant compounds that are harmful even at very low concentrations. Among all the technologies used to face such issue (e.g. Advanced Oxidation processes, Membrane processes), Adsorption constitutes a valid alternative for its ease of operation. However, the most commonly adopted solid adsorbents such as Active Carbons or Zeolites have to sustain high activation and synthesis costs respectively. In order to reduce such costs as well as to promote circular economy principles, in this thesis three different waste materials were proposed as bio-adsorbents: *Yerba Mate* (*Ilex paraguarensis*, YM) tea, *Aloe vera* (AV) rind and *Pteris Vittata* (PV) fern roots.

Yerba Mate was used for the removal of anionic and cationic compounds from wastewater. Chromium hexavalent Cr(VI), Remazol brilliant blue (RBB) and methylene blue (MB) were selected as pollutants. A calcination step was performed after the washing and drying steps to evaluate its effectiveness at increasing the adsorption capacity of the solid. Both YM and calcinated YM (CYM) were characterized by means of scanning electron microscopy (FE-SEM), Fourier transform infrared spectroscopy (FT-IR) and Brunauer–Emmett–Teller (BET) analysis. Adsorption batch tests revealed that YM was ineffective for the removal of Cr(VI) and RBB, while good results were obtained for MB (up to 80%) without pH dependency of the adsorption process, and CYM was able to remove Cr(VI) (up to 77%) and RBB (up to 65%) but not MB. The adsorption isotherm of MB on YM at 298 K was obtained experimentally and it is well represented by the Langmuir isotherm. YM's adsorption capacity for MB was estimated to be 59.6 mg/g. Kinetic batch tests were conducted and the experimental results were fitted with a mathematical model. The low influence of temperature compared to the influence of the YM concentration on the adsorption rate was explained.

The adsorption properties of *Aloe vera* (*Aloe barbadensis* Miller) for the uptake of Methylene Blue (MB) from water were investigated after pre-treating the material with water–ethanol solutions at different ethanol concentrations: 0% v/v (AV0), 25% v/v (AV25), and 50% v/v (AV50). The pretreated materials were characterized as follows: the pH of zero charge was evaluated to be 6, 5.7, and 7.2 for AV0, AV25, and AV50, respectively; from BET-BJH analysis the mesoporous nature of the material and an increase from 108.2 (AV0) to 331.7 (AV50) m²/kg of its solid surface area was observed; TG analysis revealed a significant increase in volatile compounds from the untreated (5.4%) to the treated materials (8.9%, 10.3%, and 11.3% for AV0, AV25, and AV50, respectively). Adsorption batch tests were then

performed to investigate the equilibrium, the kinetics, and the thermodynamics of the process. Results suggested that the Langmuir model was in agreement with the experimental results, and the values for the adsorption capacity were evaluated to be 199 mg/g, 311 mg/g, and 346 mg/g for AV0, AV25, and AV50, respectively. The kinetic results were used to develop a mathematical model to estimate the effective diffusion coefficient for each type of Aloe adopted. Effective diffusion coefficients of $5.43 \cdot 10^{-7}$ cm²/min, $3.89 \cdot 10^{-7}$ cm²/min, and $5.78 \cdot 10^{-7}$ cm²/min were calculated for AV0, AV25, and AV50, respectively. It was found that pre-treatment, on the one hand, enhances the adsorption capacity of the material and on the other, reduces its affinity toward MB uptake.

The perennial fern *Pteris vittata* is an Arsenic-hyperaccumulator plant able to grow in hydroponic cultures and hence used for phytoremediation of contaminated water. In order to abate the costs linked to the disposal of As-contaminated biomass, in this work *Pteris vittata* waste roots were tested for the removal of Methylene Blue (MB). The pH of zero charge was evaluated to be 6.2, hence all the adsorption tests were performed at a neutral pH. Isotherms at 20 °C and 40 °C showed a typical Langmuir trend with a maximum adsorption capacity of 112 mg/g and 154 mg/g respectively. Kinetic tests were also carried out for different solid-liquid ratios and fitted by a mathematical model. The effective diffusivity of MB in the solid was estimated using the maximum likelihood method and the values of $5.99 \cdot 10^{-8} \pm 9.6 \cdot 10^{-9}$ cm²/s and $9.56 \cdot 10^{-8} \pm 4.5 \cdot 10^{-9}$ cm²/s were obtained at 20 °C and 40 °C respectively. After calculating the Biot number it was found out that both the intra-particle resistance and the external mass transfer resistance are important for the description of the rate of the dye uptake.

Among all the three materials, *Pteris vittata* roots were selected to perform fixed bed column tests for the removal of Methylene Blue from water. As a matter of fact, swelling phenomena for *Aloe vera* induced to an excessive packing of the bed, while *Yerba Mate* tea showed a smaller adsorption capacity than *Pteris vittata*. Breakthrough curves were obtained experimentally at 20°C and the Linear Driving Force (LDF) model was used to predict their behavior. An empirical expression for the evaluation of the LDF mass transfer coefficient was then derived and validated for Reynolds number less than 0.025.

In conclusion, this thesis provides all the steps (from characterization to fixed bed applications) that are required to evaluate the feasibility of adopting an agro-waste material as an adsorbent for real industrial applications. In this sense this work constitutes a guide from both an experimental and modeling point of view setting the basis for further studies in this research field.

CHAPTER I

1. Introduction

Water is an essential resource for the quality of both natural and social environments due to its crucial impact on human health, agriculture and energy production. However, it is estimated that climate change as well as the continuous demographic increase will lead to a reduction of freshwater availability for two-thirds of the world population by 2025 [1]. For this reason, wastewater treatment and reuse will play a key role for the achievement of sustainable management of water which constitutes a fundamental goal of the United Nations' 2030 Agenda for Sustainable Development [2]. In this chapter a brief insight to the issue of wastewater treatment will be provided focusing particular attention to class of pollutants that are harmful even at very low concentrations such as dyes and heavy metals.

1.1 Freshwater Management

Approximately 99% of all liquid freshwater on Earth is stored below the ground surface and is commonly known as groundwater. The remaining part is available in surface water bodies. Freshwater withdrawal has increased strongly during the last century, and is still increasing in most parts of the world. According to recent estimates, global freshwater withdrawal increased from around 600 km³/year in 1900 to 3,880 km³/year in 2017 [3]. Such scenario was mainly driven by: population growth rate, scientific and economic progress. As a matter of fact, as highlighted in **Figure 1-1**, the agriculture, the domestic and the industrial sectors are the three principal users of freshwater led by the Asiatic continent having the largest share (64.5%) .

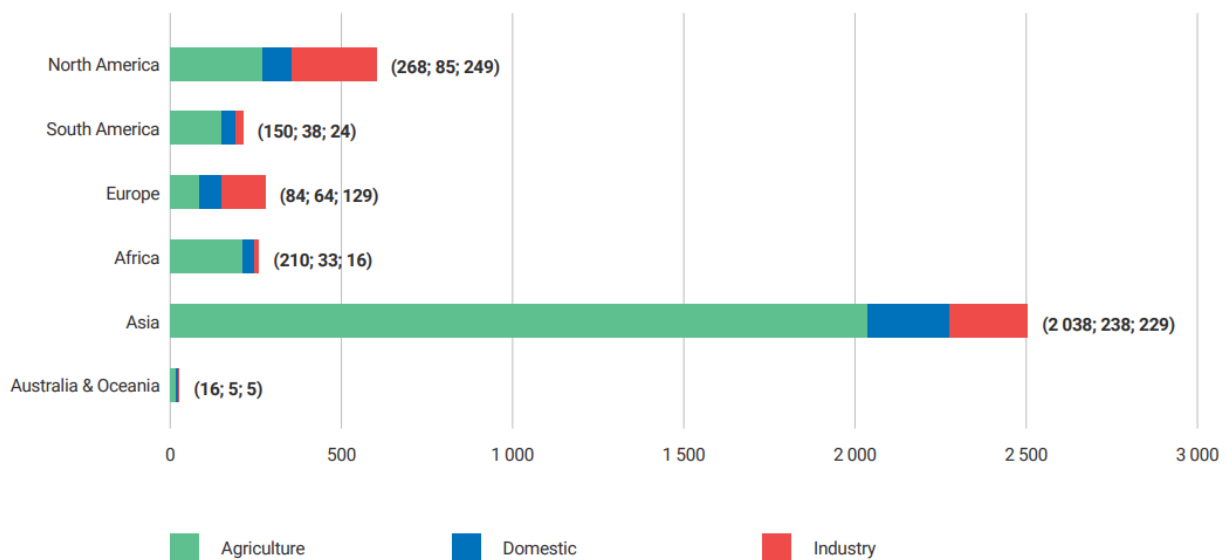


Figure 1-1 Freshwater withdrawal in 2017, aggregated by continent and by water sector use (km³/year)[3].

All the above mentioned human activities produce contaminated water effluents. The latter uncontrolled release may induce to severe environmental damages and the contamination of freshwater reservoirs leading to an overall decrease of freshwater availability. Just taking into account the European scenario, according to the European Environment Agency (EEA)¹ around 60% of surface water bodies did not achieve good ecological status in 2021 (**Figure 1-2**).

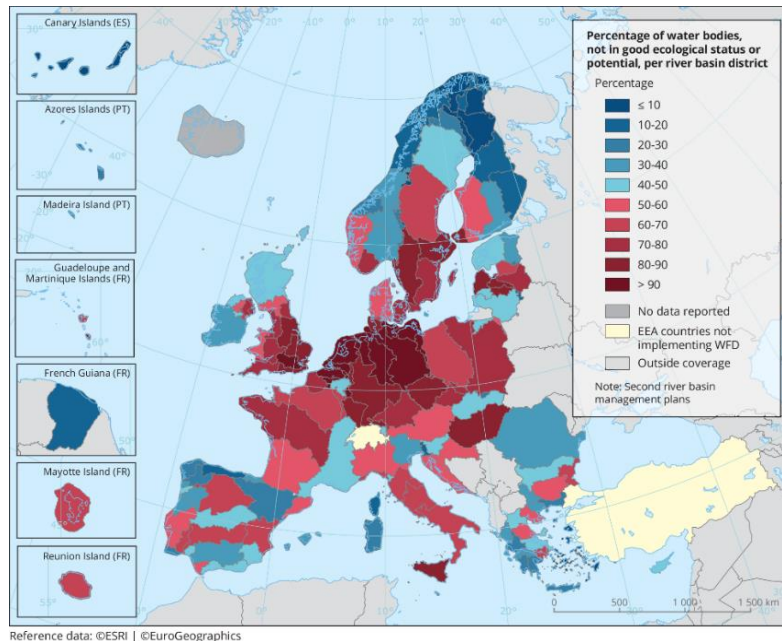


Figure 1-2 Percentage of water bodies in Europe not in good ecological status¹ in 2021.

Waste Water Treatment Plants (WWTP) play, then, a fundamental role for a safe disposal of wastewater mitigating and avoiding environmental pollution. It is worth to mention that coupled to WWTP recent technologies aim to reduce to zero the amount of liquid effluents outcoming from a process plant reusing water in a closed loop. Such approach is called Zero Liquid Discharge (ZLD) which is usually accomplished by concentrating the effluent using various techniques, including membrane-based and multi effect evaporation based systems [4].

1.2 Wastewater treatment

According to the various class of pollutants that can occur in wastewaters, each WWTP require an adequate design to achieve the desired performances. However, all the possible processes involved can be generally summarized in the following sequential steps: 1) Pre-treatment, 2) Primary treatment, 3) Secondary treatment and 4) Tertiary treatment.

1.2.1 Pre-treatment

¹ <https://www.eea.europa.eu/ims/ecological-status-of-surface-waters>

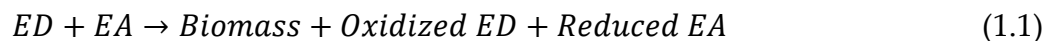
Pre-treatment is mainly focused on the equalization of the wastewater flow or pollutants concentration in order to guarantee as much as possible constant properties to the effluent avoiding the overloading of treatment units. Moreover, the pre-treatment step deals also with: pH neutralization accomplished with the addition of acid (e.g. H₂SO₄, HCl) or basin (e.g. NaOH, limestone) compounds depending on the nature of the effluent; the removal of immiscible layers of oil by skimming.

1.2.2 Primary Treatment

Primary treatment deals with the removal of suspended solids. In this case both chemical and physical methods are adopted for the purpose depending on the nature of solid involved. Screens are used as a filter to collect moderate-size particles while grit chambers permit the elimination of sand or hard inert particles. One of the most common solid separation technique is gravity sedimentation. Often the latter, especially for the removal of colloids, is preceded by Chemical precipitation using coagulants such as Aluminum sulfate, ferric chloride, ferrous sulfate, lime.

1.2.3 Secondary Treatment

Secondary treatment exploits the action of microorganisms (referred as biomass) to stabilize the liquid effluent. The metabolic pathway of the biomass is responsible of the oxidation of waste components which act as Electron Donors (ED). Different types of products are thus generated depending on the particular Electron Acceptor (EA) involved or selected. The general process of biological waste conversion was reported in Equation 1.1.



When molecular oxygen is chosen as EA, aerobic bioreactors are employed and the treatment takes the name of *Activated Sludge*. This process produces high-quality effluents (BOD₅ and Suspended Solids of 20-30 mg/L) since the combined action of adsorption and biological metabolism. As a matter of fact, many pollutants that are not degraded by biological action (e.g. carbonate/hydroxide precipitates containing heavy metals) are also removed since they remain entrapped into the biological floc made of biomass aggregates. The term *Anaerobic/Anoxic activated sludge* is instead referred to a biological process that uses another EA rather than oxygen. In particular, nitrates (NO₃⁻) are commonly used for this scope especially when they already occur in the effluent and should be removed giving place at the so called denitrification processes.

1.2.4 Tertiary Treatment

The term tertiary treatment is commonly adopted to identify chemical-physical processes that are able to remove all those pollutants that are not easily converted by biomass. The main process in this category are: Advanced Oxidation processes, Membrane Processes and Adsorption.

Advanced Oxidation Processes (APOs)

Advanced oxidation processes are able to remove all the recalcitrant organic compounds, converting them into mineral end products such as CO_2 even if their concentration is very low (<50 ppm), exploiting the extremely high oxidizing power of hydroxyl radicals. The latter are produced onsite by means of ultraviolet radiations combined with²: ozone (O_3); hydrogen peroxide (H_2O_2); Fenton's reagent (Ferrous iron and hydrogen peroxide); Titanium dioxide (TiO_2); Zinc oxide (ZnO). In the last two cases the metal oxide plays a catalytic role promoting water splitting into radical species for $\text{OH}\cdot$ formation: this phenomenon is known as photocatalysis. AOPs are considered a valid and economic alternative for the removal of very dilute solution of toxic compounds.

Membrane Processes

Selective membranes are widely used to separate contaminants from water. A first classification of membranes is linked to their physical structure: porous membranes act as a physical barrier to all those components that are larger of the membrane pores; dense membranes are permeable only to molecules they are able to solubilize and diffuse into the membrane matrix. Micro and Ultra filtration belong to the first category having pore sizes in the range of $0.1\text{--}1.0\ \mu\text{m}$ and $0.05\ \mu\text{m}$ respectively [5]. In particular, Ultra filtration is capable of separating macromolecules such as sugars and proteins. Nanofiltration and Reverse Osmosis are instead considered as dense membranes able to separate monovalent compounds such as dyes and dissolved salt and ions respectively. Often membranes are coupled with an activated sludge system leading to the Membrane Bioreactors (MBRs) technology. As shown in **Figure 1-3**, membranes may be located externally (sidestream module) or internally (submerged module) to the bioreactor. This configuration permits to generate a stable purified water stream in terms of quality standards since the membrane modules guarantee on the pollutant abatement.

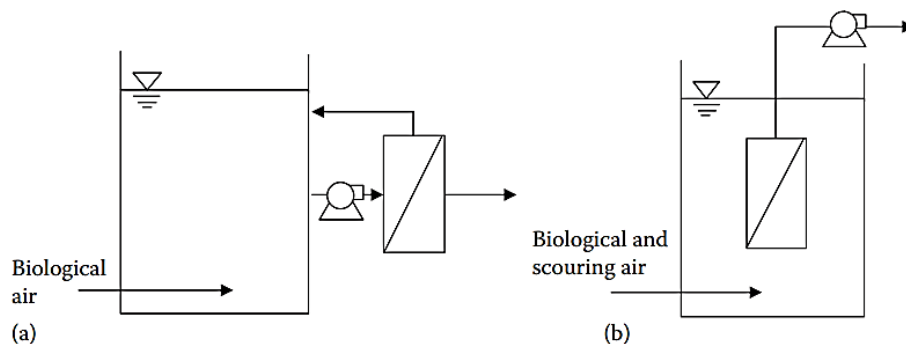


Figure 1-3 (a) MBR with sidestream membrane and (b) MBR with submerged membrane [6].

²Here were reported just the most commonly used agents, many others are available especially in the field of photocatalysis.

Adsorption

Adsorption is a physical/chemical separation method based on the principle that solute molecules are attracted by the surface of solids. Adsorption finds wide application for the removal of very diluted pollutants (<50 ppm). The working principle of this phenomenon will be extensively explained in the following chapter of this thesis. Moreover, the most used solid adsorbents for water treatment purposes are Activate Carbons (AC) and Zeolites. Both solids will be introduced in Chapter III together with the alternative adsorbent materials proposed in this study.

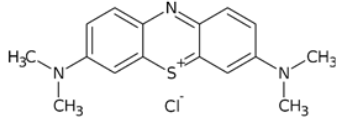
1.3 Pollutants

In this section two class of pollutants that were analysed in this thesis will be introduced: Dyes and Heavy metals.

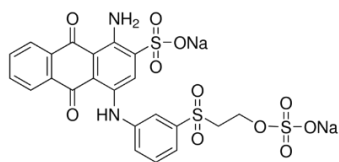
1.3.1 Dyes

Among all the possible contaminants, dyes are the first to be detected since they are highly visible even at very low concentrations (< 1ppm). It was estimated that more than 100,000 commercial dyes are used industrially with a production of about $7 \cdot 10^5 \div 1 \cdot 10^6$ tons per year [7–9] and a 10% ÷ 15% of dye is loss during dyeing processes [10,11]. The textile industry alone, which accounts 2/3rds of the dyestuff market [9], generates 120 m³ of wastewater per tons of fiber produced [12]. If released into the environment, dyes can perturb the biological activities of algae and plants by hindering light penetration in water and they can bioaccumulate in sediments and fishes. Then they can develop allergies, dermatitis, and even cancers, through contact with the gastrointestinal tract, skin, and lungs [13]. In this study the removal of two synthetic dyes will be considered: Methylene Blue (MB) and Remazol Brilliant Blue (RBB) whose properties are reported in **Table 1-1**.

Table 1-1 Properties of Methylene Blue and Remazol Brilliant Blue.

Dye	Chemical structure	Information	Contamination sources
Methylene Blue		$C_{16}H_{18}ClN_3S$ Cationic dye Mw 319.85 g/mol	Textile industry Leather industry Dyestuff industry Paper industry Plastic industry Pharmaceutical uses Laundry activity

Remazol Brilliant
Blue



$C_{22}H_{16}N_2Na_2O_{11}S_3$

Anionic dye

M_w 626.54 g/mol

Textile industry
Dyestuff industry

1.3.2 Heavy Metals

Heavy Metals is another category of pollutants with strong dangerous effects on the health of biological species, even at low concentrations, in the aquatic system [14]. Excessive concentration of, or long term exposure to, heavy metals cause several health issues such as nervous system disorders and irreversible multi-organ failure [15]. Mercury, cadmium, copper, zinc, nickel, lead, chromium, aluminum, and cobalt are considered as priority aquatic pollutants due to their toxicity [16]. This thesis dealt with Chromium (or better Cr(VI)) which is one of the most toxic heavy metals and its release in water bodies is a consequence of industrial activities such as tanneries and metal finishing plants [17]. It exists in two forms Cr(III) and Cr(VI): the first is less soluble in water body and trace concentration of Cr(III) is important in carbohydrate metabolism [18]; Cr(VI) in a non-essential element, toxic and very mobile with its high oxidizing capacity correlated to carcinogenic and mutagenic diseases [18,19]. In tanneries wastewater the Cr(VI) concentration is up to 50 mg/L [18] and 0.1 mg/L is the maximum level of Cr(VI) allowable in surfaces water [20].

CHAPTER II

2. Adsorption theory and modelling

The region of space between two phases is called *interphase*. The transition from one phase to another is not sharp but instead smooth and its extension delimits the thickness of the interphase itself. The term adsorption indicates the accumulation of molecules, present in the homogeneous phases, at the interphase. The nature of such phenomenon could be physical or chemical. In the first case the interaction forces between the molecules of one phase adsorbed to the other have a physical nature (electrostatic interactions, dipole interactions, London interactions ecc.) while in the second case the presence of covalent bonds determine the chemical nature of the phenomenon. Adsorption can occur between different types of interphases such as Liquid-Liquid, Liquid-vapor, solid-gas, solid-liquid. The latter was extensively exploited during the last decades in separation processes such as the removal of pollutants from wastewater. The aim of this chapter is to provide a theoretical background for the description of the adsorption phenomenon both from the thermodynamic and the kinetic point of view. Specific models for the representation of batch and continuous systems will be provided.

2.1 Theoretical background

2.1.1 The adsorption fundamentals

The first issue to achieve a theoretical formulation of the adsorption phenomena was to clearly define the properties of the *interphase* region. Such problem was solved by J. W. Gibbs in his work named "*influence of Surface of Discontinuity upon the equilibrium of Heterogeneous Masses*" in which it was proposed to pick arbitrarily a geometrical surface (called *dividing surface*) in the interphase to which attribute all the concentration anomalies [21]. The implication of such assumption are:

- The concentration in the bulk phases can be considered constant;
- The dividing surface can be treated from a thermodynamic point of view as a bi-dimensional phase.

A visual representation of the Gibbs's modelling was proposed in **Figure 2-1**. The thermodynamic state functions used for the description of three-dimensional phases are still valid for bi-dimensional ones. Hence, the Gibbs free energy of a bi-dimensional phase can be written as follows

$$G = U - \gamma A - TS \quad (2.1)$$

$$\gamma = \left(\frac{\partial G}{\partial A} \right)_{T, n_i} \quad (2.2)$$

where A is the interfacial area and γ is the interfacial tension defined as the amount of energy required to increase the interfacial area of ∂A at constant temperature for a fixed number of moles in the system.

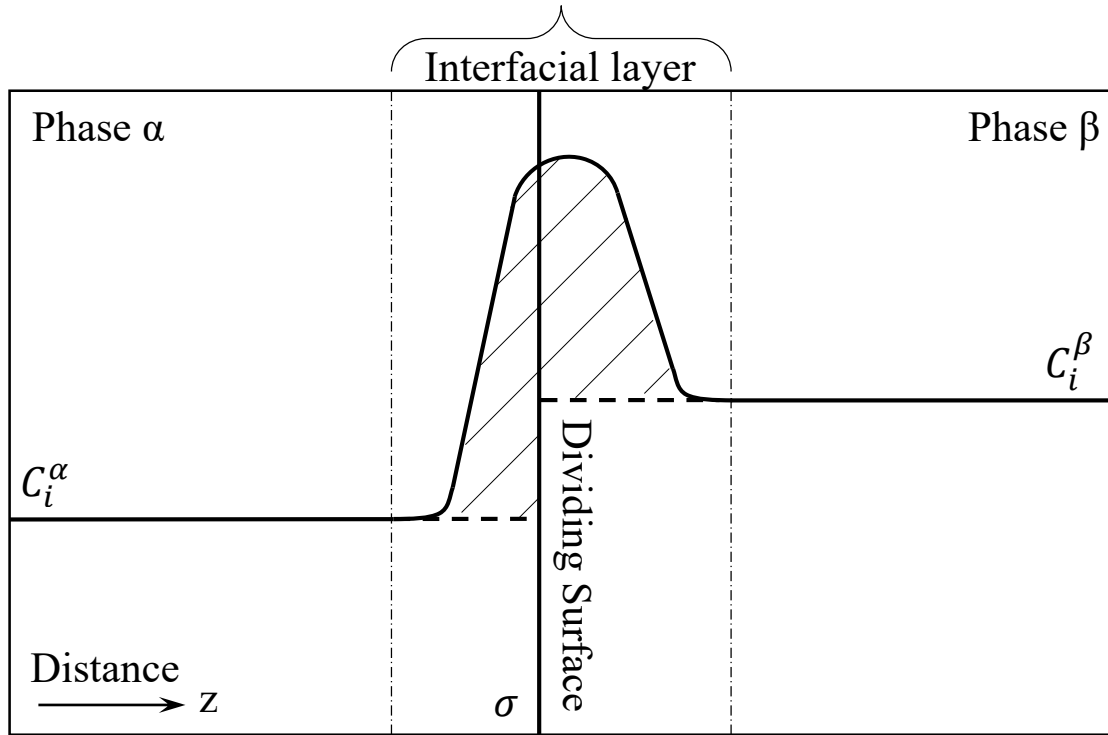


Figure 2-1 Schematic representation of the Gibbs modelling of adsorption between two bulk phases α and β .

Differentiating Equation 2.1 and using the Euler's theorem³, it is possible to obtain the Gibbs-Duhem equation which at constant temperature is also known as the Gibbs adsorption Isotherm. The latter was reported below

$$-A d\gamma = \sum_i^c n_i^\sigma d\mu_i^\sigma \quad (2.3)$$

where n_i^σ and μ_i^σ represent for each compound the moles and the chemical potential of the adsorbed species respectively, while c was used to indicate the total number of compounds at the interface. The term n_i^σ it is directly related to the so called *Surface Concentration* as shown in Equation 2.4 which is often confused with the surface excess that will be defined later in section 2.1.3.

³ The Euler's theorem states that an extensive variable can be expressed as the sum of the product of its partial molar derivative with corresponding moles involved: $\Phi = \sum n_i \bar{\phi}_i$. For further information is suggested the work "*Termodinamica degli equilibri di fasi fluide*" of L. Marrelli [120].

$$\Gamma_i = \frac{n_i^\sigma}{A} \quad (2.4)$$

It is often preferred to express Equation 2.3 in terms of the *spreading pressure* π (equivalent to a bi-dimensional pressure) which is strictly linked to the interfacial tension as shown in Equation 2.5.

$$-d\gamma = d\pi \quad (2.5)$$

Thus, using Equation 2.4 and 2.5 the Gibbs adsorption Isotherm takes the form reported in Equation 2.6.

$$d\pi = \sum_i^c \Gamma_i d\mu_i^\sigma \quad (2.6)$$

It is important to recall the definition of the chemical potential that for an adsorbed phase is expressed as follows in Equation 2.7.

$$\mu_i^\sigma = \left(\frac{\partial G}{\partial n_i^\sigma} \right)_{T, \pi, n_{j \neq i}^\sigma} \quad (2.7)$$

So far, only the bi-dimensional phase was considered while equilibrium is established when the overall Internal energy of the system reaches a minimum. The latter condition can be expressed mathematically exploiting the additive property of extensive variables as given below

$$dU = dU^\alpha + dU^\beta + dU^\sigma = 0 \quad (2.8)$$

where dU^α , dU^β , dU^σ are the variation of the Internal energy of the system related to phase α , β and σ respectively. Equation 2.8 can be further processed as follows

$$dU = \sum_{j=1}^f T_j dS_j - \sum_{j=1}^{f-\sigma} P_j dV_j - \pi dA + \sum_{j=1}^f \sum_{i=1}^c (\mu_i dn_i)_j = 0 \quad (2.9)$$

where with the symbol f it was indicated the number of phases involved. Equation 2.9 it is a general equation for the description of phase equilibria, involving the presence of the energy related to interface generation (πdA). As happens for all the others fluid phase equilibria, the following conditions must be satisfied to solve Equation 2.9:

- Thermal equilibrium. $T_\alpha = T_\beta = T_\sigma$;
- Mechanical equilibrium. $P_\alpha = P_\beta$;
- Chemical equilibrium. $\mu_i^\alpha = \mu_i^\beta = \mu_i^\sigma$ for $i = 1, 2, \dots, c$;

It is possible to notice that in the list above, the spreading pressure (π) does not appear since, at equilibrium, it is assumed that the interfacial area is constant ($dA = 0$). However, the introduction a new physical parameter such as the spreading pressure increases the degrees

of freedom of the whole system composed by the two bulk phases and the dividing surface. For this reason, the adsorption equilibrium (respect to the other fluid phase equilibria) requires an additional constraint to be completely determinate. Such bond is set by the Gibbs adsorption Isotherm which introduces a relation between the spreading pressure, the amount of adsorbed compounds and the properties of the bulk phases (through the equilibrium condition of the chemical potentials).

2.1.2 Solid-gas Isotherms

In general, for the description of a fluid-solid adsorption, the dividing surface is thought to be located at the beginning of the fluid interphase in order to allow rigorous description of the fluid phase. During this section different types of isotherms will be described according on the different assumptions made on the gaseous and the adsorbed phase. Before introducing the most famous and adopted isotherms, a simple case will be provided with the aim of understanding the importance of isotherms themselves.

The adsorption of a pure compound from a gaseous phase to a solid surface considered ideal (ideal gas layer surrounding the solid) is the easiest one to describe mathematically. As a matter of fact, in such conditions it results $f^\sigma(\pi) \rightarrow \pi$ and $f^G(P) \rightarrow P$ and hence the condition $P = \pi$ is straight forward from the equilibrium conditions of the chemical potentials. The Gibbs isotherm given in Equation 2.6 can be then manipulate to obtain the following linear adsorption isotherm similar to the Henry's law.

$$P = RT\Gamma \quad (2.10)$$

As it is easy to understand, the Equation 2.10 constitutes a fundamental relation between the measurable variables P (Pressure) and T (Temperature) with Γ (the surface concentration of the adsorbed compound). The validity of Equation 2.10 is restricted only for very small pressures and hence for low degrees of adsorption on the solid surface. The main hypothesis of such case was to consider the adsorbed phase ideal or, in other words, to have a complete knowledge of its state. Using, for example, the Van Der Waals equation of state to evaluate the fugacity of the adsorbed phase the Hill-De Boer expression [22] was obtained. The lack of knowledge of the state of the adsorbed phases implies that instead of introducing a relation between the spreading pressure and the concentration of the bulk phase (in this case the Pressure of the system) and then to use the Gibbs isotherm to obtain information about the adsorbed amount, it is convenient to proceed the other way round. For this reason, the research of model equations that could directly provide a link between the surface concentration and the bulk concentration of the fluid phase started. Such fundamental equations are identified as isotherms.

Langmuir Isotherm

The Langmuir isotherm is commonly adopted for the description of isotherms that present a saturation behaviour for high partial pressures (see **Figure 2-2**) for both chemical and

physical types of adsorption. The expression of the Langmuir isotherm was reported in Equation 2.11 and it is easily derived from the following assumptions:

- Adsorption occurs at a fixed number of distinct sites;
- All sites are energetically equivalent;
- Each site can accommodate one sorbate molecule (only monolayer adsorption is allowed);
- No interaction between sorbate molecules on adjacent sites.

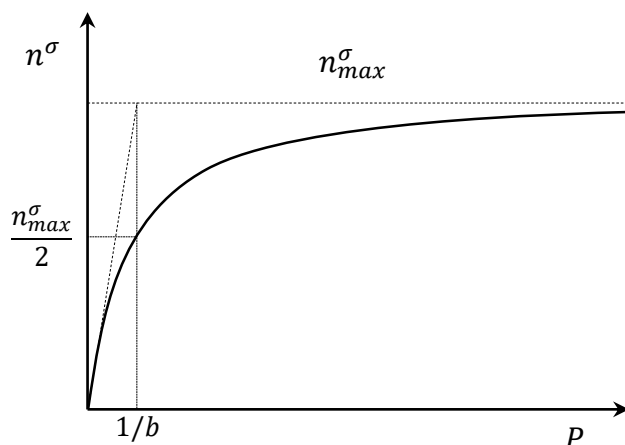


Figure 2-2 Graphical representation of the Langmuir isotherm.

$$n^{\sigma} = n_{max}^{\sigma} \frac{bP}{1 + bP} \quad (2.10)$$

The symbol n_{max}^{σ} indicates the maximum allowable molecules reached when the adsorbed monolayer is filled while b represents the Langmuir constant. The latter assumes the meaning of an equilibrium constant between the adsorption and desorption rate. According to such consideration, the equilibrium constant b is related to the free Gibbs energy variation of the reaction in a reference state ΔG° (usually the standard one) as given below.

$$-\frac{\Delta G^{\circ}}{RT} = \ln b \quad (2.11)$$

Moreover, integrating Equation 2.11 with the Gibbs-Helmoltz relation, the enthalpy variation of the phenomenon can be expressed by means of the Van't Hoff equation

$$\ln b(T) = C - \frac{\Delta h}{R} \frac{1}{T} \quad (2.12)$$

where C is a constant that arises from the integration of the Van't Hoff equation, R is the universal gas constant, Δh is the specific enthalpy variation assumed to be constant with temperature. Equation 2.12 predicts a linear relation between the natural logarithm of the equilibrium constant against the reciprocal of temperature. The physical meaning of Equation 2.11 and 2.12 is clear for chemisorption, however in case of physical adsorption it could induce to erroneous conclusions. It is worth to mention that Equation 2.12 is so much

used in literature to obtain information about the adsorption heat that even without a physical meaning the resulting value of Δh can be used to make comparison between different types of adsorbent materials.

B.E.T Isotherm

In 1938, Brunauer, Emmett and Teller [23] developed what is now known as the BET theory. As happens for the Langmuir's isotherm, the theory is based on the assumption that there are no lateral interactions between the adsorbed molecules and that they are not free to move along the solid surface. The principal property of BET isotherm is that it allows the formations of multi adsorption layers hence it describes only physical adsorption. When the number of layers admitted $n \rightarrow \infty$ the following isotherm, reported in linear form, was found:

$$\frac{P}{(P_s + P)V} = \frac{1}{V_m C} + \frac{C - 1}{V_m C} \frac{P}{P_s} \quad (2.13)$$

where V_m the volume of molecules adsorbed contained in a monolayer spread over the surface area of the adsorbent, V is the volume of gas adsorbed, P_s is the vapour tension of the adsorbed molecules and C is a characteristic constant of the system. The main advantages of the BET isotherm are two:

- It is able to represent all types of isotherms shapes (Type I, II, III, IV, V) reported in **Figure 2-3** according to the classification made by Brunauer et al. [24];
- It is adopted to evaluate the surface area of a solid adsorbent as it will be shown in section 3.4.1.

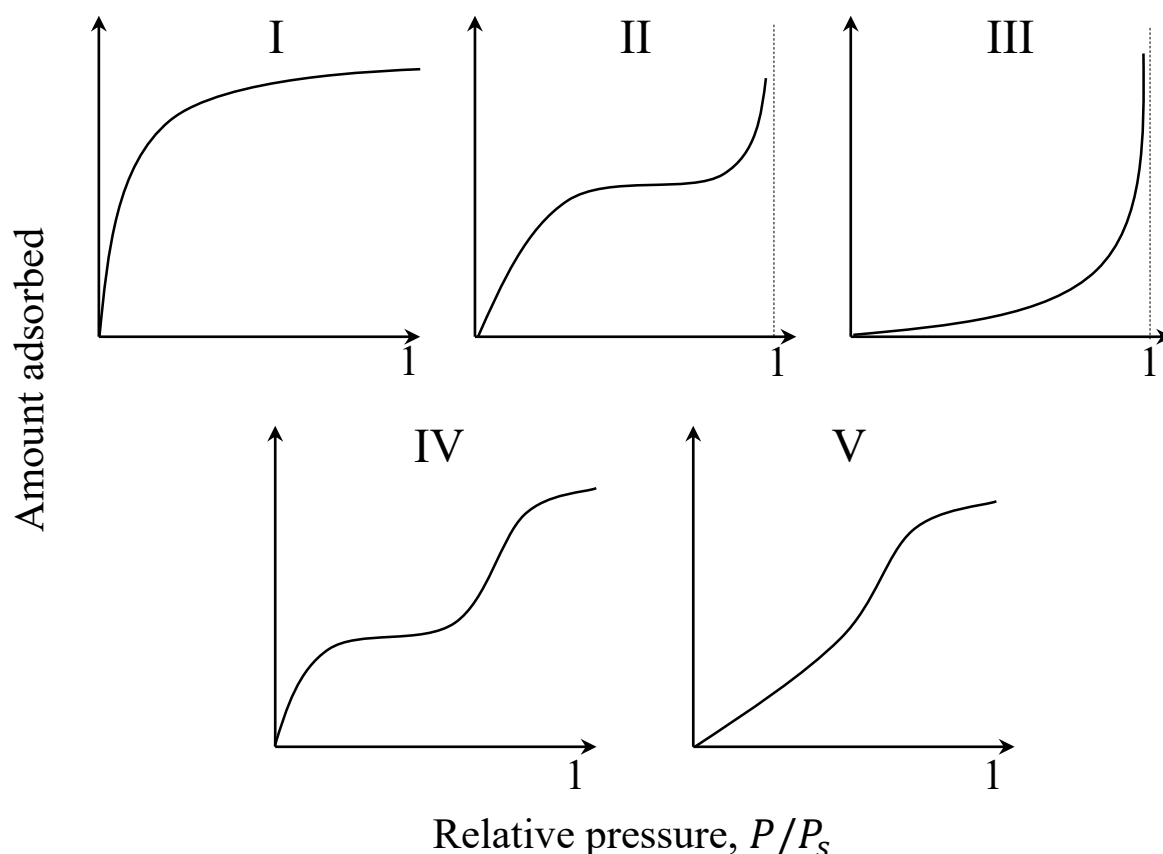


Figure 2-3 Classification of the isotherms into five types.

Freundlich Isotherm

The Freundlich isotherm is given in Equation 2.14. It was developed as an empirical expression to describe gas-solid adsorption⁴ on a heterogeneous surface. Its range of validity is limited to low degree of surface coverage since for $P \rightarrow \infty$ it happens that $n^\sigma \rightarrow \infty$.

$$n^\sigma = k_F P^{1/n} \quad (2.14)$$

where k_F is a distribution coefficient and n is a correction factor.

2.1.3 Solid-Liquid adsorption

The first aspect to clarify of the solid-liquid adsorption is that it involves at least two components: the solute and the solvent. For this reason, it is important to distinguish different possible cases depending on the nature of the liquid mixture:

⁴ It is possible to obtain the Freundlich isotherm imposing a specific heat of adsorption distribution equal to $\rho(Q_{ads}) = \alpha e^{-\beta Q_{ads}}$ and assuming valid the Langmuir isotherm for each different type of active site. The equation is then derived integrating the equation $n^\sigma = \int \frac{P}{P + k e^{-\frac{Q_{ads}}{RT}}} \alpha e^{-\beta Q_{ads}} dQ_{ads}$. For further reading is suggested the work "Aspetti cinetici della teoria del reattore chimico" by S. Carrà and L. Forni [121].

- *Completely miscible.* This is the most general case in which the entire range of concentration can be explored. In this case the terms solute and solvent are just formally attributed to the components depending on their relative quantity.
- *Partially miscible.* In this case the solubility limits establish a thermodynamic constraint that allows the presence of a homogeneous liquid phase only for a strict range of concentration. This is true both when the formation of a second liquid phase or a solid crystallization occurs.

The discussion will proceed for the description of completely miscible liquid mixtures considering partially miscible liquid mixtures a particular condition of the aforementioned case. The experimental variable commonly used to characterize solid-liquid adsorption is the *Surface excess* (q_i^E). The latter is defined as the difference between the amount of the compound i adsorbed in the unit mass of the solid and the quantity that it would be adsorbed if the composition of the solid phase was equal to of the liquid one. In mathematical terms:

$$q_i^E = \frac{n_i^E}{M} = \frac{n_T^\sigma}{M} (x_i^\sigma - x_i) \quad (2.15)$$

where n_i^E are the excess of moles adsorbed for the component i , n_T^σ are the total moles adsorbed, M is the mass of the solid adsorbent, x_i^σ is the mole fraction of component i in the adsorbed phase and x_i is the mole fraction of component i in the liquid phase.

From the manipulation of Equation 2.15 by means of material balances considering the system before and after the contact with a solid adsorbent, the following equation is derived straightforward⁵:

$$q_i^E = \frac{n_T}{M} (x_{T,i} - x_i) \quad (2.16)$$

where n_T are the total moles present in the system and $x_{T,i}$ is the mole fraction of the component i in the liquid solution before the start of the adsorption phenomenon. Thus, Equation 2.16 permits to calculate the value of the excess surface from experimental measurements of the liquid phase bulk. Moreover, Equation 2.16 (simplified to the case of a binary system) can be rewritten as shown below together with rapid mathematical passages

$$\begin{aligned} n_T &= n_1 + n_2 + n_1^\sigma + n_2^\sigma \\ x_{T,1} &= \frac{n_1 + n_1^\sigma}{n_T}; \quad x_1 = \frac{n_1}{n_1 + n_2} \\ q_i^E &= \frac{n_1^\sigma}{M} x_2 - \frac{n_2^\sigma}{M} x_1 = q_1 x_2 - q_2 x_1 \end{aligned} \quad (2.17)$$

⁵ For a complete development of the calculus see the work “*Introduzione al calcolo degli equilibri di fasi fluide*” by R. De Santis (cit) [122].

where q_1 and q_2 are the surface concentrations for unit mass of adsorbent for component 1 and 2 respectively. At this point two aspects should be stressed out:

- Equation 2.17 constitutes a relation between the surface excess (q_i^E) and the surface concentration (q_i);
- There are two different kind of isotherms depending on whether the surface excess (q_i^E) or surface concentration (q_i) are considered.

As a matter of fact, it is crucial to make a distinction between the so called “*individual isotherm*” which considers only the surface concentration for a specific component, and the “*composite isotherm*” which takes into account the surface excess and hence the role of solvent in the adsorption process. **Figure 2-4** was taken from the work of Ostwald and de Izaguirre [25] which developed a theoretical study on the possible combinations of individual and composite isotherms. Several observations are needful:

- At the extremes of each graph (in correspondence of pure compounds) $q_i^E = 0$;
- Graph a) is the only case in which the solvent B does not adsorb and $q_1^E \geq 0$ for all the range of concentration;
- When the composite isotherm assumes a negative value, hence $x_1 > x_{T,1}$ (as explained by Equation 2.16), it means that the solvent it is preferentially adsorbed with respect to the solute.

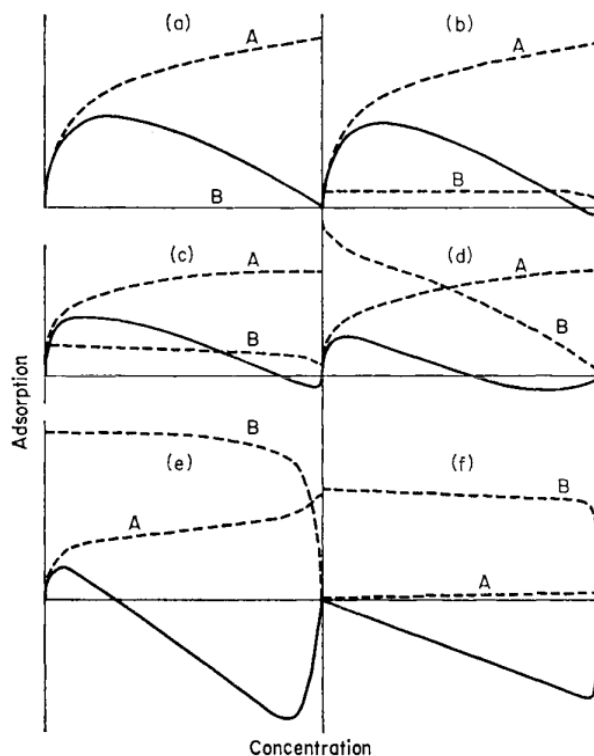


Figure 2-4 Individual and composite isotherms. Full line: composite isotherm. Broken line: A “solute, B “solvent”. For dilute conditions, the two curves overlap (for the solute) or are specular (for the solvent) [25].

Once clarified all aspects related to a general definition of isotherms for liquid solutions, it is possible to switch to a particular case: *dilute solutions*. A solution is considered diluted when the molar fraction of the solute is $x_1 < 0.01$. According to such consideration, it is reasonable to introduce the following approximation of Equation 2.17

$$q_i^E \sim q_i \quad (2.18)$$

Hence, only for dilute solutions, the surface excess coincides with the surface concentration (which is also shown graphically in **Figure 2-4**). Furthermore, in case of dilute solutions, an equivalent expression for the calculation of the surface concentration/excess can be derived (previously defined in Equation 2.16) assuming that the total number of moles in the liquid solution (or the total liquid volume V_L) remains constant during the adsorption process:

$$q_i = \frac{n_T}{M} (x_{T,i} - x_i) = \frac{V_L}{M} (C_{T,i} - C_i) \quad (2.19)$$

where $C_{T,i}$ and C_i are the molar concentration of the component i in the liquid solution before the start of the adsorption phenomenon and at equilibrium conditions respectively. Obviously all the equations, and in particular Equation 2.19, can be expressed in mass terms instead of molar ones. In such case, $C_{T,i}$ and C_i correspond to the mass concentration of the component i in the liquid solution before the start of the adsorption phenomenon and at equilibrium conditions respectively. Dilute liquid solutions are very commonly subjected to adsorption processes especially in the field of water treatment (i.e. the removal compounds that have toxic effects even at very low concentrations). Moreover, Dilute liquid solutions may occur in the cases of partially miscible liquid solutions mentioned before especially when the solubility limits are low.

The following consideration on the adopted isotherms for solid-liquid adsorption will be restricted to the case of dilute solutions since there are the types of mixture that were considered in this work. As a matter of fact, isotherms such as the Langmuir and the Freundlich one are still reliable (and commonly adopted) for the description of dilute solid liquid system. Their mathematical expression is identical to the gaseous one if the partial pressure is replaced with the concentration of the adsorbed compound liquid phase. For completeness they are reported below.

$$q_i = q_{max} \frac{bC_i}{1 + bC_i} \quad (2.20)$$

$$q_i = k_F C_i^{1/n} \quad (2.21)$$

Of course the utilization of such isotherms is convenient for their simple mathematical form and because they are somehow able to represent the behaviour of many adsorption systems. However, the loss of physical meaning should be kept in mind especially when Equations 2.11 and 2.12 are adopted to obtain information on solid-liquid systems.

2.1.4 Batch kinetic modelling

When the uptake of molecules from a fluid phase on a solid adsorbent occurs in a closed environment, the adsorption is taking place in a *batch* system. Although the majority of applications of adsorption for industrial purposes are carried out in column/continuous apparatus (see section 2.1.5), batch systems are commonly adopted to study the adsorption equilibrium and kinetics. A schematic representation of a batch system for a liquid-solid adsorption was provided in **Figure 2-5** assuming, for example, the removal of a dye: during time the colour of the liquid solution changes accordingly to the lower amount of dye remaining in the liquid. In general, the adsorption kinetics is constituted by three sequential steps:

1. *External mass transfer*. Transport of the adsorbate from the liquid bulk to the solid surface across the surrounding liquid film (**Figure 2-5 a**);
2. *Internal mass transfer*. The adsorbed compound, driven by concentration gradients, diffuses through the macro-pores (*pore diffusion* **Figure 2-5 b**) or micro-pores (*surface diffusion* **Figure 2-5 c**) of the solid;
3. *Adsorption*. The molecules are adsorbed on the solid surface.

Each step offers a distinct resistance to the adsorption kinetics and depending on their relative magnitudes any one of these resistances may be rate controlling or more than one resistance may contribute. Generally, the adsorption step is considered as instantaneous, hence its dynamics is neglected in the kinetic modelling of the system.

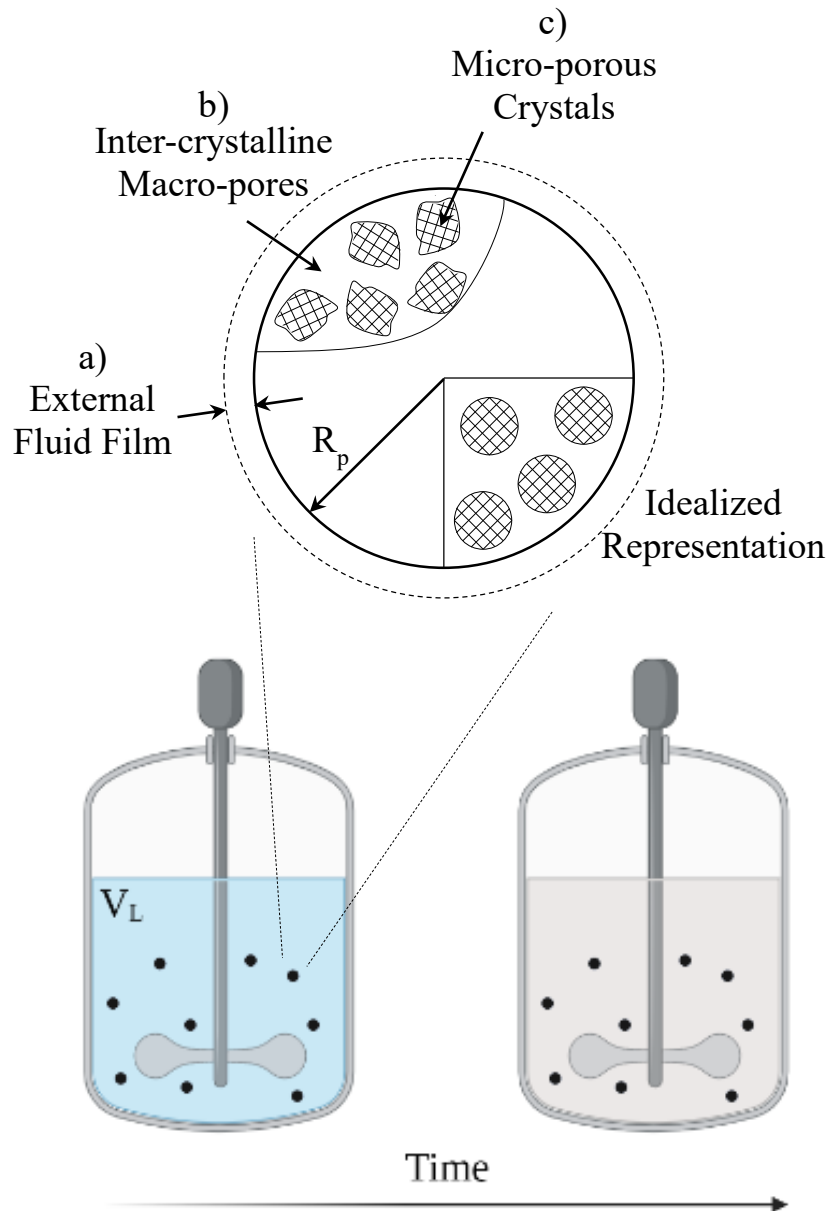


Figure 2-5 Schematic representation of a batch adsorption system that changes over time (from a coloured solution to a transparent one) with a focus on the external mass transfer resistance a) and the resistance due to the diffusion through macro-pores b) and micro-pores c).

Before to provide the complete model, a mathematical expression for each mass transfer step will be given focusing also on the differences between pore and surface diffusion. The following discussion have a general meaning but the equations will be provided in a form that could be directly applied to liquid-solid systems.

External mass transfer

Although the fluid phase is in turbulent motion, a fluid layer surrounding the solid particles is in laminar regime of motion since the fluid velocity should decrease to zero at the solid

surface to satisfy the no-slip boundary conditions. In this portion of space (whose extension depends on the fluid dynamics conditions of the fluid phase) a concentration gradient occurs. The mass flux across such layer (N_T) is linearly proportional to the concentration gradient, mathematically

$$N_T = k_L(C^L - C^i) \quad (2.22)$$

where k_L is the mass transfer coefficient referred to the fluid phase (the pedex "L" is used to indicate the liquid phase while "G" for the gasous one), C_L the adsorbate concentration in the liquid bulk and C^i the adsorbate concentration at the liquid-solid interface.

Pore Diffusion

Diffusion in the macro-pores can occur by several different mechanisms, the most important being: *molecular diffusion*, *Knudsen flow*, *surface diffusion*⁶ and *Poiseuille flow*. In vapour phase systems all four mechanisms may contribute and their relative importance varies widely depending on the system and the conditions. However, in liquid systems, molecular diffusion is almost always dominant. For this reason, in this work the discussion will be confined to the pore diffusion due to molecular mechanism⁷. For dilute solutions then, it is reasonable to assume that the solvent fills the material pores in which the solute diffuse. For the latter case (which is of main interest in this work) mass flux is simply described with the Fick'a law (already set for spherical coordinates).

$$N_p = - \left[D_m \frac{\varepsilon_p \vartheta}{\tau} \right] \frac{\partial C}{\partial r} = -D_p \frac{\partial C}{\partial r} \quad (2.23)$$

In Equation 2.23 the symbol D_m was used to indicates the molecular diffusion and C the concentration of the adsorbate in the liquid phase. Moreover the symbol ε_p represents the solid porosity to take into account that just a portion of the (supposed) spherical surface is available for mass transfer, ϑ is a correction factor that considers the variability of the pores section, τ is an empirical constant (which typically lies in the range $2 < \tau < 5$) called the tortuosity factor that considers the diffusion path tortuous. Englobing all those constants with the molecular diffusivity it is possible to obtain the so called "*Effective Diffusivity*" described in Equation 2.23 with the symbol D_p .

Surface Diffusion

When the molecules diffuse along the "surface" of the solid material or better they diffuse without escaping from the force fields of the pore walls, surface diffusion is taking place. This condition occurs mainly in micro-porous materials where surface diffusion is the main mass transfer mechanism: the molecules are already adsorbed on the material surface and

⁶ Surface Diffusion can occur also in macro-pores; however, its contribution is always negligible.

⁷ For further reading on the types of pore diffusion mechanism is suggested the book of Ruthven "*Principles of adsorption and adsorption processes*" [112].

hop randomly between neighbouring low energy sites. In surface diffusion the mass flux is expressed as follows:

$$N_s = -D_s \frac{\partial q}{\partial r} \quad (2.24)$$

where D_s is the surface diffusion coefficient. It is important to notice that the concentration gradient of Equation 2.24 was expressed with respect to the surface concentration as defined before in Equation 2.17.

Kinetic modelling

The dynamic model used to describe a batch adsorption system is based on differential mass balances applied to liquid and solid phases and mass transfer between the liquid and solid phases. The model is based on the following hypothesis:

- the process is isothermal;
- the batch system is perfectly mixed;
- solid particles are considered spherical with a constant radius;
- both pore and surface diffusion occur in the solid particles;
- equilibrium conditions are assumed at every point within the material (and therefore on its external surface).

Considering such hypothesis, the differential mass balance of the adsorbed compound in the liquid solution can be written as follows:

$$\frac{dC^L}{dt} = -k_L a (C^L - C^i) \quad (2.25)$$

where a is the specific surface area of the solid particles per volume of liquid. For the solid region the microscopic balance in the liquid phase takes the form:

$$\varepsilon_p \frac{\partial C}{\partial t} = -\frac{1}{r^2} \frac{\partial [Nr^2]}{\partial r} - \rho_s \frac{\partial q}{\partial t} \quad (2.26)$$

where C represents the concentration of the target compound in the liquid phase inside the solid region and ρ_s is the material apparent density⁸. The total flux (represented by the symbol N) should be the sum of the porous and the surface one as expressed below:

$$N = N_p + \rho_s N_s$$

$$N = - \left[D_p \frac{\partial C}{\partial r} + \rho_s D_s \frac{\partial q}{\partial r} \right] = - \left[D_p + \rho_s D_s \frac{\partial q}{\partial C} \right] \frac{\partial C}{\partial r} \quad (2.27)$$

Bearing in mind that as mentioned before, equilibrium conditions are assumed at every point within the material, the relation $\frac{\partial q}{\partial C}$ corresponds to the derivative of an isotherm form with respect to the concentration in the liquid phase. Accordingly, one may write the isotherm as

$$q = f(C) \quad (2.28)$$

and hence

$$\frac{\partial q}{\partial C} = f'(C) \rightarrow \partial q = f'(C) \partial C \quad (2.29)$$

substituting the preceding expression together with Equation 2.27 into Equation 2.26, one has

$$\left[\rho_s + \frac{\varepsilon_p}{f'(C)} \right] \frac{\partial q}{\partial t} = \frac{1}{r^2} \frac{\partial \left[\left(\frac{D_p}{f'(C)} + \rho_s D_s \right) \frac{\partial q}{\partial r} \cdot r^2 \right]}{\partial r} \quad (2.30)$$

$$(D_s)_e = \frac{D_p}{f'(C)} + \rho_s D_s \quad (2.31)$$

where with the symbol $(D_s)_e$ it was defined the effective surface diffusivity which is in general a function of the liquid concentration in the solid. It is important to underline that the isotherm (Equation 2.28) is required to link C^i to $q(r = R)$. It is now possible to

⁸ The apparent density is defined as the ratio between the solid mass and the total volume occupied by the solid. The latter includes the void volume due to the porous structure of the solid. For this reason, the bulk density (or apparent density) is not an intrinsic property of the material but it depends on the solid particular configuration. The apparent density is linked to the intrinsic density (ρ_l) as follows $\rho_s = \rho_l(1 - \varepsilon_p)$.

distinguish two cases depending on the choice made for the definition of the boundary conditions:

- CASE 1. The isotherm is used as an algebraic equation to link C^i to $q(r = R)$. Hence the boundary conditions are

$$\begin{aligned} \left(\frac{\partial q}{\partial r}\right)_{r=0} &= 0; \\ k_L(C^L - C^i) &= \left[\left(\frac{D_p}{f'(C)}\right)_{r=R} + \rho_s D_s\right] \left(\frac{\partial q}{\partial r}\right)_{r=R} \end{aligned} \quad (2.32)$$

- CASE 2. The isotherm is used as boundary condition to link C^i to q , hence an additional equation is needed to connect the material flux from the liquid bulk phase to the solid one. Such Equation is obtained by the macroscopic material balance given below

$$\frac{V_L}{M}(C_{in} - C) = \frac{3}{4\pi R^3} \int_0^R q(r) 4\pi r^2 dr \quad (2.33)$$

where C_{in} is the initial concentration of the target compound in the liquid phase. Then the boundary conditions can be expressed as

$$\begin{aligned} \left(\frac{\partial q}{\partial r}\right)_{r=0} &= 0; \\ q(r = R) &= f(C^i) \end{aligned} \quad (2.34)$$

To conclude, the initial conditions are also provided

$$t = 0 \quad \forall r \quad q = 0; \quad C^L = C_{in} \quad (2.35)$$

Special cases of the previous set of equations can be mentioned at this point:

- *Linear Isotherm.* When the isotherm has a linear expression ($q = KC$) from Equation 2.28 it results $f'(C) = K$. As an immediate consequence the effective solid diffusivity is no longer dependent from the concentration as shown in Equation 2.36, moreover,

defining a modified effective diffusivity $(\widetilde{D}_s)_e$ given in Equation 2.37, Equation 2.30 can be simplified in the form of Equation 2.38.

$$(D_s)_e = \frac{D_p}{K} + \rho_s D_s \quad (2.36)$$

$$(\widetilde{D}_s)_e = \frac{\left[\frac{D_p}{K} + \rho_s D_s \right]}{\left[\rho_s + \frac{\varepsilon_p}{K} \right]} \quad (2.37)$$

$$\frac{\partial q}{\partial t} = (\widetilde{D}_s)_e \frac{1}{r^2} \frac{\partial \left[\frac{\partial q}{\partial r} \cdot r^2 \right]}{\partial r} \quad (2.38)$$

- *Surface Diffusion is the rate controlling mechanism.* In this case the pore diffusion is neglected in the description of the kinetic model. For this reason, Equation 2.30 assumes the form below.

$$\frac{\partial q}{\partial t} = D_s \frac{1}{r^2} \frac{\partial \left[\frac{\partial q}{\partial r} \cdot r^2 \right]}{\partial r} \quad (2.39)$$

One of the most important kinetics models is based on such assumption: The “Homogeneous Surface Diffusion Model” (HSDM) which selects as boundary conditions the ones reported above in CASE 2. This model was developed by McKay to predict the adsorption of dyes from aqueous solutions on activated carbons [26] and on biosorbents derived from waste materials (i.e. bagasse pith [27]).

Interestingly Equation 2.38 and 2.39 have the same mathematical expression but a very different conceptual meaning.

Linear Driving Force (LDF) Approximation

In the previous section a general model for the description of an adsorption batch kinetic process was provided. As deeply explained, different types of diffusion mechanism can occur in the solid phase which lead to a complex mathematical form of the system as reported in Equation 2.30. The LDF model assumes valid the following expression for the batch mass transfer from the liquid to the solid phase:

$$\frac{dC^L}{dt} = -k_{LDF} a \cdot d \cdot (q^* - \bar{q}) \quad (2.40)$$

where k_{LDF} is the LDF mass transfer coefficient, d is the solid dosage (mass of solid/volume of liquid), q^* is the hypothetical surface concentration in equilibrium with the liquid bulk, $q^* = f(C^L)$, and \bar{q} is the volume-averaged adsorbate concentration in the solid particles.

$$\bar{q} = \frac{1}{V_s} \int_{V_s} q \cdot dV \quad (2.41)$$

The solid mass balance then results

$$\frac{d\bar{q}}{dt} = k_{LDF} a (q^* - \bar{q}) \quad (2.42)$$

The LDF mass transfer coefficient is a function of both the external and intra-particle resistance. The initial conditions are

$$\bar{q} = 0; C^L = C_{in} \quad (2.43)$$

A schematic representation of the Linear Driving Force model was given in **Figure 2-6**.

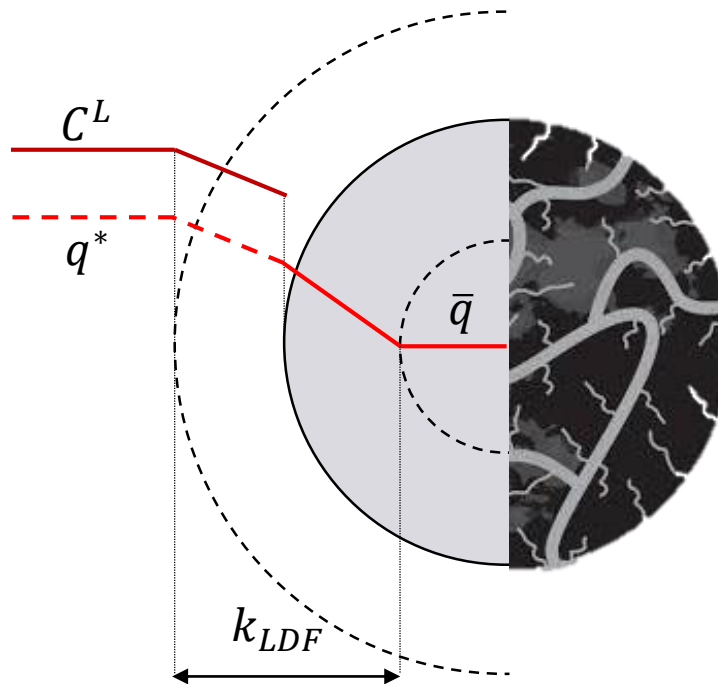


Figure 2-6 Schematic representation of the Linear Driving Force Model.

In the special case that the intra-particle resistance is the controlling one, and Equations 2.38 and 2.39 are valid, it was demonstrated a relationship between k_{LDF} and the corresponding Diffusivity coefficient [28]. In fact, Equation 2.40 is compatible with different adsorbate

concentration profiles within the particle. The parabolic concentration profile is the best known

$$q(r, t) = a(t) + b(t) \cdot r^2 \quad (2.44)$$

Then, imposing that the mass flux entering the solid particle (assumed spherical) should be the same with and without using the LDF approach

$$\left(D \frac{\partial q(r, t)}{\partial r} \right)_{r=R} = k_{LDF} (q^* - \bar{q}) \quad (2.45)$$

it results that⁹

$$k_{LDF} = \frac{5D}{R} \quad (2.46)$$

It is worth to mention that for the LDF model, when the isotherm has a linear form ($q = KC$) the system composed by Equations 2.40, 2.42 and 2.43 has an analytical solution that is provided below

$$\frac{C^L(t)}{C_{in}} = 1 - \left[\frac{d}{d + \frac{1}{K}} \right] \cdot \{1 - e^{-(k_{LDF}a)t}\} \quad (2.47)$$

2.1.5 Column kinetic modelling

In order to perform the continuous treatment of fluid effluents (both at industrial and laboratory scale), adsorption is carried out in a fixed-bed operating mode (see **Figure 2-7**). The solid adsorbent, usually in the form of porous pellets, (stationary phase) is packed into a cylindrical column and constitutes the column fixed bed. The fluid solution (mobile phase) containing the target compounds to be adsorbed, is fed at one column extremity and flows along all the column length in the void space of the column bed. The aim of an adsorption unit is to adsorb all the target compounds until their concentration goes to zero before reaching the exit of the column. During the fluid passage through the fixed bed, two main regions of the fixed bed are established:

- **Saturation region.** In this part of the column the solid is already saturated and in thermodynamic equilibrium with the inlet concentration of the adsorbed species;
- **Mass transfer zone (MTZ).** This is the area in which the mass transfer of the contaminants takes place from the fluid to the solid phase.

⁹ Considering that $\frac{\partial q(R,t)}{\partial r} = 2b(t)R$, $\bar{q} = a(t) + \frac{3}{5}R^2b(t)$ and $q^* = q(R, t) = a(t) + b(t)R^2$.

Along with time, the MTZ moves toward the length of the column and when it reaches the end it is observable as concentration profile called breakthrough curve. The moment in which the MZT shows up is called breakthrough time. Once the solid is completely saturated and no further removal of adsorbates from the fluid is possible. A sketch of the adsorption column working conditions is given in **Figure 2-7** together with a qualitative profile of a breakthrough curve.

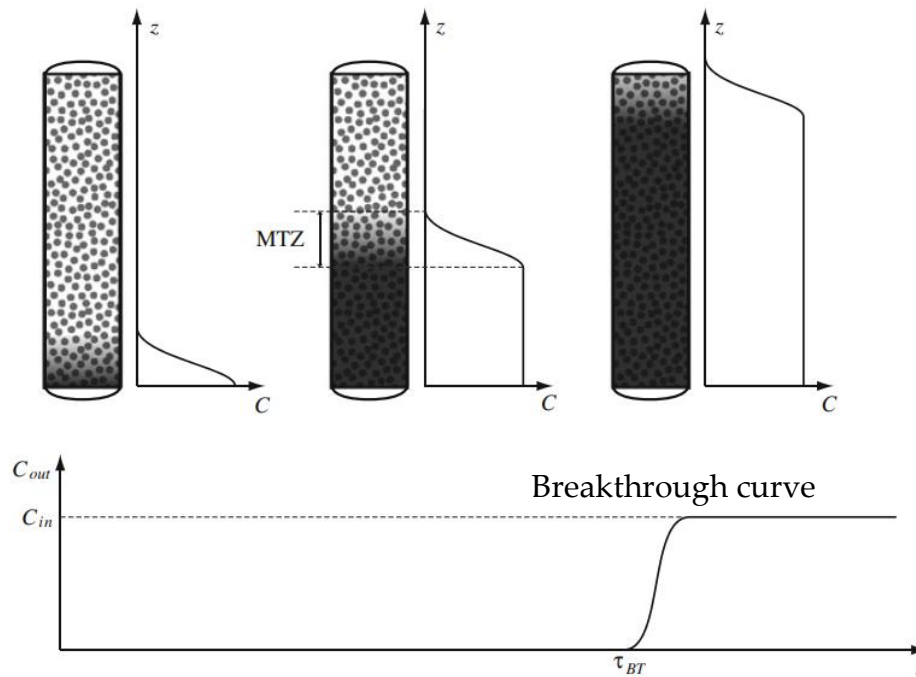


Figure 2-7 Schematic description of the typical operation cycle of a fixed-bed adsorption column. *Top* advancement of the mass transfer zone (MTZ) through the column. *Bottom* breakthrough curve [29].

The shape of the breakthrough curve provides crucial information about the fluid-dynamics and hence about the mass transfer controlling mechanism occurring in the adsorption operation. Such knowledge sets the basis for the design of an adsorption column process unit. For this reason, several mathematical models were developed in order to represent the breakthrough curve and to predict its corresponding breakthrough time. A list of the principal models developed for this scope is given in the following sections. Since all the experimental tests performed during this thesis were performed at constant temperature, thermal effects were not considered in the modelling discussion. Moreover, for the purpose of this thesis, the following discussion was limited only for diluted solid-liquid systems thus considering constant the liquid volumetric flowrate.

Ideal column

The simplest approach to an adsorption kinetic modelling is to consider that the solid is able to uptake instantaneously and avoiding losses all the target contaminants from the liquid phase. Moreover, it is assumed a plug-flow motion of the fluid phase. The partial differential

equation for a cylindrical section shown in Equation 2.48 describes the evolution of the target compound concentration during time along the column length.

$$\varepsilon \frac{\partial C}{\partial t} + \langle v \rangle \frac{\partial C}{\partial z} = -(1 - \varepsilon) \rho_s \frac{\partial q}{\partial t} \quad (2.48)$$

where ε is the bed void fraction and $\langle v \rangle$ is the superficial velocity¹⁰ (the velocity that it would exist without packing). Equation 2.48 can also be rearranged in a different form

$$\frac{\partial C}{\partial t} = - \frac{\langle v \rangle}{\left[\varepsilon + (1 - \varepsilon) \rho_s \frac{\partial q}{\partial C} \right]} \frac{\partial C}{\partial z} \quad (2.49)$$

Equation 2.49 has the same mathematical expression of a mass balance for a fluid moving in a cylindrical conduct with an average velocity equal to $w = \frac{\langle v \rangle}{\left[\varepsilon + (1 - \varepsilon) \rho_s \frac{\partial q}{\partial C} \right]}$. The term $\frac{\partial q}{\partial C}$ can be easily obtained from the isotherm function $q = f(C)$ that links C and q , thus $\frac{\partial q}{\partial C} = f'(C)$. At this point several profiles of the elution front can occur depending on the influence of the isotherm shape:

- **Ideal behaviour** - linear isotherm; $f'(C) = \frac{\partial q}{\partial C} = K$. In this case the breakthrough curve takes the shape of a step function in correspondence of the breakthrough time (τ_{BT}) which calculation is straightforward:

$$\tau_{BT} = \tau_R \left[1 + \frac{(1 - \varepsilon)}{\varepsilon} \rho_s K \right] = \tau_R + \frac{M_s}{Q} K \quad (2.50)$$

where Q is the fluid volumetric flow rate, τ_R is the fluid residence time in the column calculated as $\tau_R = \frac{L \cdot \varepsilon}{\langle v \rangle}$ and M_s is the total mass of solid in the system.

- **Compressive behaviour** - Type I isotherm according to B.E.T. classification (see section 2.1.2); in this case $f'(C)$ is high for small concentrations and low for high concentrations, thus the fluid velocity is smaller and bigger respectively. The elution front of the MTZ will therefore sharp more and more as it propagates along the column length. If the column is long enough, a constant concentration profile will establish in the MTZ moving through the column. Such condition is known as constant-pattern behaviour.
- **Dispersive behaviour** with Type III isotherm according to B.E.T. classification (see section 2.1.2); in this case the elution front of the MTZ tends to spread.

A simple sketch that reproduces the compressive and dispersive behaviour is shown in **Figure 2-8**.

¹⁰ The fluid real velocity, called interstitial velocity, is higher of the superficial one due to the presence of the backed bed which reduces the area of fluid passage. The superficial velocity is strictly related to the interstitial velocity with the expression $\langle v \rangle = \varepsilon v_i$.

Real column

In a real fixed-bed adsorption system the mass transfer is not instantaneous and a longitudinal dispersion (in contrast with the assumption of a plug-flow motion) arises due to molecular diffusion, turbulent diffusion, and the convective diffusion caused by a non-uniform velocity distribution.

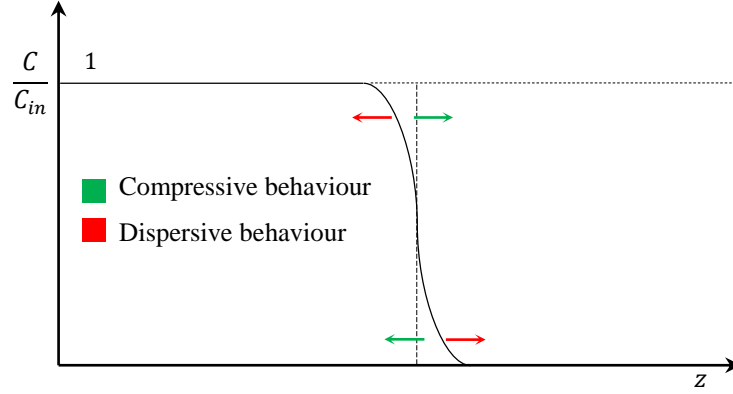


Figure 2-8 Differences between dispersive and compressive behavior.

Commonly, the most used strategy to describe the mass transfer flux is the LDF model already described in section 2.1.4. On the other hand, the “longitudinal dispersed plug flow model” or simply the “dispersion model” was widely adopted in literature to take into account the fluid-dynamic deviations from an ideal plug-flow motion. As a matter of fact, such model considers a flat velocity profile with an effective longitudinal dispersion coefficient (E_z). According to such consideration, Equation 2.48 can be rearranged as shown in Equation 2.51 and coupled with a material balance in the solid phase described by Equation 2.52.

$$\varepsilon \frac{\partial C}{\partial t} + \langle v \rangle \frac{\partial C}{\partial z} = E_z \frac{\partial^2 C}{\partial z^2} - (1 - \varepsilon) \rho_s \frac{\partial q}{\partial t} \quad (2.51)$$

$$\frac{\partial q}{\partial t} = k_{LDF} a_s (q^* - q) \quad (2.52)$$

where a_s is the specific surface area of the solid. The boundary conditions of such set of equations are

$$\left(\frac{\partial C}{\partial z} \right)_{z=L} = 0; \quad (2.53)$$

$$(C)_{z=0} = C_{in}$$

while the initial conditions are

$$\begin{aligned} C(z) &= 0; \quad 0 < z < L \\ q(z) &= 0; \quad 0 \leq z \leq L \end{aligned} \quad (2.54)$$

In order to discuss about the behaviour of an adsorption column in general terms, it is worth to express Equation 2.51 and 2.52 in a dimensionless form:

$$\frac{\partial \tilde{C}}{\partial \tilde{t}} + \frac{\partial \tilde{C}}{\partial \tilde{z}} = \frac{1}{Pé} \frac{\partial^2 \tilde{C}}{\partial \tilde{z}^2} - \frac{1}{\mu} \frac{\partial \tilde{q}}{\partial \tilde{t}} \quad (2.55)$$

$$\frac{\partial \tilde{q}}{\partial \tilde{t}} = St \left(\frac{q^*}{q(C_{in})} - \tilde{q} \right) \quad (2.56)$$

where $\tilde{C} = C/C_{in}$, $\tilde{q} = q/q(C_{in})$, $\tilde{t} = t/\tau_R$ (τ_R is the column residence time $\tau_R = \frac{L \cdot \varepsilon}{\langle v \rangle}$), $\tilde{z} = z/L$. Furthermore, $Pé$ is the Peclet number defined as $Pé = \frac{\langle v \rangle L}{E_z}$ which compares the characteristic time of convection ($\tau_c = \frac{L}{\langle v \rangle}$) with the one related to the axial dispersion ($\tau_D = \frac{L^2}{E_z}$) thus $Pé = \frac{\tau_D}{\tau_c}$; St is the Stanton number defined as the ratio between the residence time of the fluid in the column τ_R and the characteristic time of mass transfer $\tau_t = \frac{1}{k_{LDF} a_s}$ hence $St = \frac{\tau_R}{\tau_t} = \frac{k_{LDF} a_s L \varepsilon}{\langle v \rangle}$; μ is the capacity ratio, that, for a given feed, is defined as the ratio between the maximum amount of solute that can be stored in the solid and liquid phases inside the column $\mu = \frac{(1-\varepsilon)\rho_s q(C_{in})}{\varepsilon C_{in}}$. The ratio $\frac{q^*}{q(C_{in})}$ in general takes the form of the particular isotherm that represents the system. However, in many water-treatment applications the Langmuir isotherm as presented in Equation 2.20 is used. For this reason, the term $\frac{q^*}{q(C_{in})}$ was rearranged according to the Langmuir isotherm. From the definition of q^* it is easy to find that

$$\frac{q^*}{q(C_{in})} = \frac{\tilde{C}}{\lambda + (1 - \lambda)\tilde{C}} \quad (2.57)$$

where λ is called the *linearity* parameter defined as $\lambda = \frac{1/b}{1/b + C_{in}}$ that shapes the isotherm from linear ($\lambda \rightarrow 1$) to rectangular ($\lambda \rightarrow 0$). The plot of the dimensionless form of the Langmuir isotherm as a function of the *linearity* parameter is shown in **Figure 2-9**.

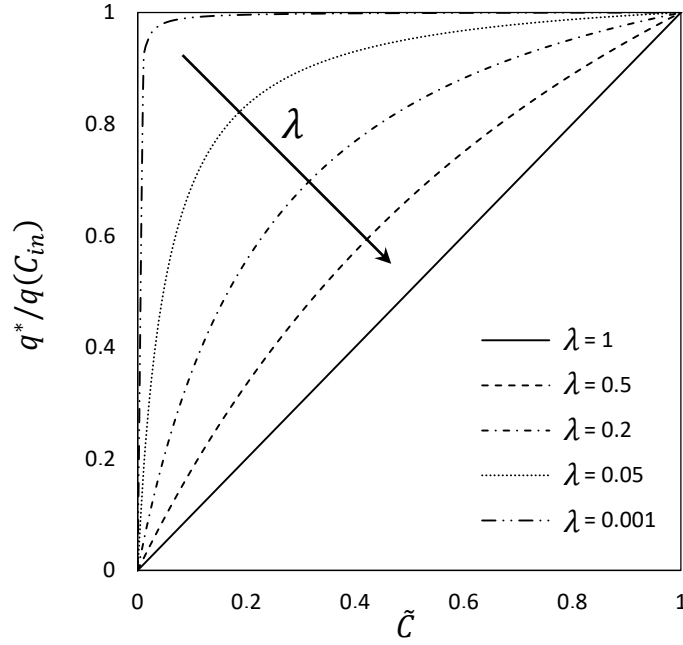


Figure 2-9 Linearity parameter of a Langmuir isotherm: relation with isotherm shape.

Introducing Equation 2.57 into Equation 2.56 it is possible to obtain the following set of dimensionless equations:

$$\frac{\partial \tilde{C}}{\partial \tilde{t}} + \frac{\partial \tilde{C}}{\partial \tilde{z}} = \frac{1}{Pé} \frac{\partial^2 \tilde{C}}{\partial \tilde{z}^2} - \frac{1}{\mu} \frac{\partial \tilde{q}}{\partial \tilde{t}} \quad (2.58)$$

$$\frac{\partial \tilde{q}}{\partial \tilde{t}} = St \left(\frac{\tilde{C}}{\lambda + (1 - \lambda)\tilde{C}} - \tilde{q} \right)$$

The boundary conditions in a dimensionless form then become

$$\left(\frac{\partial \tilde{C}}{\partial \tilde{z}} \right)_{\tilde{z}=1} = 0; \quad (2.59)$$

$$(\tilde{C})_{\tilde{z}=0} = 1$$

while the initial conditions are

$$\tilde{C}(\tilde{z}) = 0; \quad 0 < \tilde{z} < 1$$

$$\tilde{q}(\tilde{z}) = 0; \quad 0 \leq \tilde{z} \leq 1 \quad (2.60)$$

It is worth noting that the solution of Equation 2.58 depends the value of four dimensionless numbers: St , $Pé$, μ and λ .

CHAPTER III

3. Adsorbent materials for water treatment

Adsorption occurs when molecules diffusing in the fluid phase are held for a period of time by forces emanating from an adjacent surface. The solid surface represents a sharp discontinuity for the solid structure. In fact, differently of the atoms in the solid bulk, the ones at the surface have some unbalanced forces which attract molecules from the surrounding phase. These residual forces are common to all surfaces and the only reason why certain solids are classified as “adsorbents” is that they can be manufactured in a highly porous form, giving rise to a large internal surface. In those cases, the contribute of the external surface to the total surface of the solid is negligible.

In this chapter a brief introduction to the main solid adsorbents for waste water treatment was provided focus on the attention on a new class of emerging adsorbents: low-cost adsorbents from agro-waste materials.

3.1 Activated Carbons

“What is activated carbon? Activated carbon is porosity (space) enclosed by carbon atoms [30]”.

Activated carbons are porous carbonaceous adsorbents having a high adsorptive surface area that ranges between 500–1500 m²/g [31]. Commercially available activated carbons are prepared from naturally occurring carbonaceous materials such as coal, lignite, wood, peat, nut shell, coconut shell, lignin, petroleum coke and synthetic high polymers. It is mainly used in the form of powdered activated carbon (PAC) or granular activated carbon (GAC). PAC has an average dimension between 15-25 µm (passes through a sieve 0.177 mm according to ASTM D5158 standard) while GAC have sizes ranging from 0.2 to 5 mm. Both are widely used for wastewater treatment reminding that GAC has a slower adsorption rate than PAC due to a higher intra-particle resistance but at the same time GAC is easier to recover for regeneration purposes.

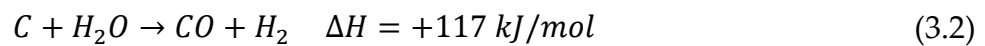
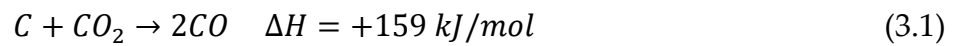
The main approaches for activate carbon preparation are:

- *Physical.* The material goes through a two-step preparation in which is firstly carbonized and secondly thermally activated;

- *Chemical.* The activation process takes place directly during the carbonization step thanks to the action of a chemical agent (H_3PO_4 , $ZnCl_2$, KOH) of which the material was previously impregnated.

3.1.1 Physical activation

Carbonization (or pyrolysis) is a heat treatment that takes place at 400-600°C in an inert atmosphere. The aim of this stage is to obtain a solid carbon matrix removing all Oxygen and Hydrogen present in the solid with the generation also of some undesirable (responsible for carbon loss) by-products such as CO_x , tar and other hydrocarbons. At this point a gasification process is carried out at 800-1000°C as an additional activation step to reach the desired porosity of the solid. For this purpose, carbon dioxide and water vapor are introduced as gasifying agents used either singly or together. In fact, such components attack the solid surface removing carbon atoms with the endothermic chemical reactions reported below which are able to create new pores inside the material structure.



Air is added as well to produce heat with the oxidation of the products of the reactions described in Equation 3.1 and 3.2 (CO and H_2). However, the presence of oxygen should be carefully managed because it could lead to an uncontrolled combustion (consumption) of the material and hence to an uncontrolled increase of temperature. It is worth to mention that at the same time some oxygen is adsorbed on the material surface forming some oxygen complexes that act as retardants (inhibitors) of the combustion reaction rate thus helping to control the gasification and subsequent porosity development.

3.1.2 Chemical activation

Chemical activation, known as wet oxidation, is commonly used for raw materials containing cellulose. The first step of activation is called the "*impregnation step*" followed by a heat treatment in neutral atmosphere. During the impregnation step the material is immersed in a liquid solution of the selected activating agent kept at 85°C. Such temperature promotes the material swelling and hence promotes the access of the chemical agent in the material pores. In an inert atmosphere lignocellulosic materials, also called biomass resources, mainly degrade at 200-350 °C [32] and the removal of heavier hydrocarbons (tar) occurs in the range 350-500°C and above 500°C. For this reason, the chemical activation is then conducted at 450-600°C. The most used activating agents are H_3PO_4 , $ZnCl_2$, KOH , K_2CO_3 , $NaOH$ which are able to interact with the solid surface and remove carbon atoms for the generation of new pores.

3.1.3 AC production and Market

The synthesis of Activated Carbons occurs in furnaces specifically designed to control the reaction of combustion and the pores development. The main reactor used is the rotary kiln which guarantees a major residence time with respect to other reactor configurations such as fluidized bed or a multiple-hearth furnace [30]. The rotary kiln has two main configurations: Direct-fired kilns (**Figure 3-1 a**) in which the gas combustion occurs inside the furnace; indirect-fired kilns (**Figure 3-1 b**) in which the furnace is isolated from the heat source.

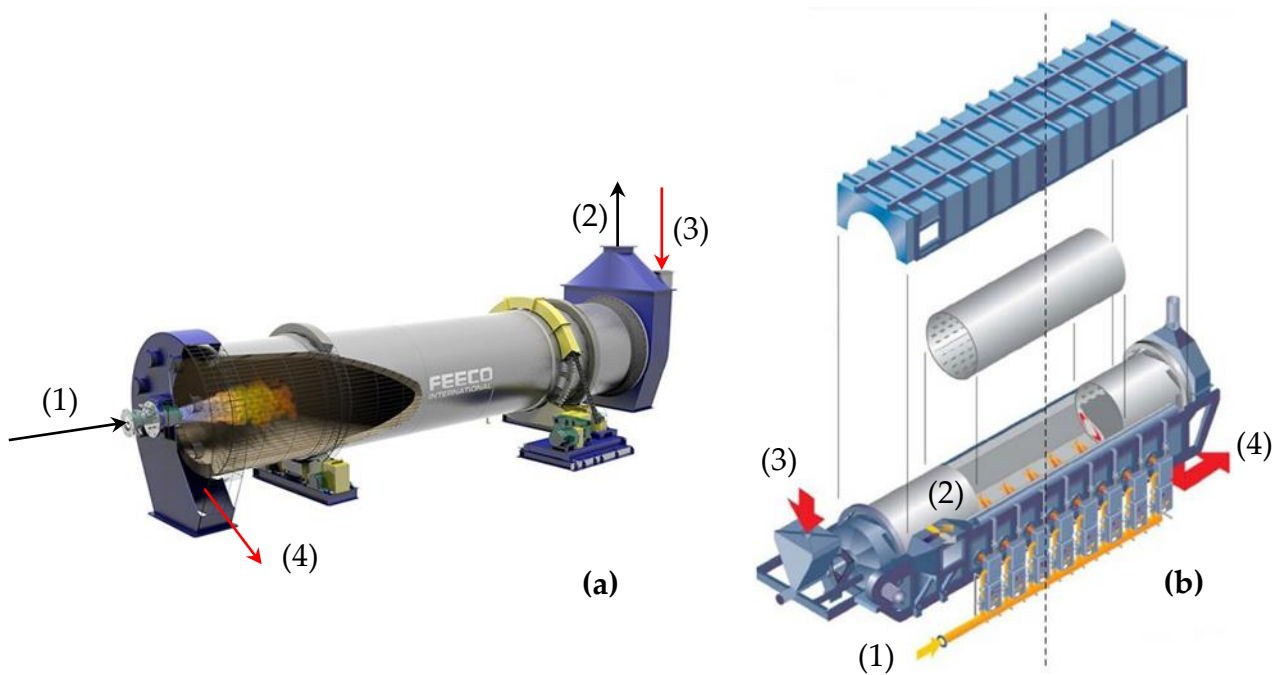


Figure 3-1 Direct-fired rotary kiln (a); Indirect-fired rotary kiln (b). Configuration: air, steam and CO₂ inlet (1); Gas exit (2) for the indirect configuration are just the gas resulting from the combustion of a fuel while for the direct one are included the product of activation (mainly H₂, CO); Char inlet (3); Activated carbon exit (4).

The global activated carbon market is estimated to be USD 5.7 billion in 2021 and is projected to reach USD 8.9 billion by 2026, at a CAGR of 9.3% from 2021 to 2026¹¹. The production of AC is expected to grow related to the need of improving air and water quality mainly for reducing CO₂ emissions and for freshwater availability. In 2020, the average activated carbon import price amounted to 2.3 \$/kg¹².

¹¹ <https://www.marketsandmarkets.com/Market-Reports/activated-carbon-362.html>

¹² <https://www.globenewswire.com/en/news-release/2021/12/16/2353239/0/en/Global-Activated-Carbon-Market-Rising-Demand-for-Water-Purification-Drives-U-S-Trade-IndexBox.html#:~:text=In%202020%2C%20the%20average%20activated,amongst%20the%20major%20supplying%20countries.>

3.2 Zeolites

Zeolites or “*molecular sieves*” are crystalline aluminosilicates formed by the union of SiO_4 and AlO_4 -type tetrahedrons. The basic structure of Zeolites can be described by the generic formula

$$M_x(\text{AlO}_2)_x(\text{SiO}_2)_y \cdot c\text{H}_2\text{O} \quad (3.3)$$

where $x \leq y$ and M represents the compensation cation (Na^+ , K^+ , Li^+ , Ca^{2+} , Mg^{2+} ecc.) which balances the negative charge introduced by every Al atom. The zeolitic structure can be thought of as an assemblage of polyhedral units made of several SiO_4 and AlO_4 tetrahedral on which the catalytic/adsorption active sites are available. Moreover, specific cavities or “*windows*” define the effective diameter of the zeolite pores and determine the access to the crystalline structure only to selected molecules. The specific surface area of zeolites lies in the range of 200-600 m^2/g . According to the different molecular structure, it is possible to distinguish three groups of zeolites: *sodalite*, *mordenite*, *chabazite*. The most used zeolites in the field of adsorption (and catalysis) belong to the sodalite group in which is worth to mention the zeolite A and the *faujasite*-type zeolites (e.g. zeolite X and Y). A sketch of a Zeolite A and and faujasite-type zeolites X and Y was provided in **Figure 3-2**.

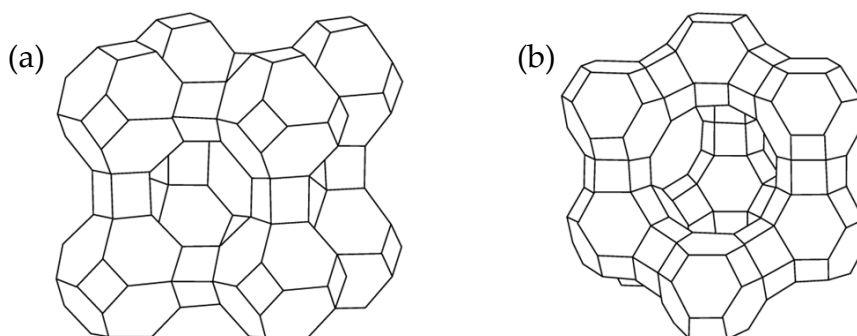


Figure 3-2 Zeolite A (a) and faujasite-type zeolites X and Y (b) formed by sodalite cages.

3.2.1 Zeolite synthesis

The synthesis of zeolites can occur both in solid or liquid state. The second choice is often preferred because it is faster, requires lower operating temperatures (80-150°C) with respect to the first one that occurs at around 300°C and, hence, it is least costly [33]. This procedure is known with the general term *Solvothermal synthetic method* which indicates that the zeolite synthesis is occurring in a liquid solvent. Several researches reported a successful synthesis of zeolite using different solvents such as alcohols (e.g., methanol, ethanol, pentanol), ethylene glycol, hydrocarbons and pyridine [34]. Moreover, when ionic solvents (ionic liquids) are adopted this term is assigned as *ionothermal*, while when water is employed as solvent it takes the name of *hydrothermal*. The Hydrothermal Method (HM) is considered

one of the least costly for zeolite synthesis [33] and hence it is one of the most used. It consists of three steps which are schematically reported in **Figure 3-3** and explained below:

1. **Crystallization.** A water solution of silicon and aluminum sources together with mineralizing agents such as OH⁻ and F⁻, metal cations, and structure-directing agent (usually an organic surfactant)[35] is prepared and placed into an autoclave reactor. The reaction (crystallization) takes place at a temperature range of 80-150°C at autogenous pressures up to 15 bar [36].
2. **Filtering step.** The reaction product is filtered and washed several times in order to collect the solid and remove from its surface the residual reagents.
3. **Drying step.** The material is oven dried.

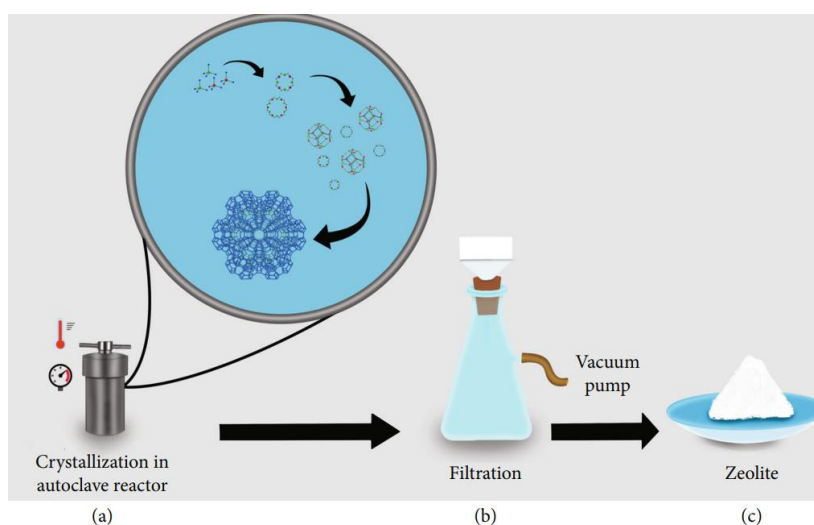


Figure 3-3 Hydrothermal synthesis process. The crystallization occurs in an autoclave (a). Then, the product is filtered and oven dried (b). The remaining solid is the zeolite (c) [33].

3.2.2 Zeolites production and Market

The global zeolite market size was \$4,326.2 million in 2019 and is projected to reach \$6,190.0 million by 2027, exhibiting a CAGR of 4.7% in forecast period¹³. The price of synthetic zeolites is subjected to big differences according to the specific type of zeolite considered. According to wastewater treatment purposes, it is worth to highlight the prices of zeolite 3A and 13X 1.15-1.35 \$/kg¹⁴.

¹³ <https://www.fortunebusinessinsights.com/industry-reports/zeolite-market-101921>

¹⁴ https://www.made-in-china.com/products-search/hot-china-products/Zeolite_Price.html

3.3 Low-cost agro-waste adsorbents

Low-cost adsorbents are mainly waste materials used without, or with a little, pre-treatment. In this section will be briefly introduced the waste materials that have been studied in this thesis as bio-adsorbents.

3.3.1 Yerba Mate Tea

Yerba Mate (*Ilex paraguariensis*), shown in **Figure 3-4**, is a tea-like produced in South America countries, nowadays 280000 tons per year represents the domestic production in Argentina [37] and an increase of its consumption will be expected [38]. The global Yerba Mate market size is expected to gain market growth in the forecast period of 2020 to 2025, with a CAGR of 4.3% and will be expected to reach USD 1807.9 million by 2025, from USD 1527.3 million in 2019¹⁵. The tea called “mate” is prepared by infusion of mate leaves and this extract is rich in polyphenols, xanthines, alkaloids, flavonoids, vitamins and minerals [39,40]. The potential benefits of this material can also be found in its waste. The extract can be used as reducing agent for the green synthesis of nanoparticles [38] or the re-use of solid residue for the production of materials for thermal insulation purposes [41]. The solid is a prominent material for adsorption processes: activated carbon can be produced from Yerba Mate (YM) due to the presence of oxygenated acid groups which make it ideal for phenols adsorption [42] and the presence of several functional groups suggested its possible application also for the adsorption of dyes without pre-treatment [43].



Figure 3-4 Yerba mate plant and Tea.

3.3.2 Aloe Vera

Aloe vera (*Aloe Barbadensis* Miller) is a perennial, drought-resistant succulent herb, called the healing plant or the silent healer because of its wound and burn healing properties. The *Aloe* leaf consists of three layers as shown in **Figure 3-5** i.e. Gel (inner layer), Latex (middle layer) and Rind (outer layer) [44]. The Gel is made of 99 % water, amino acids, lipids, sterols,

¹⁵ www.marketstudyreport.com/reports/global-yerba-mate-market-2020-by-manufacturers-regions-type-and-application-forecast-to-2025?gclid=CjwKCAjwIbr8BRA0EiwAnt4MTv2K-HnnJfjwPpbt6xsvI4FfRPjETD3z9YHix_He04fE5XaQH_pP4RoCJloQAvD_BwE

vitamins and polysaccharides (such as glucomannans) to whom are associated most of the health benefits of *Aloe* [45]. For this reason, the industrial interest is mainly focused in collecting the *Aloe vera* Gel rejecting both Latex and Rind (schematically represented in **Figure 3-5**) producing 400 kg of solid waste per month in local agroindustry of Yucatàn and Mexico [46]. The global *Aloe Vera* market size reached a value of almost USD 602 million in the year 2020. The market is further expected to grow at a CAGR of 8.5% between 2021 and 2026 to reach a value of almost USD 982.4 million by 2026¹⁶. According to the amount of *Aloe Vera* involved in industrial processes and hence the amount of waste produced accordingly, *Aloe Vera* rind was tested as a bio-adsorbent material.

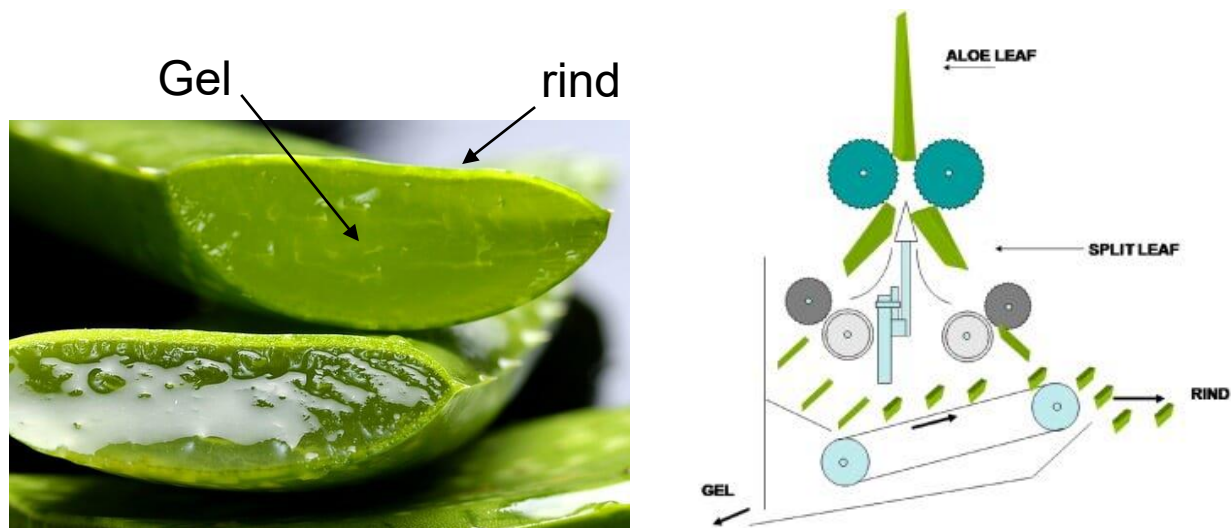


Figure 3-5 Focus on the *Aloe Vera* structure (left); example of an industrial rind and gel separation unit.

3.3.3 *Pteris vittata* Fern

Pteris vittata (PV) is an herbaceous fern with tropical and subtropical distribution. Several researches documented the ability of PV to uptake large amounts of Arsenic (As) (up to 23.000 mg/kg) from soil [47], which is mainly accumulated in fronds [48,49]. Interestingly, several studies reported that PV can grow in hydroponic culture systems as documented in **Figure 3-6**, showing a fully developed root apparatus and an efficient uptake of As from contaminated water [50,51]. In addition, it was shown that PV can be reused in multiple phytofiltration cycles and that, when introduced in non-contaminated water, there is no release of any As previously accumulated [52], highlighting the sustainability of this approach.

¹⁶ <https://www.expertmarketresearch.com/reports/aloe-vera-market#:~:text=Global%20Aloe%20Vera%20Market%20Outlook%20The%20global%20aloe,value%20of%20al most%20USD%20982.4%20million%20by%202026>.

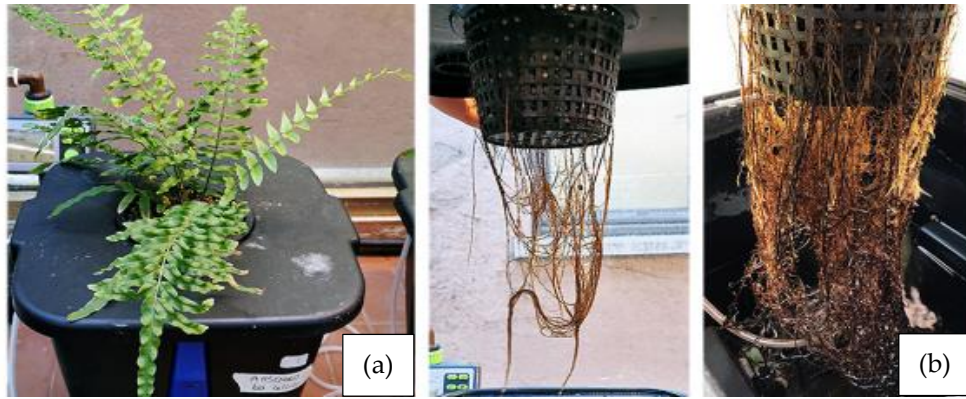


Figure 3-6 *Pteris Vittata* fern hydroponic culture with a focus on fronds (a) and roots (b) [52].

3.4 Material Analysis

In this section will be explained the principle of a material analysis technique that was deeply used in the experimental work of this thesis (that is also based on the phenomenon of adsorption): the BET analysis.

3.4.1 BET analysis

The BET analysis was developed as a technique to measure the Specific Surface Area (*SSA*) of a solid. Such method is based on the experimental evaluation of the adsorption isotherms of gases that approximate a perfect gas law behavior (to simplify the calculation of the volume from pressure measurements) such as nitrogen, argon or krypton. Then, the data collected are fitted with the linearized form of the B.E.T isotherm expression provided in Equation 2.12 to calculate the gas volume adsorbed on a monomolecular layer (V_m) per unit mass of solid adsorbent. The relationship between V_m and *SSA*, is simply the area of each adsorbate molecule on the surface multiplied by the total number of molecules in the monolayer capacity

$$SSA = \frac{V_m \rho_L N_A \Omega_A}{PM} \quad (3.4)$$

where ρ_L is the liquid density of the adsorbed compound (since physical gas adsorption is similar to a condensation phenomenon), N_A is the Avogadro number, PM is the molecular weight of the adsorbed compound and Ω_A is the area occupied by a single molecule. Ω_A can be determined by the assumption that each molecule of adsorbate occupies a hexagonal close-packed system in which each molecule has twelve nearest neighbors. This gives:

$$\Omega_A = 1.091 \left(\frac{PM}{\rho_L N_A} \right)^{2/3} \quad (3.5)$$

where 1.091 is the packing factor for hexagonal close packing. In **Table 3-1** are reported the temperatures and the suggested values for the cross sectional area for the most commonly used compounds in BET analysis.

Table 3-1 Commonly adopted compounds for BET analysis together with their isotherm temperature and cross-sectional area[53].

Compound	<i>T</i> , K	Ω_A , Å
<i>N</i> ₂	77	16.2
<i>Ar</i>	77	13.8
<i>Kr</i>	77	20.2
<i>n</i> - <i>C</i> ₄ <i>H</i> ₁₀	273	44.4
<i>C</i> ₆ <i>H</i> ₆	293	43.0

CHAPTER IV

4. Yerba Mate (*Ilex paraguarensis*) as Bio-Adsorbent for the Removal of Methylene Blue, Remazol Brilliant Blue and Chromium Hexavalent: Thermodynamic and Kinetic Studies

In this chapter it was investigated the use of YM solid waste on adsorption of Cr(VI) and dyes pigments. In particular, Methylene blue (MB) and Remazol Brilliant Blue (RBB) were used as cationic and anionic dyes respectively. Adsorption tests were performed at different pH condition (from 3 to 10), different temperature (from 283 K to 313 K) and different dosage of YM and concentration of pollutants. Scanning Electron Microscopy (FE-SEM), Fourier Transform Infrared Spectroscopy (FT-IR), BET and X-Ray diffraction (XRD) analysis were done to offer a complete characterization of the adopted material. Good results in term of MB removal (up to 80%) were observed while low Cr(VI) removal and limited RBB adsorption rate were recorded although at low condition of temperatures and pH ideal for the adsorption of the anionic species. This critical aspect was overcome by proposing a calcination step as pre-treatment. The content of the chapter was taken from its corresponding publication of Mazzeo et al. [54].

Materials and Methods

4.1 Materials preparation and characterization

4.1.1 Bio-adsorbent preparation

The Yerba Mate (YM) waste was obtained as residue of the beverage production. The waste was washed for 5 times in boiled demineralized water, dried in oven at 333 K and chopped with a twin-function mill. A standard stainless-steel sieve system was used for the solid particles separation and the particles with a diameter in the range of 1.19-2.00 mm were tested as bio-adsorbent.

Additional tests were carried out by using Calcinated Yerba Mate (CYM) [55] to evaluate a possible activation effect of waste on the adsorption of anionic species. The calcinated material was produced by treating the selected solid fraction in a muffle furnace at 600 °C for 1 h.

4.1.2 Chemicals

Methylene blue ($C_{16}H_{18}ClN_3S$; MB), remazol brilliant blue ($C_{22}H_{16}N_2Na_2O_{11}S_3$; RBB), potassium dichromate ($K_2Cr_2O_7$), 1,5- diphenylcarbazide ($C_{13}H_{14}N_4O$), hydrochloric acid (HCl) and sodium hydroxide (NaOH) were purchased from Sigma Aldrich (United States). All chemicals were of analytical reagent grade and used without any further purification. The solutions used in the experimental tests were prepared by providing a dilution in ultrapure water.

4.1.3 Analysis

A morphological investigation of YM and CYM was performed using a field-emission scanning electron microscope (HR-FESEM AURIGA, Zeiss, Germany). The samples were prior sputter-coated with 10 nm thin layer of chromium using a Quorumteach Q150T sputter coater.

The functional groups on the surface of the samples were detected by a Fourier-transform infrared (FT-IR) spectroscopy. Infrared measurements were carried out with a Bruker Vertex 70 spectrometer (Bruker Optik GmbH, Germany) equipped with a single reflection Diamond ATR cell. Spectra were recorded with a 3 cm^{-1} spectral resolution in the mid infrared range ($400\text{--}4000\text{ cm}^{-1}$) using 512 scans. Yerba Mate samples were ground, quartered and run in triplicate.

The specific surface area (SSA) was measured by N_2 adsorption-desorption isotherms acquired at 77 K using a Micromeritics 3Flex analyser (Micromeritics Instrument Corp., USA). The adsorption-desorption isotherms were acquired in the p/p^0 range from 0.01 to 0.99. Samples were previously outgassed at 423 K for 3 h. The BET (Brunauer-Emmett-Teller) and BJH (Barrett-Joyner-Halenda) equations were used to determine the specific surface area, pore volume and average pore diameter, respectively [56]. A detailed explanation of the method was provided in section 3.4.1.

Zero charge point (pH_{PZC}) was determined according to the pH drift method [57]. 0.5 g of YM were added to 50 mL of ultra-pure water. Before the solid addition, the pH of solution was adjusted from 2 to 12 by the addition of HCl (0.1 M) and NaOH (0.1 M). The suspension was placed on orbital shaker for 24 h to reach the equilibrium condition. After that, the final pH was measured and the pH_{PZC} was determined as point where the final pH is equal to the initial pH of the solution. The pH measurement was performed by using a Crison GLP 421 pH meter (Crison, Spain).

The adsorption of dyes was measured by spectrophotometric analysis using a PG Instruments (United States) T80+ UV/Vis spectrophotometer (with glass cells of 1 cm path length) at $\lambda = 674\text{ nm}$ (MB) and $\lambda = 591\text{ nm}$ (RBB). The spectrophotometer analysis was adopted also for the Cr(VI) adsorption tests by colorimetric method using 1,5-diphenylcarbazide [58].

4.1.4 YM Characterization

The infrared spectra of samples of neat YM waste shown in **Figure 4-1** exhibits the characteristic bands of a lignocellulosic material. A detailed assignment of the main bands in Yerba Mate waste spectra is reported elsewhere [59]. Upon calcination the complete removal of main bands related to hemicellulose (1732 , 1238 and 591 cm^{-1}), cellulose (1422 , 1318 , 1107 , 664 and 559 cm^{-1}), xanthines (1644 cm^{-1}) and lignin (1594 , 1504 and 1455 cm^{-1}) components, initially present in the YM residue was assessed.

The extremely sharp band at 3642 cm^{-1} in CYM could be ascribed to OH stretching which may arise to keeping of some hydroxides, such as $\text{Ca}(\text{OH})_2$, $\text{Mg}(\text{OH})_2$, Si-OH etc. The absorption bands at 1457 and 870 cm^{-1} are assigned to different vibration modes C-O of carbonate groups CO_3^{2-} . The other bands at 1399 , 1112 and 1050 cm^{-1} are attributed to C-H, C-O-H (OH deformations of carboxyl-C) and C-O (alkyl/aryl ethers), respectively [60].

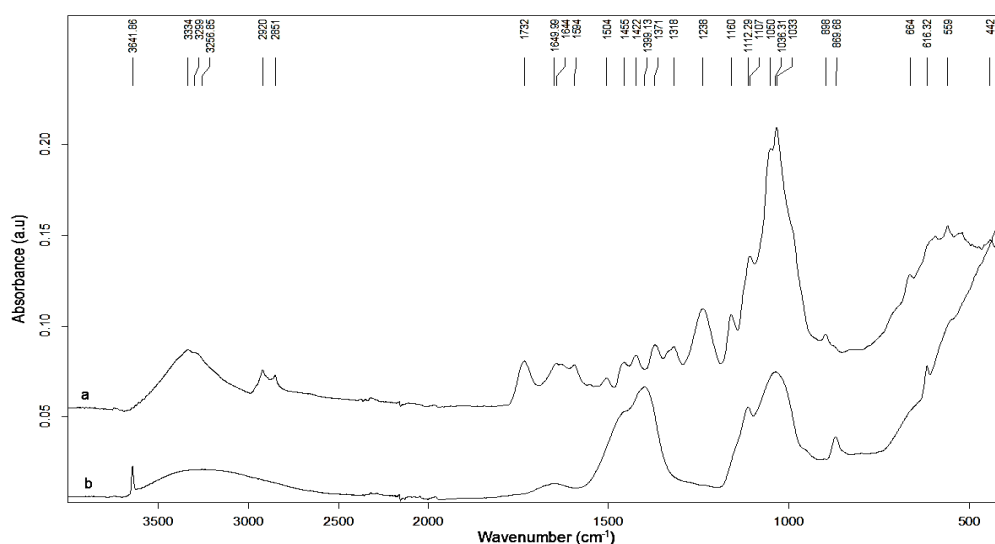


Figure 4-1. Infrared spectra of the YM (a) and CYM (b) samples [54].

In the FE-SEM micrographs of YM showed in **Figure 4-2** a-b a coarse surface topography with a large number of pores can be observed. This morphology could provide a greater dye adsorption capacity of the dye by such bio-adsorbent due to the capture of contaminants in its irregular internal surface area. The internal structure of the Calcinated YM (CYM) was different and a fibrous aspect (**Figure 4-2** c) with a large prismatic hexagonal crystal of calcium hydroxide (**Figure 4-2** d) can be clearly detected.

The the specific surface (BET SSA) showed an important increase by 1.08 ± 0.02 m^2g^{-1} to 13.84 ± 0.06 m^2g^{-1} when the YM samples were thermally treated (**Table 4-1**). This result supports the employment of that material as an adsorbent in the treatment of refractory organic pollutants such as dyes. Similar values of YM specific surface were found in [43].

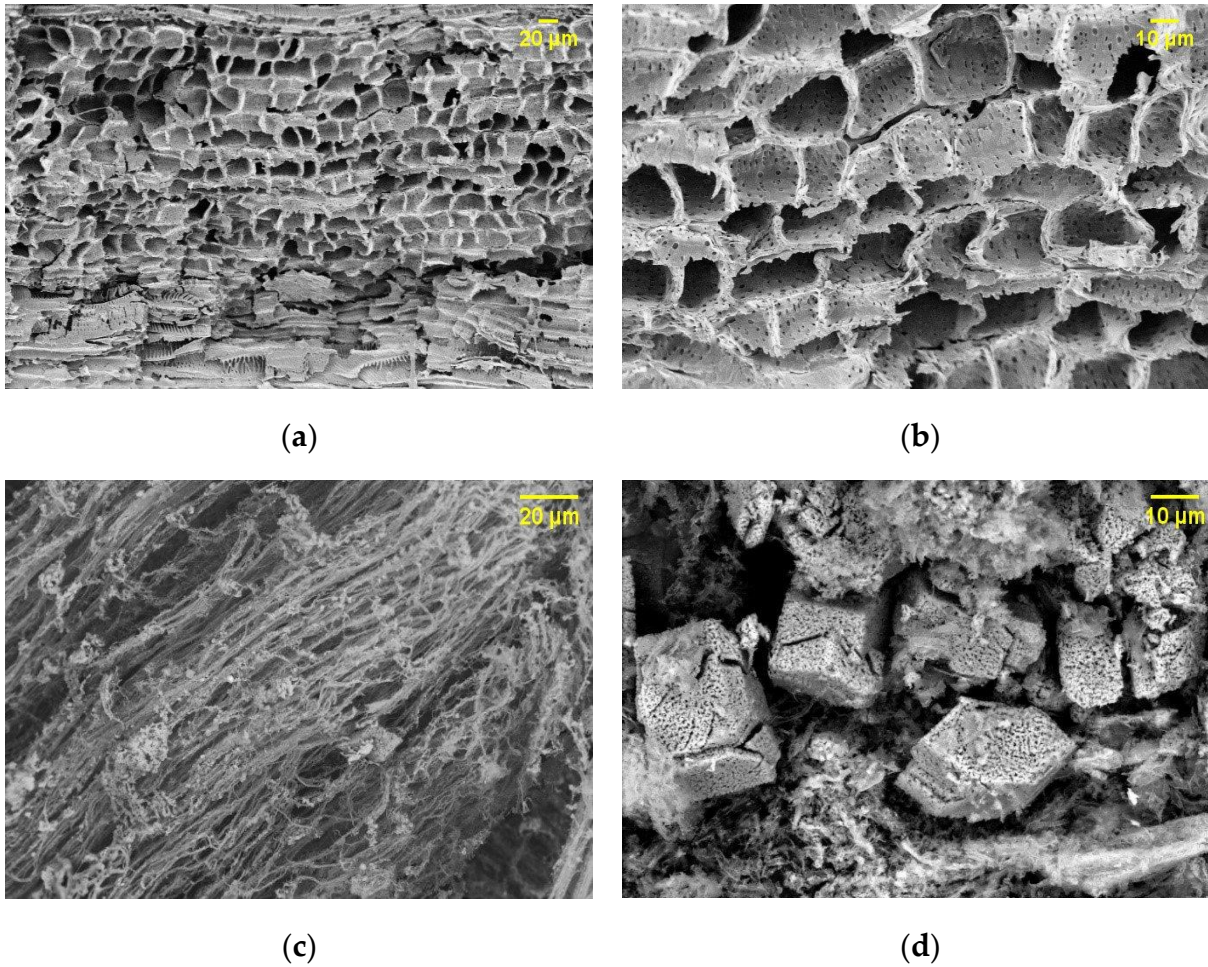


Figure 4-2. FE-SEM micrographs of the YM (a-b) and CYM (c-d) samples [54].

Table 4-1. Specific surface area (SSA) of YM samples.

Sample	Surface area [m ² /g]	Pore volume [cm ³ /g] (x 10 ⁻³)	Average pore diameter [Å]
YM	1.08	0.48	17.85
CYM	13.84	59	183.39

From the data displayed in **Figure 4-3**, pH_{PZC} of YM was estimated equal to be 6.52. At pH conditions lower than pH_{PZC} the presence of positive charge on YM surface could promote the adsorption of anionic species, whilst, due to the absence of any protonation, for pH condition higher than pH_{PZC} the adsorption of cationic species will be promoted [61].

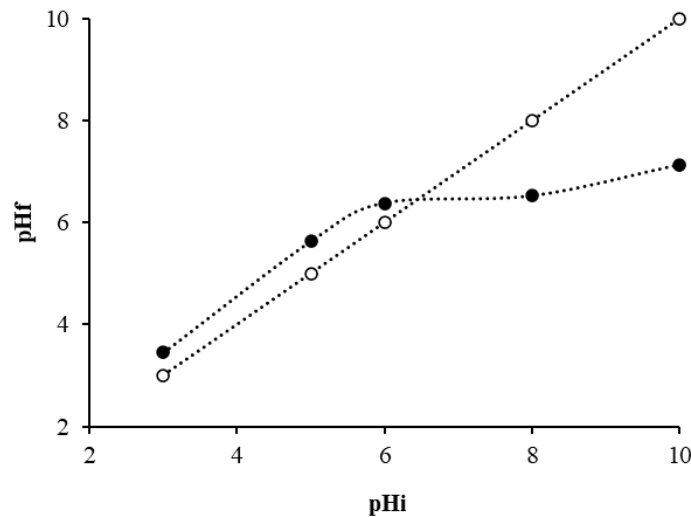


Figure 4-3. Zero Charge point (pHpzc) of YM, determined by the pH drift method. The Zero Charge point is represented by the intersection of the two curves: the black dotted (●) curve shows the final pH (pHf) of the suspension respect to the initial one (pHi); the white dotted curve (○) represents the condition pHi=pHf [54].

4.2 Adsorption tests

Preliminary tests as investigation of the adsorption efficiency of both dyes and Cr(VI) were performed at different pH condition by mixing 0.2 g of bio-adsorbent (YM or CYM) in 50 mL with a pollutant concentration of 20 mg/L. The solutions were stirred in an orbital shaker until equilibrium (72 h) at 298 K. The percentage of the pollutant i removed (E_i) was calculated with the following equation:

$$E_i\% = \left(\frac{C_i^{in} - C_{i,e}}{C_i^{in}} \right) \times 100 \quad (4.1)$$

where C_i^{in} is the concentration (mg/L) of the pollutant at the beginning of the test and $C_{i,e}$ is the concentration of the pollutant at the equilibrium (mg/L). Using YM, surprisingly, no adsorption effect of RBB and Cr(VI) was observed, while a removal of MB of 81.85 %, 71.58 %, 74.36 % and 72.90 % at pH=10, pH=8, pH=6 and pH=4 was calculated, respectively. These results are quite different from those observed by Aldbadarin and co-workers where a removal of an anionic dye (Orange II sodium salt) and MB was successfully obtained in different pH conditions (2.04 and 8.98, respectively) thanks to the presence of different functional groups on the fraction of YM used [43]. The discussion on the adsorption process of the anionic species will be reported later. Although there is no significant effect of pH, the dosage of adsorbent material plays a key role in the adsorption process. In attempt to define the best operative condition of MB adsorption process, tests at different YM dosage were performed at 298 K with 50 mL of MB solution (20 mg/L). After 72 h, the MB residue concentration was measured and the results are reported in **Figure 4-4**. An initial growing trend was observed with the increase of YM dosage up to 1.6 g/L, where a slowdown in the process was observed. Beyond this value, a further increase in the dosage of solid did not

contribute significantly to MB removal, that reached a value of 80%. At low dosages of YM, the availability of active sites for the adsorption was the limiting factor, while at dosage higher than 1.6 g/L the efficiency of the process was controlled by the mass transfer of MB diffusion onto YM [62].

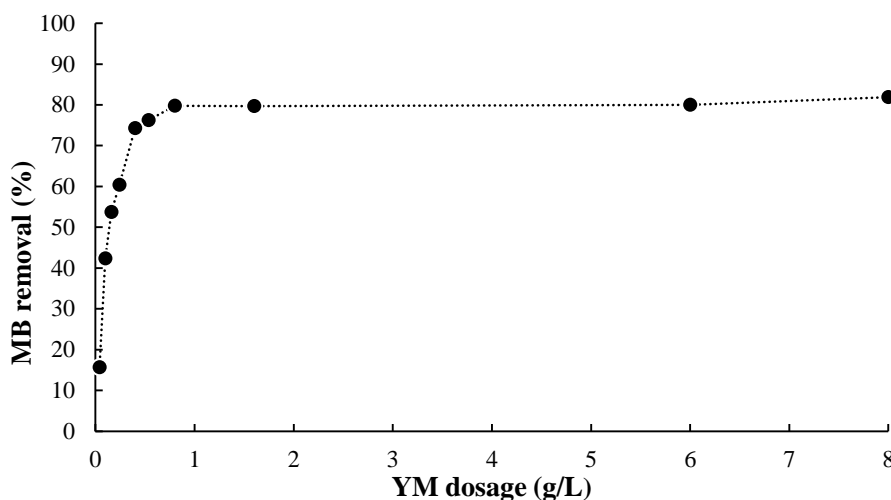


Figure 4-4. MB adsorption removal efficiency after 72h of equilibrium tests at different YM dosage. Conditions: 20 mg/L of MB, 50 mL of volume, pH=6 and 25 °C [54].

The reusability of the YM was investigated by performing desorption cycle in 0.1 M of HCl solution according to other authors [18]. After 24 h of desorption cycle, the solid was washed several times, then dried and re-used in adsorption test with 0.5 g of YM in 50 mL of MB solution (20 mg/L) at room condition (298 K) and pH=6. In such condition a removal of 58% and 41% were reached after the first and the second pre-treatment cycle, respectively, compared to a removal of 64% obtained with the first use of YM. This result highlighted that after the second regeneration cycle a significant decrease of the MB removal of about 36% was calculated demonstrating that further evaluations on type of pretreatment and removal efficiency are required if the reuse of the material is necessary for over to three times.

4.3 MB adsorption batch tests using YM

4.3.1 Isotherm and thermodynamic studies

A solution of 50 mL of MB with 4 g/L of YM was placed in a 100 mL conical flask and shaken for 72 h. The concentrations of MB ranged from 20-350 mg/L and the temperature was fixed at 298 K. The suspension was centrifuged and the supernatant was analyzed for the detection of MB concentration. To determine the equilibrium adsorption capacity of YM, the equilibrium concentration of MB, were compared to Langmuir (Equation 2.20) and Freundlich (Equation 2.21) isotherm models already expressed in section 2.1.3. The surface concentration at equilibrium q_e (mg/L) was calculated using Equation 2.19 here reported again for completeness:

$$q_e = \frac{V}{M_S} (C_{MB}^{in} - C_e) \quad (4.2)$$

where V (mL) is the liquid volume, M_S (g) is the mass of the adsorbent material, C_{MB}^{in} (mg/L) is the initial concentration of MB and C_e (mg/L) is the MB concentration at equilibrium.

The standard free energy change ΔG° (kJ/mol) at 298 K was then calculated with Equation 2.11 opportunely adjusted as shown below:

$$-\frac{\Delta G^\circ}{RT} = \ln[b \cdot PM \cdot 10^3] \quad (4.3)$$

where R (8.314 J/mol K) is the universal gas constant, T (K) is the absolute temperature and PM (g/mol) is the molecular weight of the adsorbed compound.

4.3.2 Kinetic studies

The kinetic batch tests were performed in 100 mL conical flask with 50 mL of MB solution at pH 6 shaken for 4 h (time enough to reach the equilibrium) in an oscillator system. During the tests the suspension was centrifuged and the supernatant was analyzed for the detection of MB concentration. Adsorption tests were performed at different bio-adsorbent dosage and pollutant concentration in a fixed ratio R as outlined by Equation 4.4

$$R = d/C_{MB}^{in} \quad (4.4)$$

where d is the bio-adsorbent concentration (g/L) and C_{MB}^{in} is the concentration (mg/L) of MB at the beginning of the test. The adsorption process was studied at different R by varying the operative temperature (283 K, 293 K and 313 K). More precisely, for each temperature, the parameter R was varied changing the bio-adsorbent dosage while keeping constant the starting concentration of MB. **Table 4-2** reports all the concentrations of bio-adsorbent adopted for each temperature.

Table 4-2. Bio-adsorbent concentrations in batch tests

R [mg/mg]	d [g/L]		
	283 K	293 K	313 K
100	2.6	2.4	2.5
200	5.3	4.8	5.1
300	7.9	7.3	7.7

The system was analyzed by means of the Linear Driving Force (LDF) model provided in section 2.1.4. with the assumption (later verified) of a linear isotherm which leads to the analytical expression of Equation 2.47 here reported for completeness.

$$\frac{C_{MB}(t)}{C_{MB}^{in}} = 1 - \left[\frac{d}{d + \frac{1}{bq_{max}}} \right] \cdot \{1 - e^{-(k_{LDF}a)t}\} \quad (4.5)$$

A non-linear regression, based on the minimization of the mean square error, was performed for the determination of the parameters bq_{max} and $k_{LDF}a$ for each test. It is important to underline that the Specific surface area a is dependent from the solid concentration (d) and hence from the parameter R as follows:

$$a = \frac{3}{\rho_s R_s} d = \frac{3 C_{MB}^{in}}{\rho_s R_s} R \quad (4.6)$$

where ρ_s is the material density (g/L) and R_s is the radius of the solid sphere. Thus, the parameter $k_{LDF}a$ is expected to be linearly dependent respect to the solid concentration and R . Additional tests at $R=200$ and $R=400$, both at 298 K, with a solid concentration of 3.54 and 7.08 g/L respectively, were carried out to validate the model.

Results and discussion

4.4 Isotherm and Thermodynamic studies

In order to compare Yerba Mate with other types of bio-adsorbents, isotherm data at 298 K were collected: Langmuir and Freundlich constants, derived from fitting, were used to quantify the maximum adsorption capacity of YM. The experimental results reported are a mean value of at least three repetitions and are plotted in **Figure 4-5** together with the Langmuir and Freundlich isotherms. The mean square error obtained from isotherms fitting was 9.3 for Langmuir and 15.6 for Freundlich. According on such consideration and, since the experimental data in **Figure 4-5** show a saturation behavior typical of the Langmuir isotherm, it is clear that the Langmuir isotherm gives a better representation of the system.

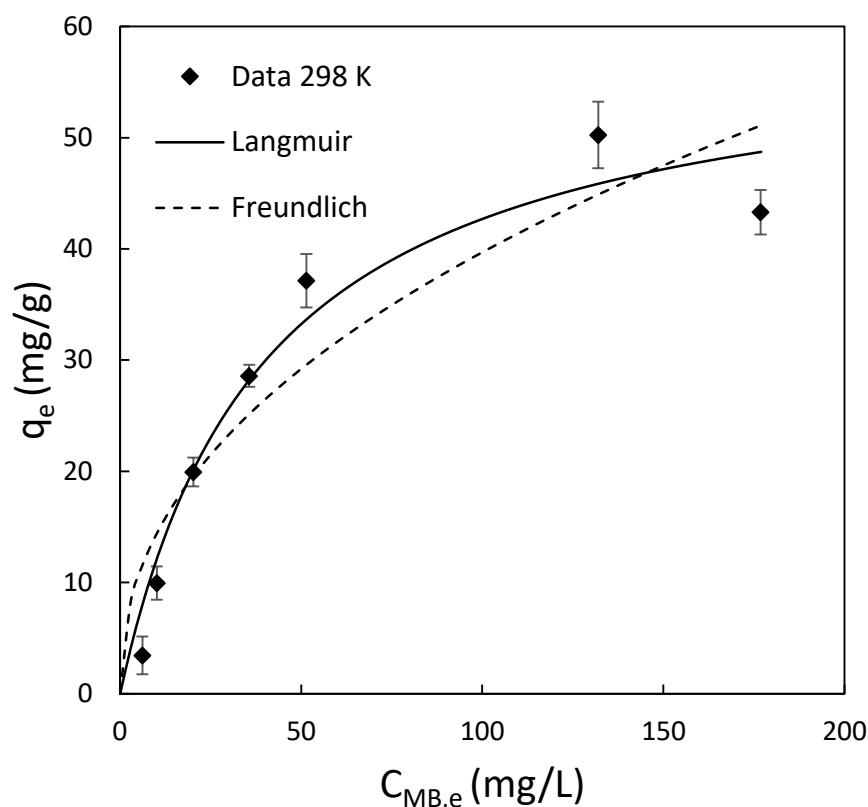


Figure 4-5. Langmuir and Freundlich Isotherms obtained by a non-linear fitting of the adsorption data of MB using Yerba Mate at 298 K. The error bars represent the standard deviation [54].

The Langmuir and Freundlich constants obtained are reported in **Table 4-3** where they are compared with the same parameters calculated for other bio-adsorbent materials reported elsewhere. The comparison shows that YM has a higher adsorption capacity (q_{max}) than many other bio-adsorbents such as Chaff [63], Peanut hull [64], Banana peel [65], Orange peel [65], Rice husk [66], Apricot shells [67], Wheat shells [68], Spent coffee grounds [69] and Passion fruit waste [70]. It is possible to affirm that Yerba Mate constitutes a promising solid adsorbent in this field.

The variation of the standard free energy calculated by Equation 4.3 is $\Delta G^\circ = -22.3$ kJ/mol confirming the spontaneity of the process.

Table 4-3. Comparison of the Langmuir and Freundlich constants for different types of food waste bio-adsorbents.

Bio-adsorbent	T (°C)	pH	q_{max} (mg/g)	b (L/mg)	Reference
Papaya seeds	30	7	555.5	0.0028	[71]
Grass waste	30	7	457.6	0.0023	[72]
AV50 ¹⁶	20	7	346.52	0.018	[73]

Rice husk	20	7	312.2	0.0171	[74]
AV25 ¹⁶	20	7	311.81	0.12	[73]
Cotton waste	20	7	277.7	0.009	[74]
AV0 ¹⁷	20	7	199.13	0.17	[73]
Pteris waste roots	20	7	112.3	0.62	[75]
Tea waste	25	8	85.1	1.26	[76]
Peanut hull	20	5	60.05	0.16	[64]
Yerba Mate	25	6	59.6	0.02	[This study]
Passion fruit waste	25	8	44.70	0.002	[70]
Apricot shells	25	5	24.31	0.002	[67]
Banana peel	30	7	20.8	0.06	[65]
Chaff	25	7	20.03	0.22	[63]
Spent coffee grounds	25	5	18.72	0.27	[69]
Orange peel	30	7	18.6	0.05	[65]
Wheat shells	30	7	16.56	0.02	[68]

4.5 Kinetics experiments and fitting of model parameters

Kinetics batch tests were carried out to assess the influence of temperature and the adsorbent concentration on the adsorption rate. The experimental results are given in terms of the ratio between the adsorbate concentration measured along time and the initial concentration: this allows a better comparison of the graphs. In **Figure 4-6** the experimental points are presented together with the curve of the model outcome from fitting. The values of the parameters bq_{max} and $k_{LDF}a$ derived from fitting are resumed in **Figure 4-7**. As it is possible to see from **Figure 4-6**, the increase of the bio-adsorbent concentration from $R=100$ to $R=300$ enhanced the velocity of the adsorption process and an increase in MB removal was observed. To evaluate the influence of temperature on the adsorption behavior, more information are given in **Figure 4-7**. In **Figure 4-7 a)** were reported the values obtained from fitting of the parameter bq_{max} for each temperature. It was observed that the parameter bq_{max} could be considered constant in all the range of temperatures (283 K - 313 K) under analysis. In **Figure 4-7 b)** the values of the parameter $k_{LDF}a$ were plotted versus R showing a linear behavior as expected according to Equation 4.6. Even in this case it was not observed

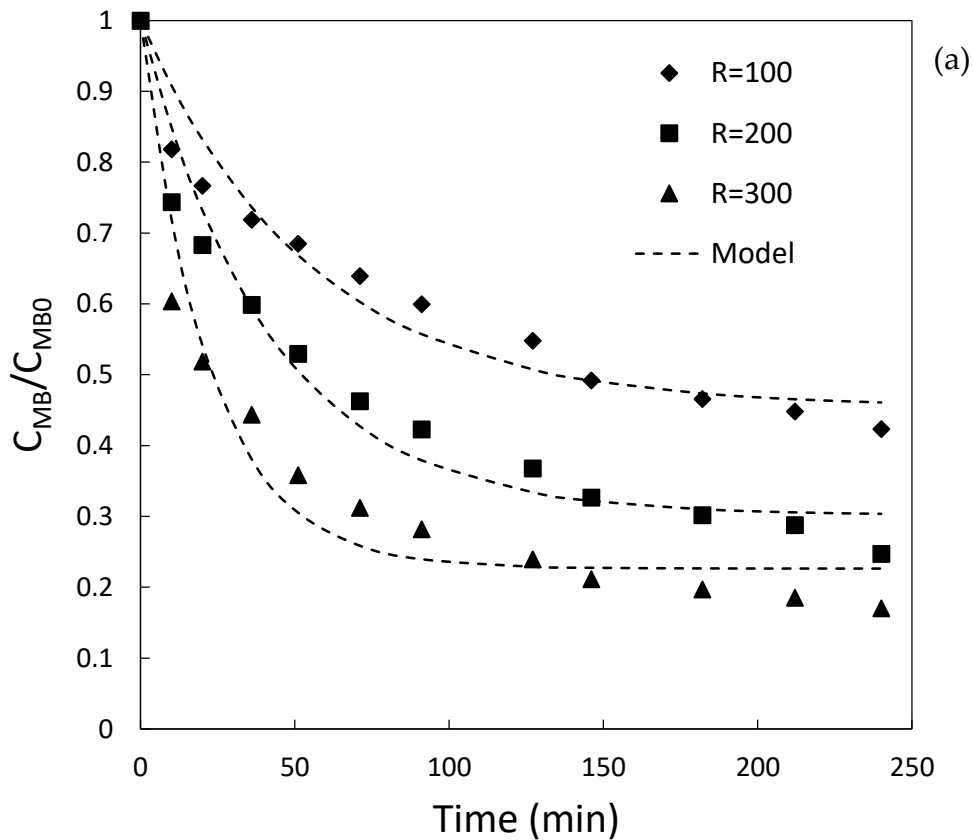
¹⁷ AV stands for Aloe Vera as introduced in Chapter 5.

a significant variation (the standard deviation of each point was <10% of the referring value) of the parameter with temperature (the error bars in **Figure 4-7 b** represent the effect of temperature oscillation).

This result can be explained with the following considerations:

- the variation of temperature did not induce a significant change on the liquid properties nor on the effective diffusivity of MB through YM pores and k_{LDF} , the overall LDF transport coefficient, remained constant;
- the concentration of MB in the liquid phase at equilibrium was so small that the variation of the isotherm slope was not appreciable (bq_{max} remains constant).

Due to the nature of the LDF Model, in this case it was not possible to obtain information on which between the intra-particle or the external resistance is the limiting one.



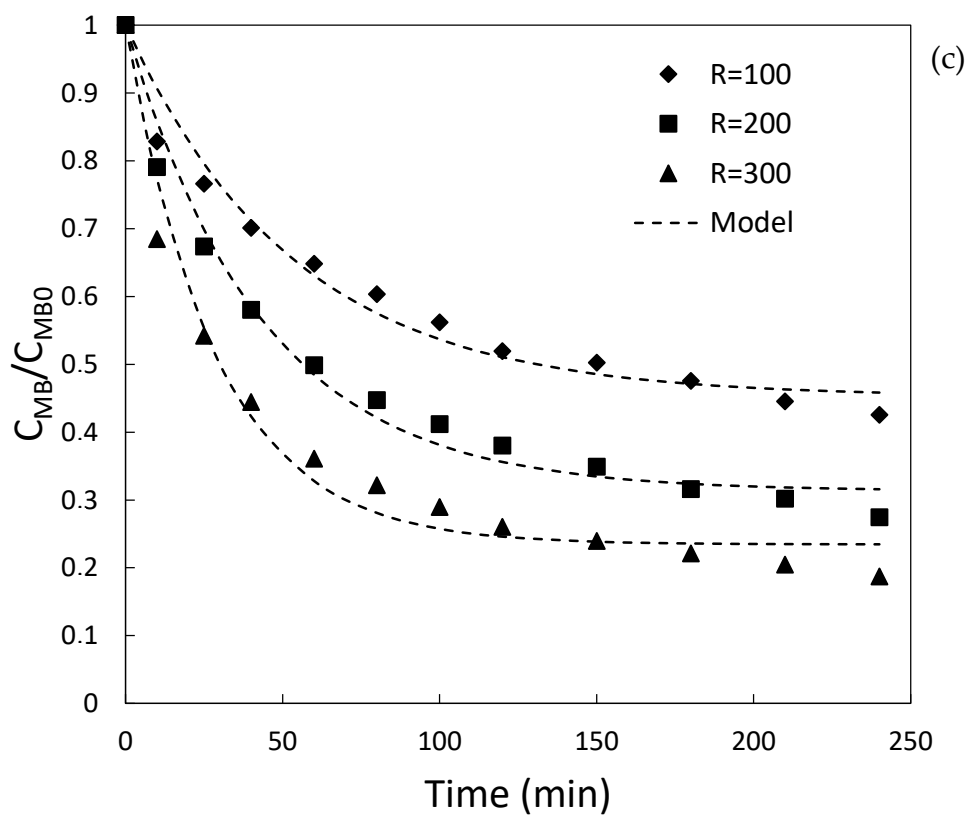
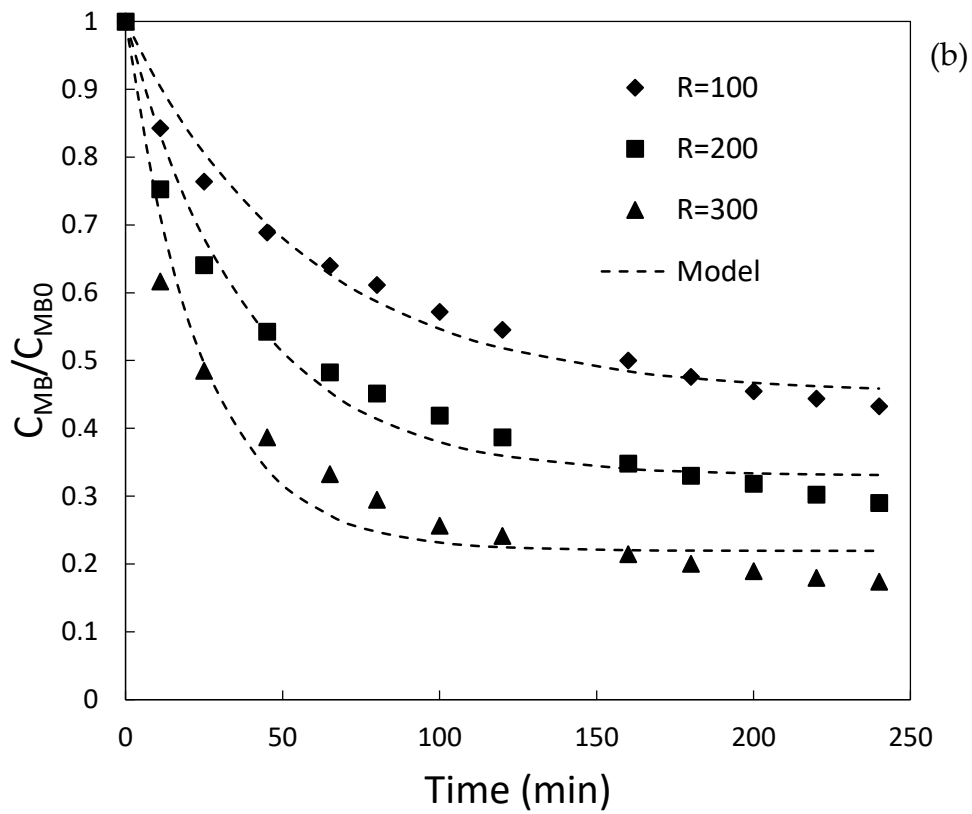


Figure 4-6. MB adsorption on Yerba Mate at different R (100, 200, 300 for each graph) and temperatures 283 K (a), 293 K (b) and 313 K (c) [54].

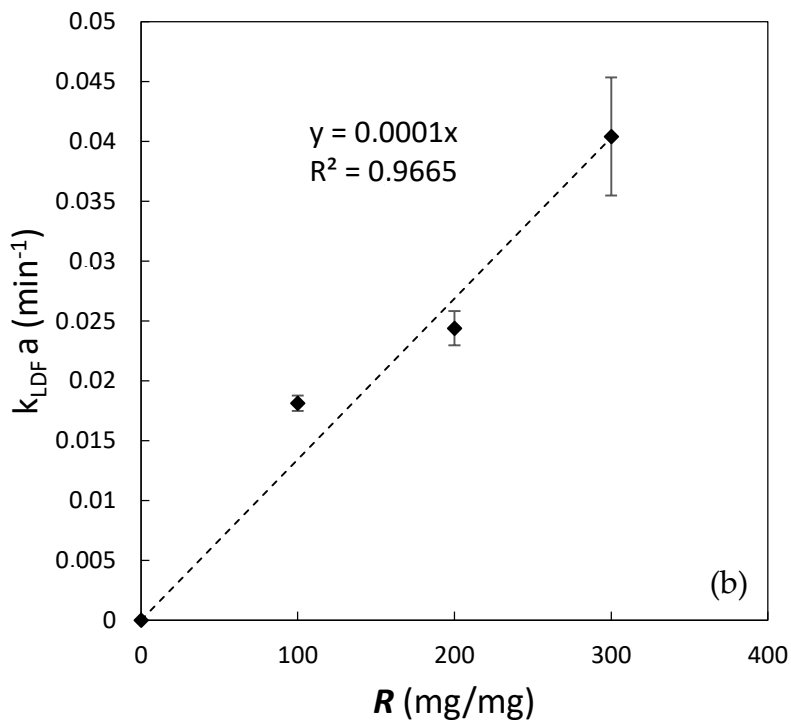
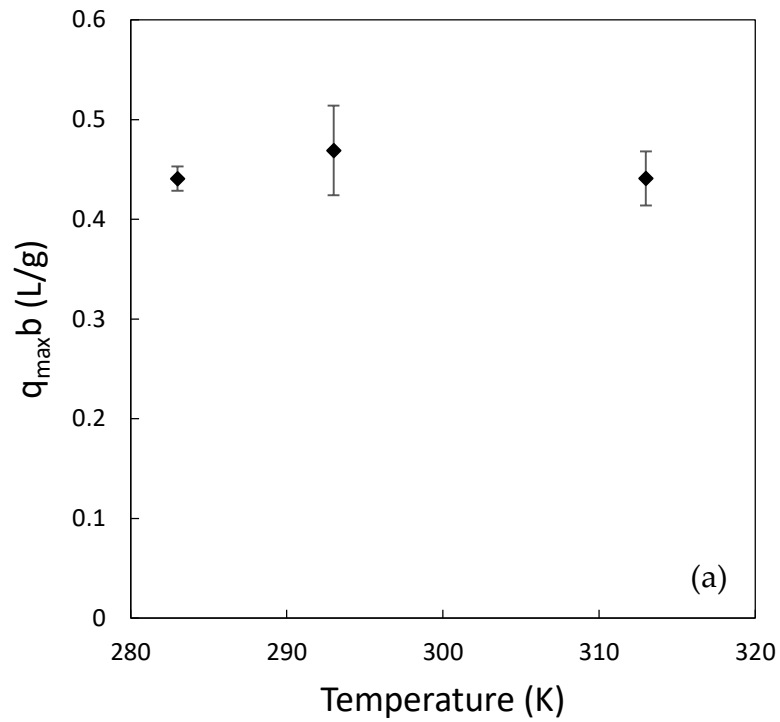


Figure 4-7. Variation of the parameters of fitting bq_{\max} (a) and $k_{LDF}a$ (b) with temperature and the ratio between the solid dosage and the initial concentration of MB respectively. The points reported are the mean of the fitting values [54].

4.5.1 Model validation

Based on the results previously reported it is evident that Langmuir isotherm best represents the equilibrium of the system. At the same time, temperature proved not to be a crucial parameter on the adsorption kinetic of MB on Yerba Mate in the operative conditions adopted in this work. To confirm the hypothesis of linear isotherm in the range of concentrations involve in the kinetic tests, the condition $bC_{MB} \ll 1$ must be satisfied for all the duration of the test. The maximum value of bC_{MB} is reached at the beginning of the experiment where $C_{MB} = C_{MB}^{in}$. For all the tests conducted, the maximum initial concentration adopted was $C_{MB}^{in} = 26$ mg/L., hence it was always $bC_{MB} \leq 0.52$ ($b=0.02$ L/mg calculated from isotherm fitting). Such value was considered small enough to satisfy the hypothesis of Equation 4.5.

In order to validate the model proposed in Equation 4.5, two additional tests were run at 298 K. Such experimental results are compared in **Figure 4-8** against the numerical results (dotted line) of Equation 4.5, now implemented for the prediction of the adsorption kinetics. The values of the fitting parameter for this simulation were:

- $bq_{max} = 0.45$ [L/g] taken as the mean of all the values of bq_{max} obtained from the fitting (see **Figure 4-7 a**);
- $k_{LDF}a = 0.0001 \cdot R$ [1/min] (see **Figure 4-7 b**); hence for $R = 200$ $k_{LDF}a = 0.02$ [1/min] and for $R = 400$ $k_{LDF}a = 0.04$ [1/min]

As depicted in **Figure 4-8** the model well predicted the experimental data with a mean square error of 0.17 for the case of $R = 200$ and 0.22 for the case of $R = 400$.

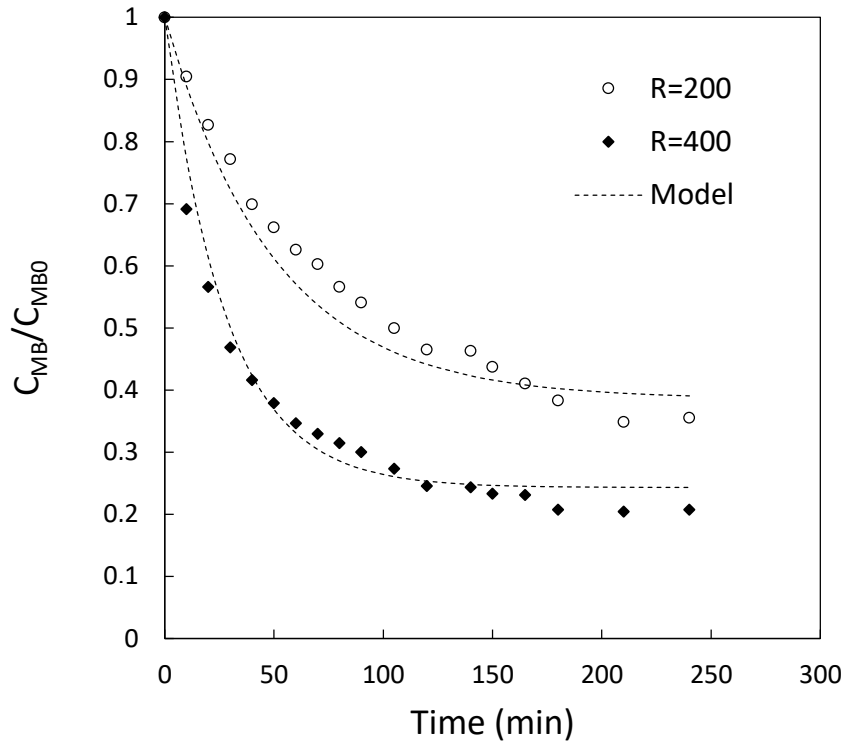


Figure 4-8 Adsorption kinetics of Methylene Blue on Yerba Mate at 298 K for $R=200$ and $R=400$. The dashed lines represent how the model (with $bq_{max} = 0.44$ [L/g] and $k_{LDF}a=0.02$ and $k_{LDF}a=0.04$ [1/min] for $R = 200$ and $R = 400$ respectively) predicts the trend of adsorption [54].

3.2.2. Characteristic time of adsorption

To quantify how the rate of adsorption was influenced by the amount of bio-adsorbent in terms of the parameter R , a characteristic time of adsorption (from Equation 4.5) was defined:

$$\tau = \frac{1}{k_{LDF}a} \quad (4.7)$$

The characteristic time τ (min) depends from the concentration of the bio-adsorbent, included in the specific surface area, and the temperature. The characteristic time τ (min) was calculated for the tests at 283 K, 293 K and 313 K using for each test the values of $k_{LDF}a$ derived from fitting. Since it has been previously observed that temperature did not significantly influence the values of $k_{LDF}a$, the variation of τ was reported only in function of R in **Figure 4-9**. As expected, the characteristic time of adsorption decreased linearly when the concentration of the solid adsorbent increased. In fact, it was observed that doubling the amount of solid adsorbent (from $R = 100$ to $R = 200$) the characteristic time of

adsorption was reduced of 15 min; tripling the amount of solid adsorbent (from $R = 100$ to $R = 300$) the characteristic time of adsorption was reduced of 30 min.

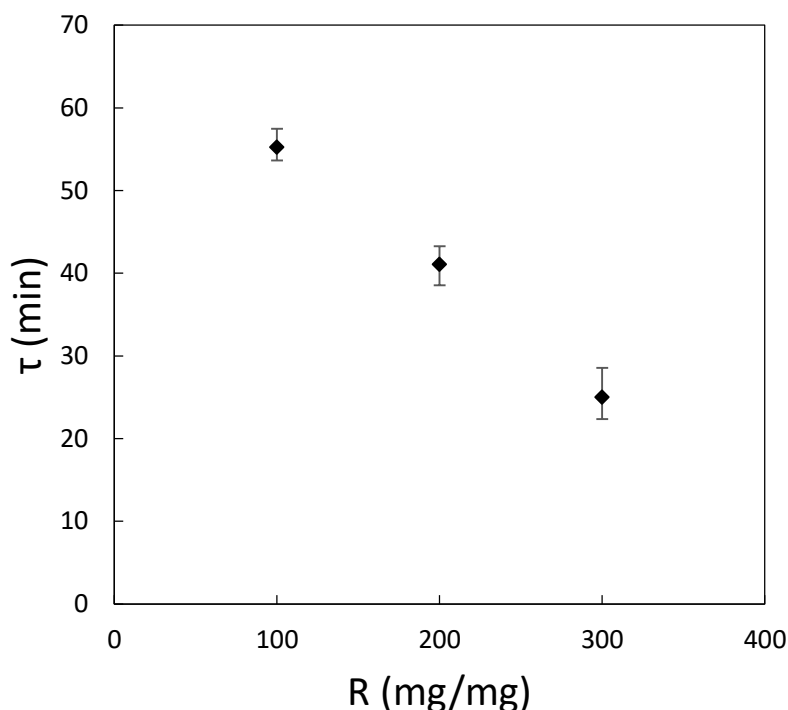


Figure 4-9. Variation of the characteristic time of adsorption of Methylene Blue using Yerba Mate versus R . The points reported are the mean of the fitting values. Moreover, the error bars represent the maximum and minimum difference between the values of fitting and the mean [54].

4.6 Adsorption of RBB and Cr(VI) using YM and CYM

According to the pH_{ZC} of YM (**Figure 4-3**), adsorption tests of the RBB were conducted at pH-values at maximum equal to 6 because the anionic nature of the dye. Unlike the previous results on MB, no satisfying RBB removal were obtained, under any experimental condition. The maximum value of RBB removal (27%) was observed at low pH condition (pH=3) and low temperature (283 K). This suggested the inapplicability of YM material for the removal of anionic species because the low availability of protonated species on the coarse fraction of YM waste (as nitrogen based groups [77]) and the presence of functional groups [43] that limit the occurrence of a low distribution of the positive charge (**Figure 4-3**). On the contrary, this low presence of positive charge allows to promote the adsorption of the cationic species in the investigated pH conditions.

Similar results were obtained during the adsorption tests of Cr(VI). Under acidic pH condition (up to 3) Cr(VI) existed in form of $HCrO_4^-$ and $Cr_2O_7^{2-}$ [19] while and above pH 7 Cr(VI) exists only in form of CrO_4^{2-} ions according to the reaction below [78]:



Acidic pH conditions are required to promote the electrostatic attraction between the negative charge of Cr ions and the surface of YM. However, also in this case, due to the low attitude to protonation, a lower Cr(VI) adsorption was observed than MB: a 50% removal of Cr(VI) was calculated at 283K and pH=3. These results represent the best results obtained in the experimental campaign. In the attempt to improve the removal of the anionic species, an activation effect of YM was stimulated by calcinating the waste material. The results of the adsorption test performed at 298K and pH=6 with YM in the calcinated and not calcinated form, are reported in **Table 4-4**.

Table 4-4. Removal efficiency of MB, RBB and Cr(VI) on YM and CYM samples.

Sample	T [K]	pH	E _{RBB} %	E _{Cr(VI)} %	E _{MB} %
YM	283	3	27.00	50.00	70.00
YM	298	6	0	2.80	74.36
CYM	298	6	77.00	65.00	0

Table 4-4 shows that the activation of YM produced a positive effect on RBB and Cr(VI) adsorption; at neutral pH condition and 298 K, the removal of MBB and Cr(VI) reached a 77% and 65%, respectively, suggesting that it is not necessary to operate in extreme operating conditions (283 K and pH=3) to ensure a good removal of the species. On the contrary, the removal of MB was completely reset suggesting that the calcination resulted in the removal of the functional groups responsible of the removal of cationic species.

Conclusions

In this work Yerba Mate (*Ilex paraguariensis*), an agro-food waste, was tested as a bio-adsorbent for the removal from an aqueous solution of Methylene Blue (MB), Remazol Brilliant Blue (RBB) and Cr(VI). It was observed that YM is an excellent bio-adsorbent for the removal of MB while it resulted less effective for the adsorption of RBB and Cr(VI). For this reason, MB adsorption was investigated more in detail leading to the following conclusions:

- Adsorption of MB using YM is a spontaneous process. The adsorption isotherm follows the Langmuir expression and an adsorption capacity of 59.6 mg/g was calculated. Compared to other food-derived bio-adsorbents tested in literature, YM shows one of the highest adsorption capacity;
- The concentration of YM is the most important operative parameter of the bio-adsorption process: an increase in bio-adsorbent concentration speeds up the adsorption

process and reduces the residual amount of pollutant in the aqueous solution. The effect of temperature and pH are negligible in the range of concentration of MB considered.

An additional calcination step of the Yerba Mate waste resulted in a physio-chemical modifications of the original material including an important increase of its specific surface area. The calcinated product proved to be suitable for the adsorption of RBB and Cr(VI) at low pH and temperature values.

CHAPTER V

5. Effect of Water–Ethanol Extraction as Pre-Treatment on the Adsorption Properties of Aloe vera Waste

In this chapter the aim was to investigate on the effects that a possible pre-treatment step could induce to the adsorption properties of Aloe Vera waste rind.

Several studies were conducted for the extraction of high value molecules from Aloe vera. For example, Acemannan was extracted from both Gel and Aloe skin with water or water-ethanol solutions as explained in the review of Liu et al. [79] or anthraquinones were extracted from Aloe peel powder in a 60 % ethanol-water solution by Tan et al. [80].

Aloe vera wastes were used also for water treatment purposes mainly for the removal of dyes and heavy metals [81]. Giannakoudakis et al. [82] pointed out different classes of pre-treatment steps before utilization of Aloe as bio-adsorbent: no-treatment; air-dried treatment at $T < 110$ °C; chemical treatment with strong acids; thermal treatment at 300 °C $< T < 700$ °C from which activated carbons or ash are obtained depending on the absence or the presence of oxygen respectively. However, all the aforementioned pre-treatments do not focus on the recovery valuable compounds that are still present in the Aloe waste matrix (i.e. anthraquinones) which could be instead recovered promoting economic advantages. For this reason, solvent extraction was selected as the best pre-treatment option which could achieve simultaneously an increase of the adsorption properties of the material and benefits from the economical point of view.

To the best of our knowledge, there are no studies that utilize solvent extraction on Aloe vera as a pre-treatment for the preparation of a new bio-adsorbent material. Although the aim of this work was far from optimizing the particular extraction step adopted, it was given a first analysis on its influence on the adsorption properties of a waste material. Thus, the purpose of this work is to couple an extraction (as pre-treatment) step using as solvent water or a solution of ethanol-water (adopted for extraction on Aloe as previously explained) followed by a batch adsorption of Methylene Blue and to investigate how the adsorption properties of Aloe vera change depending on the solvent used.

In the work of Hanafiah et al. [83] Aloe vera rind powder washed with water was tested as adsorbent material of Methylene Blue, however several points of interest were not studied: no information was given regarding the amount of substances released during the washing step with water; the equilibrium data are focused in a concentration range which is below 25 mg/L and possible information about the behavior of the system at higher concentration were lost; no physical model was developed for the analysis of the adsorption kinetics.

In this work the equivalent Gallic Acid concentration (GA) was quantified after the pre-treatment step and experimental data of adsorption equilibrium with Methylene Blue are reported for the material treated with different extracting solvents. Moreover, experimental data are also reported about the batch adsorption kinetics of Methylene Blue from the aqueous phase. Such data were analyzed by a mathematical model to estimate the Methylene Blue diffusion coefficient inside the bio-adsorbent and to compare the results related to the different pre-treatment step. The content of the chapter was taken from its corresponding publication of Mazzeo et al. [73].

Materials and Methods

5.1 Chemicals

Methylene blue (C₁₆H₁₈ClN₃S; MB), pure ethanol (C₂H₅OH), hydrochloric acid (HCl), sodium hydroxide (NaOH), sulfuric acid (H₂SO₄), sodium carbonate (Na₂CO₃), Folin Ciocalteu reagent (C₁₀H₅NaO₅S) were purchased from Sigma Aldrich and used without any further purification.

5.2 Bio-adsorbent preparation

The outer layer (rind) of *Aloe vera* (*Aloe Barbadensis* Miller) leaves was obtained from residues of a cosmetic industry located in Lazio region, Italy. The solid was firstly dried at 60 °C for 24 h in order to remove the moisture initially present. Then it was drilled and sieved in order to collect particles in the size range of 0.5-1 mm. Three different aqueous solutions were tested for the pre-treatment: water, water-ethanol (25% v/v), water-ethanol (50% v/v). The acronyms AV0, AV25 and AV50 were adopted to identify the *Aloe vera* treated with water, with the water-ethanol (25% v/v) and with the water-ethanol (50% v/v) solution respectively. The pre-treatment step was carried out at room temperature in 500 mL magnetically stirred flasks with a solid concentration of 20 mL/g (in the range adopted by Gironi et al. [84] and Fanali et al. [85]) for 2h. The total amount of organic compounds in the aqueous solution was evaluated by Total Organic Carbon (TOC) measurement (TOC-L Analyzer- Shimadzu) while the equivalent Gallic Acid (GA) concentration was measured by means of the Folin Ciocalteu reagent (using gallic acid as standard). The latter (0.144 mL) was mixed together with 5 mL of HCl (0.1 M), 4.656 mL of Na₂CO₃ (10% w/w) and 0.2 mL of the sample. The solution was kept reacting in the dark for 1h before spectrophotometric analysis using a PG Instruments (United States) T80+ UV/Vis spectrophotometer (with glass cells of 1 cm path length) at the wavelength of 700 nm.

5.3 Bio-adsorbent characterization

The zero-charge point pH of the pre-treated materials (pH_{ZC}) was determined according to the pH drift method [16]. An amount of 0.04 g of Aloe was added to 10 mL of ultra-pure water. Before the introduction of the solid, the pH of the solution was adjusted from 2 to 12 by the addition of H₂SO₄ (0.1 M) and NaOH (0.1 M). The pH of the solution was then

measured (Crison GLP 421) after 24 h which was estimated to be the time required for the system to reach the equilibrium condition. Analysis of the adsorbent's surface area was performed by N₂ adsorption isotherms acquired at -196 °C using a Micromeritics Triflex analyzer (Micromeritics Instrument Corp.) in the p/p⁰ range from 0.01 to 0.99. Isotherm analyses were carried out using the 3Flex Version 4.05 software. Samples were previously outgassed at 100 °C for 3 h. The Brunauer–Emmett–Teller (BET) and Barrett–Joyner–Halenda (BJH) equations were used to determine the specific surface area (SSA), pore volume and average pore diameter, respectively as shown in section 3.4.1. A thermal-gravimetric analyzer (TGA-SDTQ600, TA Instruments, USA) was employed to investigate the degradation profile of the prepared samples over a temperature range of 30-700 °C. The dried *Aloe vera* samples were ground into very fine powder using a non-metallic electric grinder, and approximately 10 mg was placed onto a platinum crucible and heated at 10 °C/min under 100 mL/min N₂ flow.

5.4 Batch Tests

To evaluate the affinity between the solid adsorbent and the model compound (MB) to be removed, batch tests were performed. In all the tests the concentration of MB was determined by Infinite M200 PRO Tecan microplate spectrophotometer (Tecan Trading AG, Switzerland) at the wavelength of 664 nm.

5.4.1 Equilibrium tests

All equilibrium experiments were carried out in magnetically stirred beakers of 100 mL contacting 50 mL of MB solution of known concentration in the range of 8.5 mg/L – 212.5 mg/L. Each test lasted at least 24 h since preliminary tests showed that it was an enough time for the system to reach equilibrium. The stirring speed was kept constant at 220 rpm while the solid dosage was fixed to 0.2 g/L unless in the case of 212.5 mg/L MB starting solution in which it was set to 0.4 g/L. The temperature was fixed to 20 ± 0.2 °C. Each test was performed for AV0, AV25 and AV50 alone at least in duplicate. Only for AV0 the equilibrium was evaluated at 10 ± 0.2 °C and 40 ± 0.2 °C in order to understand the nature of the adsorption mechanism. The surface concentration at equilibrium (q_e) was calculated from experimental data as follows (as defined by Equation 2.19):

$$q_e = \frac{V}{M_S} (C_{in} - C_e) \quad (5.1)$$

where V (mL) is the liquid volume, M_S (g) is the mass of the adsorbent material, C_{in} (mg/L) is the initial concentration of MB and C_e (mg/L) is the MB concentration at equilibrium.

5.4.2 Kinetic tests

All kinetic experiments were carried out in magnetically stirred beakers of 250 mL contacting 100 mL of MB solution at a starting concentration of 8.5 mg/L. The stirring speed was kept constant at 220 rpm while the temperature was set at 20 ± 0.2 °C verifying that

such condition was satisfied before the beginning of the tests. The solid to liquid ratio was fixed to 0.2 g/L. Samples were taken at definite time intervals by removing 200 μ L from the liquid. Since the number of samples collected was less to 10, the error made on the final volume was <2%. Each test was performed for AV0, AV25 and AV50 alone at least in duplicate. A mathematical model (deeply discussed in the following section) was adopted to fit the experimental data by means of the process simulator gProms (Process System Enterprises, London, UK) and to evaluate the controlling resistance of the system.

Results and Discussion

5.5 Bio-adsorbent pre-treatment

The solid preparation with the only drying and milling steps is not sufficient to obtain a clean material to be adopted for adsorption tests because of the interference of released compounds during the tests on MB spectrophotometer detection. For this reason, different pre-treatments (as washing cycles) were adopted and the effect of the washing solution composition was investigated. To this purpose water and a water-ethanol solution (25% v/v and 50% v/v of ethanol) were adopted. The pre-treatment procedure was repeated replacing fresh solvent for the same amount of solid until the concentration of polyphenols in the liquid phase reached about the detectable limit of the spectrophotometer. The results of the pre-treatment are reported in **Figure 5-1** where it is possible to show that three cycles were enough to reach such threshold. The Total amount of Polyphenolic Compounds (TPC) was evaluated to be 0.4 mg/g of Equivalent GA per gram of Aloe. A similar result was observed by Di Scala et al. [86] for a pre-treatment conducted at 0.1Mpa. In **Figure 5-1**, it is also noticeable that the water-ethanol solutions have a higher extraction potential in agreement to the higher solubility of polyphenolic compounds in such mixtures respect to water alone [87,88]. Furthermore, **Figure 5-1** highlights the decrease of the GA concentration along the pretreatment cycles. To evaluate the concentration of the total organic compounds that can be removed from AV solid (not only limited to polyphenolic compounds) the TOC of the final solution was measured: this was conducted for the only water test and a value of 79.4 mg/L (10% of which were polyphenols) was observed as a sum of the three washing cycles. This result suggests that, many other components are extracted and, in an attempt to adopt such pretreatment as possible extraction process of added value compounds, an optimization of the operative parameters (temperature, solid/liquid ratio) of the process and purification of the extracts are required. The aim of this work was to study the adsorption properties of AV waste even in the case of a residue outcoming from an extraction process.

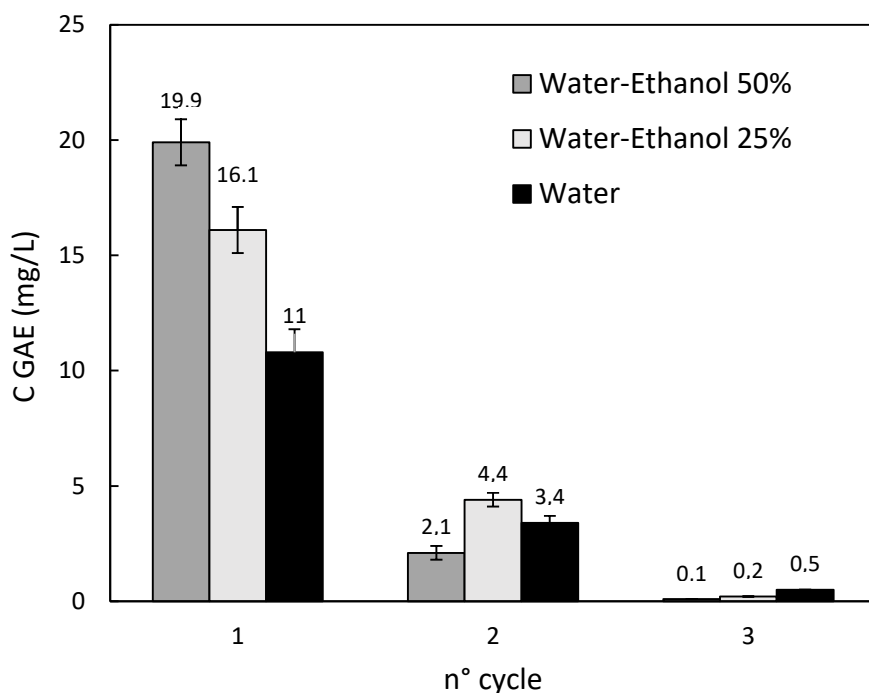


Figure 5-1. Equivalent Gallic Acid concentration (C GAE) along three pre-treatment cycles using water, water-ethanol (25% v/v) and water-ethanol (50% v/v) solutions as solvents [73].

The pH_{zc} was evaluated graphically and reported in **Figure 5-2**: values of 6, 5.7 and 7.2 for AV0, AV25 and AV50, respectively were determined. As reported in **Figure 5-2**, AV0 and AV25 have similar behaviours while AV50 showed a higher affinity for protonation. These results suggest that the pre-treatment could induce some changes in term of protonating/deprotonating functional groups on the solid surface when solvent at higher percentage than 25% v/v respect to water are adopted.

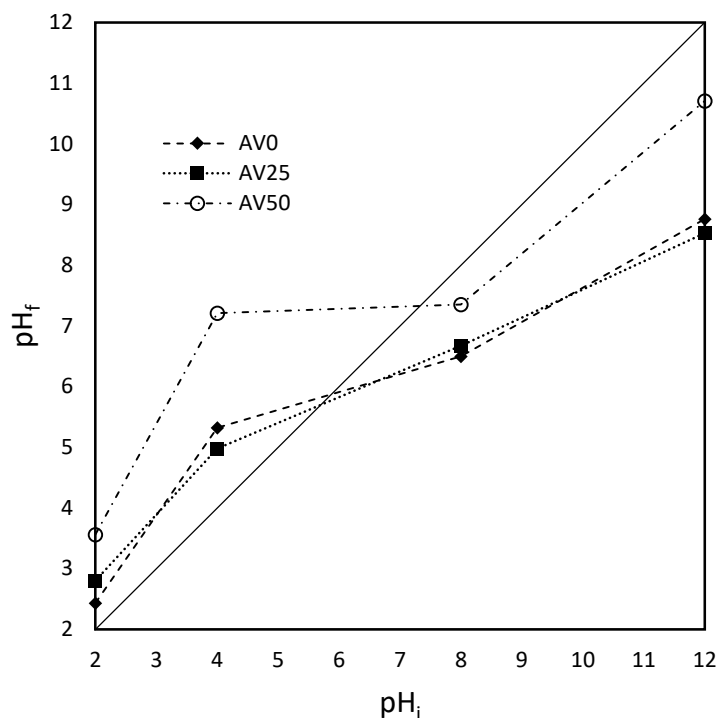


Figure 5-2. Zero-point charge (pHZC) determination for AV0, AV25 and AV50. The zero-point charge is represented by the intersection of the characteristic lines for all the samples with the bisector of the graph [73].

Figure 5-3 a) shows the TG curve of as-received *Aloe vera* waste. The first weight loss region in this curve can be seen between room temperature and 150 °C, which is due to the removal of adsorbed/bound water and other trapped volatile compounds, which constitute approximately 5.4 wt% of the total weight. The second weight loss region is observed at 150-380 °C, and this corresponds to decomposition of hemicellulose and pectin (43.6 wt%). Beyond 380 °C, weight loss is very fast due to the presence of cellulose (34.5 wt%). The last slow weight loss occurring between 540 °C and 750 °C is due to the presence of lignin, which account approximately 4.8 wt% of the total weight. The amount of solid residue remaining at 700 °C was about 11.6 wt% [83]. In **Figure 5-3 b)** the DTG curves of AV0, AV25 and AV50 are reported and a decrease in thermal stability of the pre-treated materials is observed with the increase of ethanol percentage adopted in the pre-treatment solutions. No significant modification as hemicellulose, cellulose and lignin amount were detected and values of 51.83%, 30.26% and 3.40% were determined respectively. The difference respect to the untreated one is related to the reduction of solid residue in the analysed samples from 11.60%±0.84% to 4.33%±0.61% that contributed to increase the percentage of these species respect to the untreated AV. A significant increase on volatile compounds was measured from the untreated (5.4%) to the treated materials (8.9%, 10.3% and 11.3% for AV0, AV25 and AV50 respectively) probably due to a strong absorption of ethanol on the active sites of lignocellulosic material. With the increase of ethanol content (higher than 25%v/v) on the

pre-treatment solution, the modification in term of pH_{ZC} have to be associated to possible protonation/deprotonation ethanol mechanism [89].

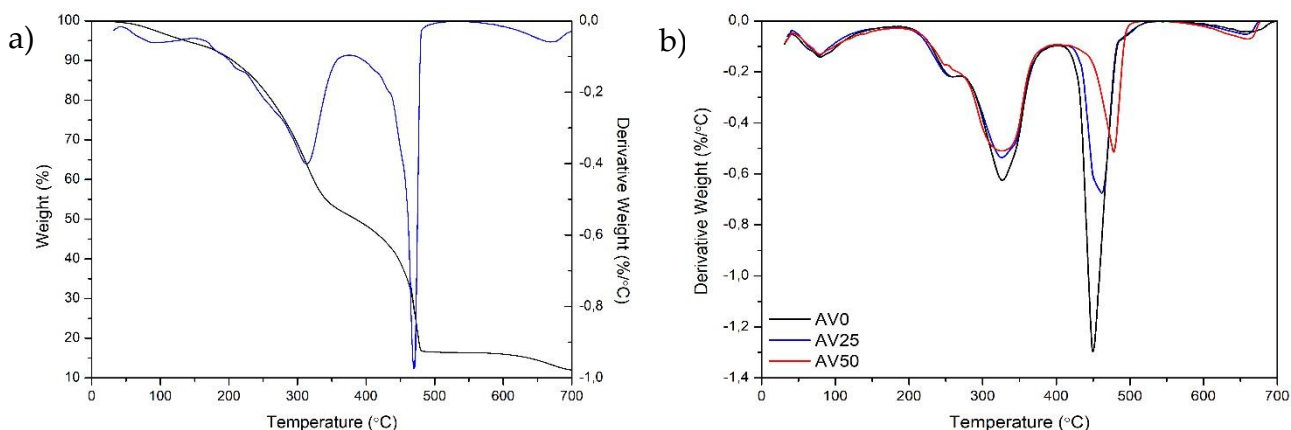


Figure 5-3. a) TG-DTG curves of as-received Aloe vera; b) DTG curves of AV0, AV25 and AV50 [73].

5.6 Equilibrium

The equilibrium experimental data for the bio-sorbents AV0, AV25 and AV50 are reported in **Figure 5-4**. It is immediately noticeable that the isotherms for AV0 and AV25 showed a typical saturation behaviour. Hence, the Langmuir model (Equation 5.2) was chosen to analyse the experimental data of these two isotherms and only for completeness it was made a comparison using also the Freundlich model (selected for its wide usage in literature). Different considerations should be done for AV50 isotherm: in the range of concentration considered, it was not possible to affirm that the curve goes to saturation. For this reason, both Langmuir and Freundlich (Equation 5.3) models must be considered for data description. The Langmuir equation is given below in Equation 5.2

$$q_e = q_{max} \frac{bC_e}{1 + bC_e} \quad (5.2)$$

where b (L/mg) is the equilibrium constant of the Langmuir model correlated to the affinity of binding sites, q_{max} (mg/g) is the maximum adsorption capacity. The Freundlich equation is also reported in Equation 5.3

$$q_e = k_F C_e^{1/n_F} \quad (5.3)$$

where k_F ((mg/g)(L/mg)^(1/n_F)) is the distribution coefficient and 1/n_F is a correction factor. According on such considerations, the experimental data were fitted by means of a non-linear regression using the least square method. The Langmuir and the Freundlich parameters q_{max}, b and $k_F, 1/n_F$ respectively were estimated for AV0, AV25 and AV50 and were reported in **Table 5-1** together with their corresponding Root Mean Square Error (RMSE). According to such results, it was observed that the Langmuir isotherm provides a better representation of the system for all the samples under analysis. For this reason, the Langmuir model was selected as representative also for the thermodynamic analysis of the adsorption mechanism discussed later in this section. In **Figure 5-4** it was chosen to plot only for AV50 the curve obtained from the regression with the Freundlich model since for AV0 and AV25 the graphical results were unsatisfactory. Moreover, in **Table 5-2** the adsorption capacities of other bio-sorbents regarding the uptake of MB were collected and compared with the ones obtained in this study. From **Table 5-2** it is possible to observe that all the pre-treated Aloe Vera wastes considered in this work showed good performances for the adsorption of MB, in particular the sample AV50.

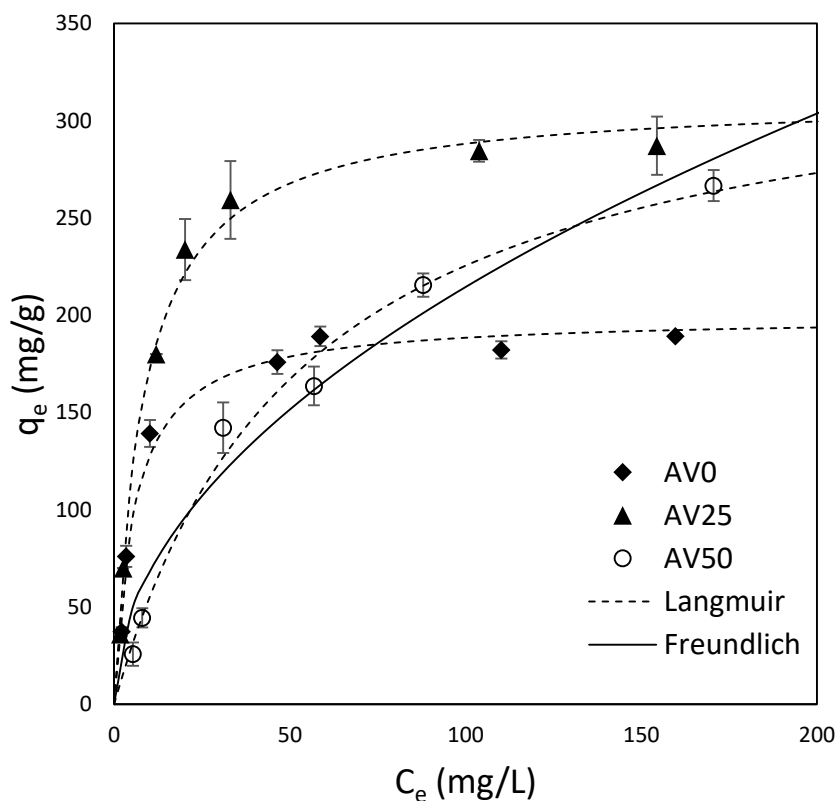


Figure 5-4. Isotherms at 20°C for AV0, AV25 and AV50 fitted with Langmuir model. Only for AV50 it was provided the fitting with Freundlich model [73].

Table 5-1. Langmuir and Freundlich isotherm parameters at 20 °C for AV0, AV25 and AV50.

Sample	Langmuir	Freundlich
--------	----------	------------

	q_{max} (mg/g)	b (L/mg)	RMSE (mg/g)	K_F ((mg/g)(L/mg) ^(1/n_F))	n_F	RMSE (mg/g)
AV50	346.52	0.018	9.01	4.92	2.83	17.02
AV25	311.81	0.12	10.84	46.81	1.51	41.95
AV0	199.13	0.17	8.74	5.17	2.26	23.48

Table 5-2. Langmuir isotherm parameters for agro-waste adsorbents.

Bio-adsorbent	T (°C)	pH	q_{max} (mg/g)	b (L/mg)	Reference
Papaya seeds	30	7	555.5	0.0028	[71]
Grass waste	30	7	457.6	0.0023	[72]
AV50	20	7	346.52	0.018	[This study]
Rice husk	20	7	312.2	0.0171	[74]
AV25	20	7	311.81	0.12	[This study]
Cotton waste	20	7	277.7	0.009	[74]
AV0	20	7	199.13	0.17	[This study]
Pteris waste roots	20	7	112.3	0.62	[75]
Tea waste	25	8	85.1	1.26	[76]
Peanut hull	20	5	60.05	0.16	[64]
Yerba Mate	25	6	59.6	0.02	[90]
Passion fruit waste	25	8	44.70	0.002	[70]
Apricot shells	25	5	24.31	0.002	[67]
Banana peel	30	7	20.8	0.06	[65]
Chaff	25	7	20.03	0.22	[63]
Spent coffee grounds	25	5	18.72	0.27	[69]
Orange peel	30	7	18.6	0.05	[65]
Wheat shells	30	7	16.56	0.02	[68]

Table 5-1 shows that both *Aloe* AV50 and *Aloe* AV25 have a higher adsorption capacity than AV0 of 74% and 56.5% respectively toward the uptake of Methylene Blue from water. Moreover, the value of q_{max} of AV50 respect to the one of AV25 is 11.13% higher. It is possible to ascribe this enhancement in term of q_{max} to the increase of exposed surface area how demonstrated by the results of BET analysis shown in **Table 5-3**. This result, linked to the pre-treatment operated with water-ethanol solution, is not related to the solubilisation of polyphenolic compounds (that were completely removed as discussed in the previous section) but to other soluble molecules present in the AV rind matrix such as tannins [91] whose solubilisation increases with the percentage of ethanol in water [88].

Using the International Union of Pure and Applied Chemistry (IUPAC) definition for microporous (less than 2 nm in diameter) and mesoporous (less than 50 nm in diameter) materials, the pore diameter patterns reported in **Figure 5-5** and in **Table 5-3** showed that all samples are mainly mesoporous material. This result is in agreement with the study of El-Azazy et al. [92].

Table 5-3. BET-BJH data for treated *Aloe vera* samples.

Sample	SSA (m ² /kg)	Mean pore diameter (nm)	Total pore volume (cm ³ /kg)
AV0	180.2	9.60	0.11
AV25	313.3	5.11	0.37
AV50	331.7	7.27	0.59

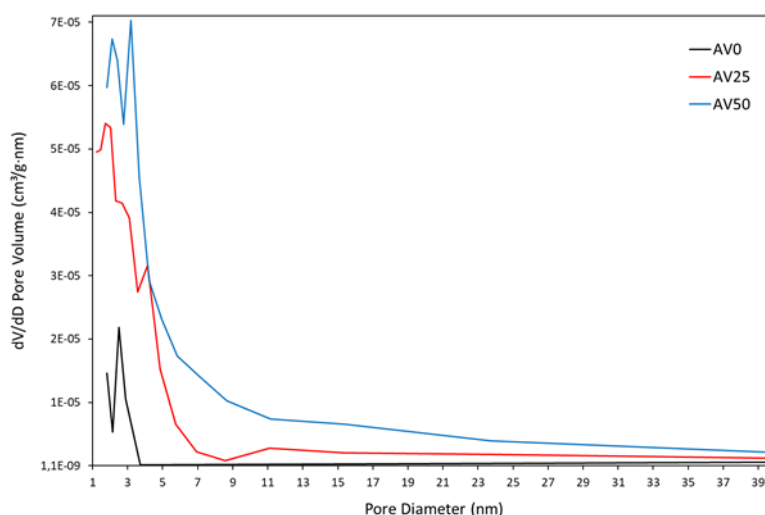


Figure 5-5. Relation between pore volume and diameter for AV0, AV25 and AV50 [73].

On the other hand, as reported in **Table 5-1**, a decrease of the Langmuir equilibrium constants b was observed. In fact, the reduction of such parameter was of 29.4% (AV25) and 89.4%(AV50) respect to AV0. This result suggests that the pre-treatment in presence of ethanol on one hand enhances the solubility of species with, as a consequence, the increase of the sites available for the adsorption, but, on the other hand, reduces the affinity with MB molecules, significantly in the case of AV50 in line with the observation on pH_{Zc}.

Considering a batch system having an initial concentration C_{in} of MB in the liquid solution, with the only knowledge of thermodynamic information it is possible to calculate the concentration of the solution and hence the percentage of MB removed ($R\%$) at equilibrium by solving together Equation 5.1 and Equation 5.2 as follows:

$$R = 1 - \frac{C_e}{C_{in}} = 1 - \frac{1}{2} \left[- \left(\frac{1}{bC_{in}} + \frac{M_S q_{max}}{V_L} - 1 \right) + \sqrt{\left(\frac{1}{bC_{in}} + \frac{M_S q_{max}}{V_L} - 1 \right)^2 + \frac{4}{bC_{in}}} \right] \quad (5.4)$$

In **Figure 5-6 a)** was reported the R calculated for AV0, AV25 and AV50 for different initial concentrations of MB. As it is possible to notice in **Figure 5-6 a)**, the value of R for AV25 is always bigger than the one for AV0 as expected since the higher adsorption capacity of AV25. For this reason, as shown in **Figure 5-6 b)**, the ratio between the R referred to AV25 (R_{AV25}) and the one referred to AV0 (R_{AV0}) it is always >1 independently of the variation of C_{in} . The same scenario occurs in **Figure 5-6 c)** as a consequence that for all the range of C_{in} explored AV25 removes a higher amount of MB respect to AV50. Moreover, in **Figure 5-6 c)** it is also noticeable the presence of a maximum which indicates the initial concentration of MB (which was calculated to be 50 mg/L) for which the bio-adsorbent AV25 shows the best performance respect to AV50.

In **Figure 5-6 a)** happens also that R_{AV50} and R_{AV0} intersect each other. This means that depending on the starting concentration of MB, AV50 may perform better than AV0 and vice versa. In fact, in this case (**Figure 5-6 d)** the ratio between R_{AV0} and R_{AV50} it is not always >1 : for $C_{in} < 100 \text{ mg/L}$, $\frac{R_{AV0}}{R_{AV50}} > 1$ and AV0 removes more MB than AV50; for $C_{in} > 100 \text{ mg/L}$, $\frac{R_{AV0}}{R_{AV50}} < 1$ and AV50 removes more MB than AV0. The range of initial concentration explored is limited to the one analyzed experimentally.

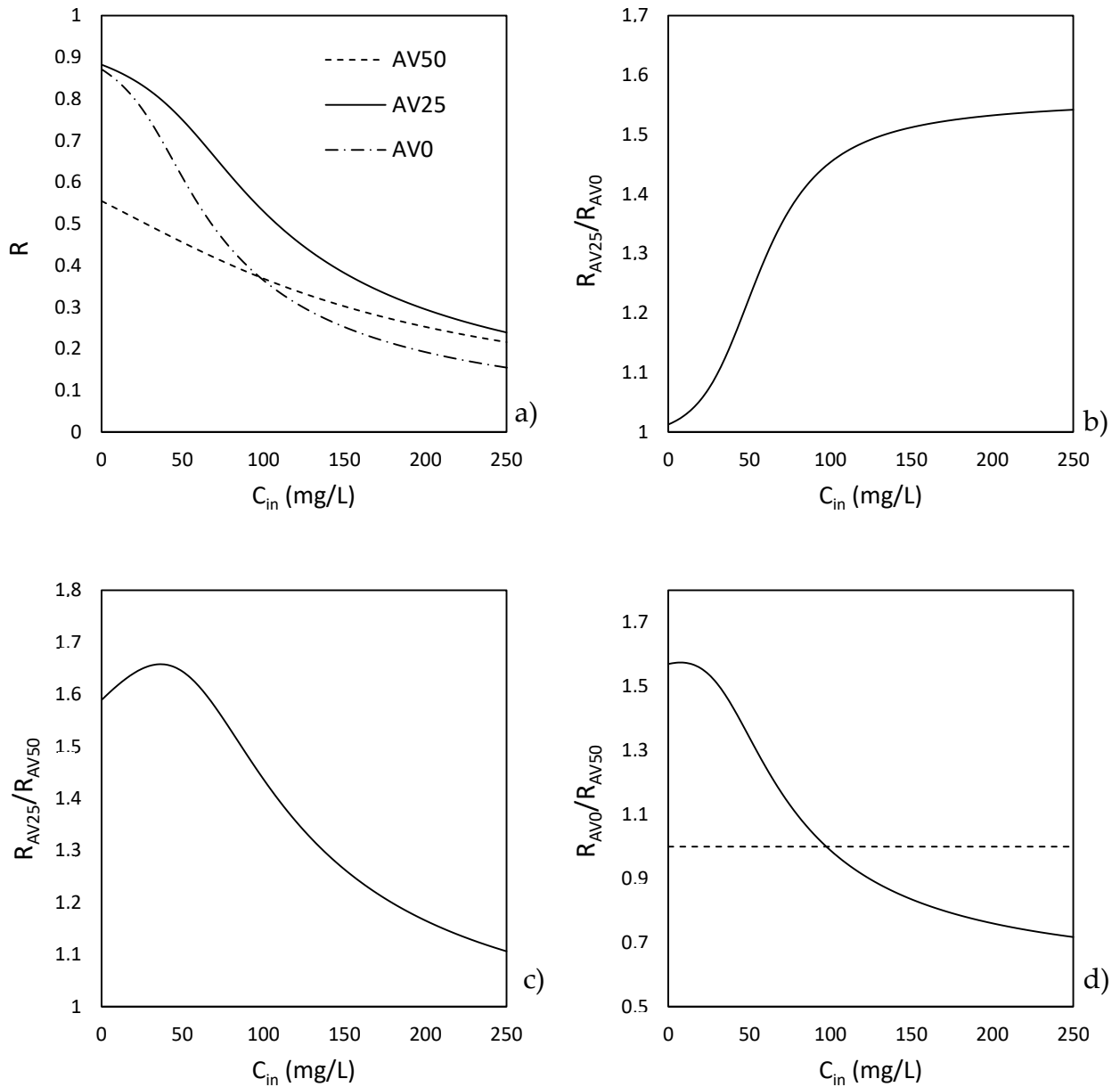


Figure 5-6. a) Plot of the removal percentage at equilibrium of MB (R) versus the initial concentration for AV0, AV25 and AV50; b) plot of the ratio R_{AV25}/R_{AV0} versus the initial concentration; c) plot of the ratio R_{AV25}/R_{AV50} versus the initial concentration; d) plot of the ratio R_{AV0}/R_{AV50} versus the initial concentration [73].

AV0 was chosen as a representative sample to understand the nature of the adsorption mechanism since it has a higher affinity toward MB adsorption respect to the other samples considered. Moreover, to evaluate if, in the case of AV0, it is possible to promote the adsorption mechanism, the effect of temperature was considered. In **Figure 5-7** are reported the equilibrium data for AV0 at different operative temperatures (10 °C, 20 °C, 40 °C). Also for this case, the data were analysed by means of the Langmuir isotherm. The values of q_{max} and b were calculated for each temperature and given in **Table 5-4**. It can be immediately observed a decrease of both q_{max} and b with temperature.

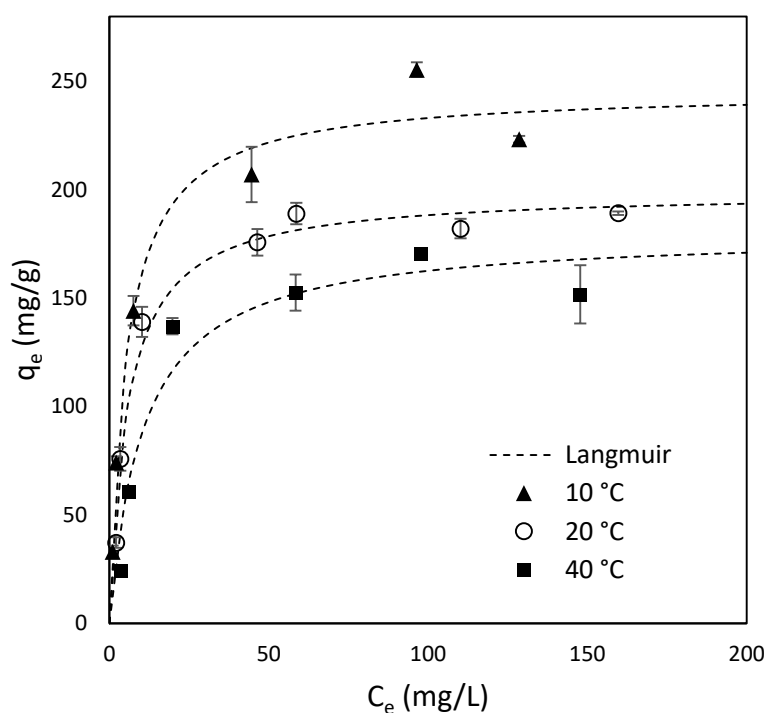


Figure 5-7. Isotherms of AV0 at 10 °C, 20 °C and 40 °C fitted by Langmuir model [73].

Table 5-4. Langmuir isotherm parameters at 10 °C, 20 °C and 40 °C for AV0.

Parameter	10 °C	20 °C	40 °C
q_{max} (mg/g)	245.59	199.13	180.21
b (L/mg)	0.18	0.17	0.09

An increase on q_{max} value was calculated but such results is lower respect those related to AV25 and AV50 at 20°C. On the contrary, b , even in a small extent, increased. According to the Langmuir theory of adsorption, b is directly connected to the enthalpy variation of the process by means of the Van't Hoff equation already reported in section 2.1.2.

As shown in **Figure 5-8** the experimental data have a linear behaviour as suggested by Van't Hoff equation. By means of a linear regression the value of Δh was calculated to be -4.3 kcal/mol which is included into the typical range associated to physical adsorption of -1 to -10 kcal/mol [93]. Moreover, the variation in enthalpy is negative revealing the exothermic nature of MB adsorption on *Aloe* as expected from the decrease of b with the increase of the temperature (see **Table 5-4**).

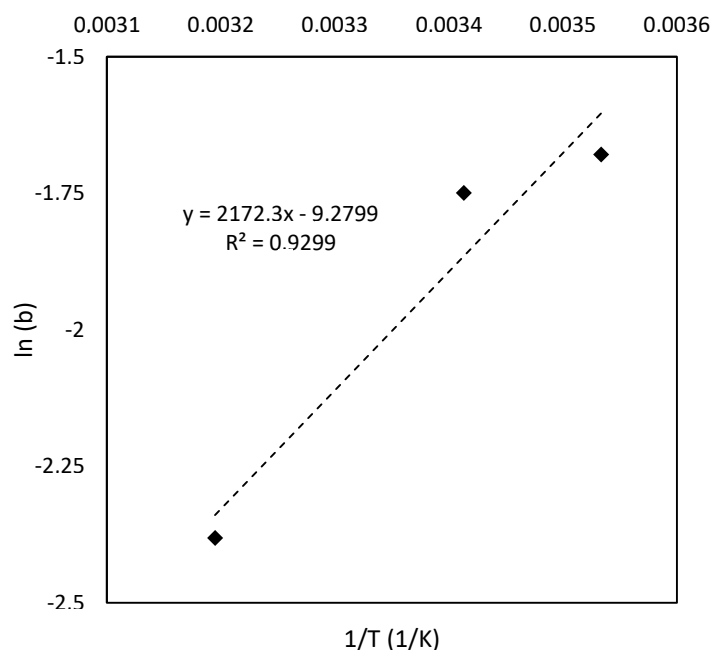


Figure 5-8. Natural logarithm of the Langmuir constant b versus the reciprocal of temperature. The dotted line represents the result of the linear regression which equation is reported in the graph together with the value of R^2 [73].

As previously observed, the adsorption capacity q_{max} decreases with temperature. Despite the fact that the Langmuir isotherm well describes the equilibrium conditions of the system, Langmuir theory do not admit a change in q_{max} with temperature. In fact, Langmuir assumes a monolayer coverage of the solid surface with a constant amount of active sites available which is not related to the system conditions but only on the morphology of the adsorbent material. Even if the variation of q_{max} with temperature is quite common in adsorption of dyes (and in particular of Methylene Blue), this aspect is often neglected (for example see [68,94–96]). In this work the aim is only to highlight this topic underlining the lack of a rigorous theoretical isotherm suitable to describe the adsorption of electrolytic non-volatile compounds such as dyes. However, Polanyi's theory associates physical adsorption to a phenomenon of solid precipitation [97]. According to this point of view, the "apparent" increase of the adsorption capacity at lower temperatures may be due to a decrease of the salt solubility in water.

5.7 Kinetic tests

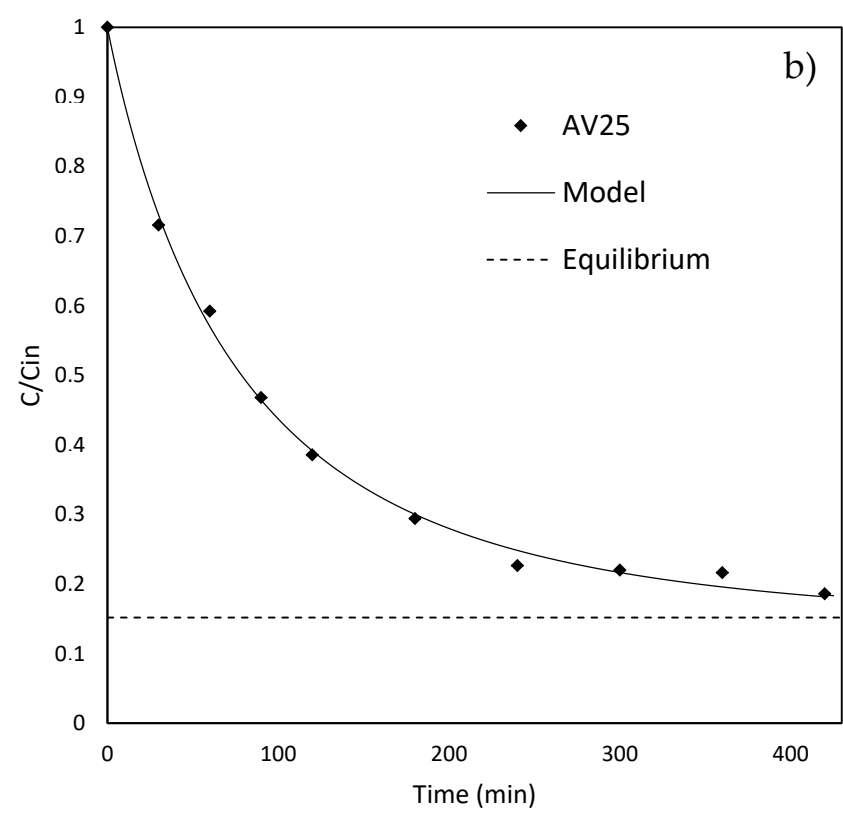
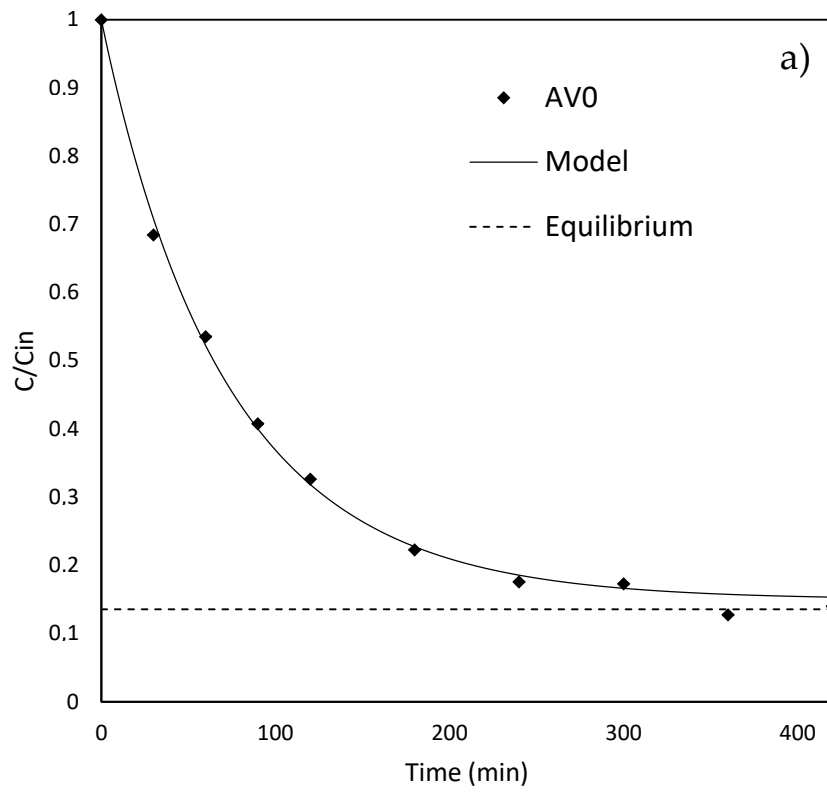
The dynamic model used to describe the adsorption of MB on the types of *Aloe* considered (AV0, AV25 and AV50) was the rigorous model described in the section 2.1.4. It was selected an opportune initial concentration (8.5 mg/L) to operate in the linear region of the isotherm

(see **Figure 5-4**) in order to avoid the dependence of the diffusion coefficient from concentration [98]. Moreover, the boundary conditions were expressed as the CASE 2 shown in section 2.1.4. For these reason, Equation 2.38 is valid and the values of $k_L a$ and the modified effective diffusivity $(\widetilde{D}_s)_e$ were then estimated by fitting the kinetic experimental data using the maximum likelihood method

Commonly, the fitting of such kind of model was focused on finding k_L alone [99] which it is possible to estimate by knowing the density of the solid ($a = \frac{3 M_S}{R V_L \rho_S}$ where ρ_S is the solid density). Since especially for waste derived adsorbents materials the solid density may be of difficult determination, it was decided to fit the entire term $k_L a$ to obtain sufficient information on the liquid film transfer resistance. The value of the particle diameter used in the model was 0.075 cm (the average of the particle size range).

In **Figure 5-9** are reported the kinetic data for AV0, AV25 and AV50 in terms of the variation of the ratio between the concentration of MB in water and its initial concentration. It was decided to not report the error bars in the graph because of the very small experimental error observed. As it is possible to notice in **Figure 5-9**, the theoretical model well represents the experimental behaviour of the system. Furthermore, the χ^2 test was performed to verify the goodness of fit for each estimation imposing a significance level of $\alpha=0.05$ (data not shown).

In order to detect how far the system was from equilibrium at the end of the kinetic test, the ratio between the concentration at equilibrium respect to the initial concentration of the system was calculated by Equation 5.4 and plotted in the graph.



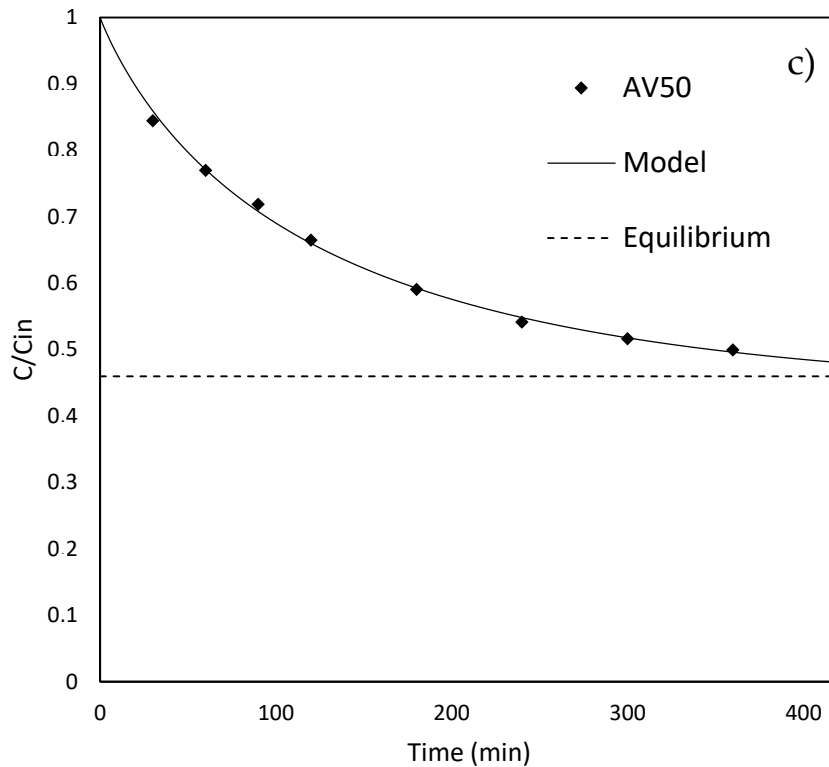


Figure 5-9. Experimental kinetic data for a) AV0, b) AV25 and c) AV50 reported as the ratio between the concentration of Methylene Blue in water and its initial concentration (C/C_{in}) versus time. The solid line represents the model prediction while the dotted line the expected equilibrium threshold [73].

The values of $k_L a$ and $(\widetilde{D}_s)_e$ derived from fitting are reported in **Table 5-5**. As expected, the $k_L a$ calculated for AV0 AV25 and AV50 are of the same order of magnitude since the fluid dynamic conditions set in each test were the same. In particular, the $k_L a$ estimated for AV0 is 7.6% smaller than the one obtained for AV25 and 62.5% higher than the one obtained for AV50. This result could be attributed to some oscillation of the average particle size which in the model was chosen to be 0.75 mm but that can be included in the range of 0.5-1 mm (as explained in the Materials and methods section) or by the lack of setting perfectly the same agitation speed for each test.

As shown in **Table 5-5**, the effective diffusion coefficient $(\widetilde{D}_s)_e$ follows the order of AV50>AV0>AV25. In contrast with the common feeling that the effective diffusion coefficient must increase with the material porosity which it is true only for the pore diffusion coefficient \mathcal{D}_p (for information about the pore volume of the materials see Table 3), $(\widetilde{D}_s)_e$ resulted higher for AV0 than for AV25. This behaviour can be easily explained by means of Equation 2.37 (section 2.1.4) in which the relation between $(\widetilde{D}_s)_e$ and ε , $q_{max}b$ was given. It was discovered that in this case the effective diffusion coefficient follows the same order of $1/q_{max}b$ for each material which is again AV50>AV0>AV25. In other words, it was

find out that the equilibrium terms rather than the porosity play a major role on the determination of the effective diffusion coefficient.

The values calculated in this work for the effective diffusivities of Methylene Blue are comparable with the ones founded in literature. For example, Sáenz-Alanís et al. [100] estimated a diffusivity of $1.7 \cdot 10^{-7}$ cm²/min for the adsorption kinetics of MB on commercial bituminous granular activated carbon (GAC) and a diffusivity of $2.8 \cdot 10^{-7}$ cm²/min for the adsorption kinetics of MB on heat-treated activated carbon (HGAC).

Table 5-5. kinetic fitting parameters at 20 °C for AV0, AV25 and AV50.

Parameter	AV0	AV25	AV50
$k_L a$ (1/min)	$0.013 \pm 5.30 \cdot 10^{-4}$	$0.014 \pm 5.43 \cdot 10^{-4}$	$0.008 \pm 3.9 \cdot 10^{-4}$
$(\widetilde{D}_s)_e$ (cm ² /min)	$5.43 \cdot 10^{-7} \pm 9.02 \cdot 10^{-8}$	$3.89 \cdot 10^{-7} \pm 5.92 \cdot 10^{-8}$	$5.78 \cdot 10^{-7} \pm 4.30 \cdot 10^{-8}$
Bi	12.1	13.6	17.9

The evaluation of the limiting resistance of the process was performed calculating the dimensionless Biot number. The latter is defined as the ratio between the characteristic time of diffusion in the solid (τ_D) respect to the characteristic time of mass transfer (τ_t) from the liquid to the solid phase. By imposing the continuity of the mass flux at the solid boundary [101], the following expression was obtained:

$$Bi = \frac{\tau_D}{\tau_t} = \frac{R^2}{(\widetilde{D}_s)_e} k_L a \frac{V_L}{M_S} \frac{C_{in}}{q_e(C_{in})} \quad (5.5)$$

where $q_e(C_{in})$ (mg/g) is the solid concentration in equilibrium with the initial concentration of MB (C_{in}) in the liquid bulk. As shown in **Table 5-5**, the values of the Biot number for AV0, AV25 and AV50 are all $Bi > 1$ and hence $\tau_D > \tau_t$. This result indicates that the controlling resistance of the adsorption process is the intra-particle one. However, in this case the value of Bi it is still not big enough ($Bi \in [1; 100]$ [102]) to neglect the external mass transfer resistance for the description of the adsorption kinetics.

Conclusions

This chapter investigates the effects that a water-ethanol pre-treatment (not optimized) induces on the adsorption performances of an agro-waste material. In particular, the *Aloe vera* rind was treated with water alone (AV0), with water-ethanol 25% v/v (AV25) or with a water-ethanol 50% v/v (AV50) solution. It was observed that with the increase of the ethanol concentration on the pre-treatment solution, an increase of the adsorption capacity of AV50 and AV25 of about 74% and 56.5% higher than the one of AV0, respectively was calculated and supported by BET-BJH analysis. On the other hand, the affinity of *Aloe vera* respect to the Adsorption of MB (represented by the Langmuir constant) dramatically decreased when the ethanol is used following the order AV0>AV25>AV50. This phenomenon was attributed to the possible adsorption of ethanol on the material surface during pre-treatment. As a matter of fact, TGA analysis revealed a major presence of volatile compounds in the Aloe matrix treated with a higher percentage of ethanol. By means of a thermodynamic analysis it was also confirmed the physical nature of the adsorption mechanism. The implementation of a mathematical model was used to calculate the effective diffusion coefficient for AV0, AV25 and AV50 and it was find out that the affinity toward MB plays a major role for its final value. It was also developed a dimensionless analysis from which the number of Biot was calculated. It was concluded that both intra-particle and film transfer mechanism are important in the adsorption kinetics in the operating condition adopted.

The results obtained increase the knowledge on the effects that a possible extraction step may induce on the adsorption performances of a agro-alimentary waste material. Moreover, it opens a new prospective for the twofold valorisation of *Aloe* waste material.

CHAPTER VI

6. Characterization of waste roots from the As-hyperaccumulator *Pteris vittata* as low-cost adsorbent for methylene blue removal

The ability of the fern *Pteris Vittata* to uptake Arsenic from contaminated water in hydroponic cultures and to store it in its fronds was already highlighted in section 3.3.3. The possible development of long-lasting hydroponic decontamination systems, raises the question of the disposal of As-rich biomass, which constitutes a major cost and hence a crucial issue for the development of phytoremediation technology. As a matter of fact, the phytoremediation project in Huanjiang which lasted two years attributed the 10% of the total cost to the safe disposal of the As-rich biomass [103]. Although several methods were adopted to generate valuable products (bio-oil, bio-char, bio-gas, heat, and As-rich ash) from As-rich PV such as gasification [104], Hydrothermal liquefaction [105], and combustion [106], the income produced is still not enough to make such strategies economically convenient to offset the cost of phytoremediation [107]. To overcome such problem, Cai et al. [107] successfully extracted bio-active compounds (BACs) (i.e. flavonoids, proanthocyanidins, phenolic acids) from PV abating the costs linked to the disposal of PV. In this thesis, another possible approach to this challenge is proposed by giving PV a second life as a new bio-adsorbent for waste-water treatment. From this point of view PV is a by-product of phytoremediation that can be distributed as an adsorbent material avoiding the costs linked to the biomass disposal. The content of the chapter was taken from its corresponding publication of Mazzeo et al. [75].

Materials and methods

6.1 Chemicals

Methylene Blue ($C_{16}H_{18}ClN_3S$; dye content $\geq 82.0\%$), sodium hydroxide (NaOH, purity $\geq 98\%$), sulfuric acid (H_2SO_4 , 95.0 – 98.0 % purity), were purchased from Sigma Aldrich (United States) and used without any further purification.

6.2 Bio-adsorbent preparation

Pteris vittata (PV) plants were grown in hydroponic culture systems according to Marzi et al. [52] using tap water. Waste roots were pretreated before the adsorption tests. The washing step was performed at room temperature by inserting 2 g of PV roots in a 500 ml

beaker filled with 250 mL demineralized water vigorously agitated by a magnetic stirrer for 1h. After that, the roots were dried at 50°C for 24h and cut to reduce their length between 1 – 2 cm. The material was then observed under a High Resolution-Field Emission Scanning Electron Microscope (HR-FESEM, AURIGA Zeiss) operated at 15 kV. The micrographs obtained (a sample is shown in **Figure 6-1**) were processed using the software ImageJ to measure the diameter of each PV root. The average PV diameter was estimated to be 216 μm .

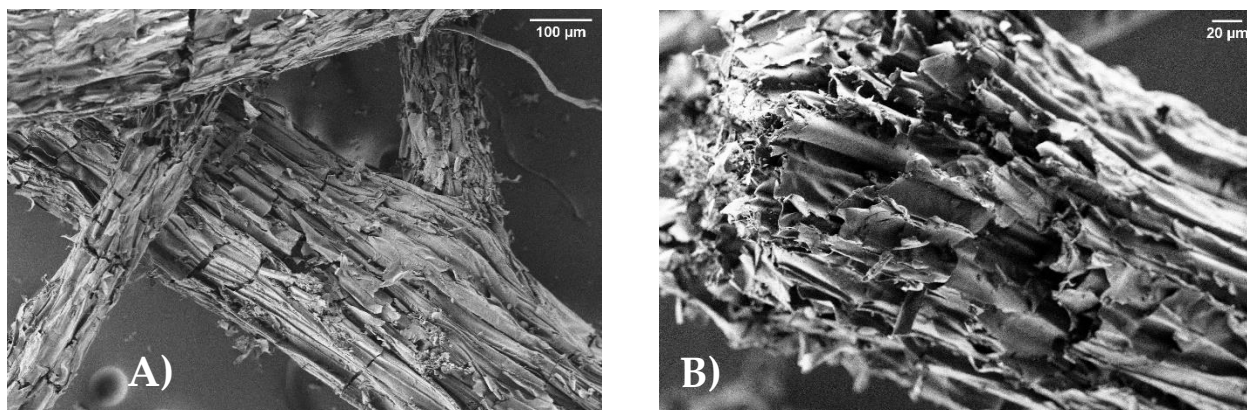


Figure 6-1. Scanning Electron Microscope (SEM) micrographs of pre-treated PV. A) Top view of the root; B) Root section [75].

6.3 Bio-adsorbent characterization

The pH drift method [57] was used to evaluate the zero-point charge (pH_{ZC}) of the PV roots. An amount of 0.04 g of PV was added to 10 mL of ultra-pure water. Before the introduction of the solid, the pH of the solution was adjusted from 2 to 12 by the addition of H_2SO_4 (0.1 M) and NaOH (0.1 M). The pH of the solution was then measured after 24 h which was estimated to be the time required for the system to reach the equilibrium condition. The pH measurement was performed using a Crison GLP 421 pH meter (Hach Company, Crison, Spain). The pH_{ZC} was evaluated graphically in **Figure 6-2** as the point at which the final pH (pH_f) is equal to the initial pH (pH_i) of the solution and was calculated to be 6.2. Since the adsorption on cationic compounds (such as MB) is promoted for $\text{pH} > \text{pH}_{\text{ZC}}$, a neutral pH was selected to perform the adsorption tests.

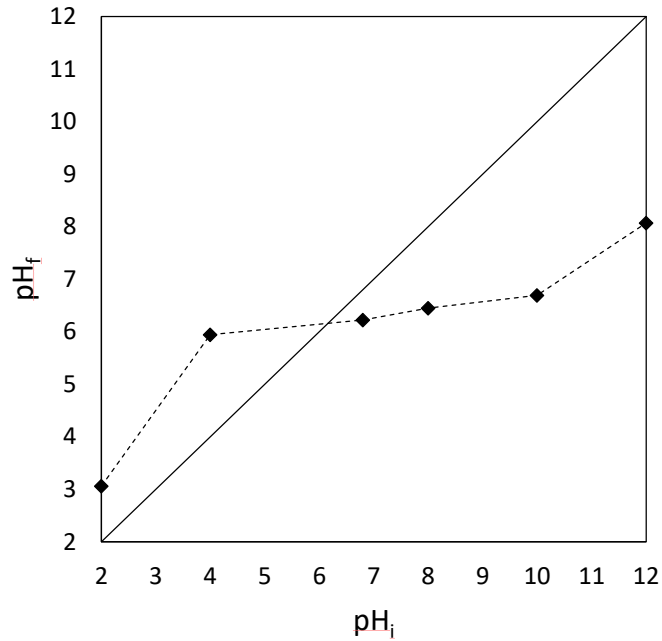


Figure 6-2. Zero-point charge (pH_{zc}) determination for PV. The zero-point charge is represented by the intersection between the characteristic lines for PV and the bisector of the graph [75].

6.4 Batch Tests

Batch tests were performed to characterize the PV roots as an adsorbent material. As commonly used in literature, MB was used as target compound for achieving this scope. In all the tests the concentration of MB in the liquid solution was calculated by PG Instruments (United States) T80+ UV/Vis spectrophotometer (with glass cells of 1 cm path length) at the wavelength of 664 nm.

6.4.1 Equilibrium tests

Equilibrium tests were performed in beakers of 100 mL filled with 50 mL of MB solution in the concentration range of 8.5 mg/L – 212.5 mg/L under constant stirring (220 rpm) for 24 h which was verified from preliminary tests to be enough time for the system to reach the equilibrium condition. The solid dosage was fixed to 0.2 g/L. To investigate the effect of temperature on the system, isotherms were obtained at 20 ± 0.2 °C and 40 ± 0.2 °C. The solid concentration at equilibrium (q_e) was calculated using the following material balance (reported already in Equation 2.19):

$$q_e = \frac{V}{M_S} (C_{in} - C_e) \quad (6.1)$$

where V (mL) is the liquid volume of the solution, M_S (g) is the mass of the solid adsorbent, C_{in} (mg/L) is the concentration of MB at the beginning of the test and C_e (mg/L) is the concentration of MB at equilibrium. Each test was reproduced at least in triplicate.

6.4.2 Kinetic tests

All the tests of this section were performed in a 100 mL beaker filled with an opportune amount of liquid to obtain the desired solid dosage (solid-liquid ratio). Moreover, the stirring speed was kept constant at 220 rpm while the initial concentration of Methylene Blue (MB) was set at 4.5 mg/L.

To establish at which solid dosage the kinetic tests had to be performed, preliminary experiments were conducted. The latter consists of measuring the concentration of MB after 110 minutes and calculating the corresponding removal percentage (R%) of MB for different solid-liquid ratios at a constant temperature of 20 ± 0.2 °C. The amount of solid, liquid volume and the resulting solid dosage adopted, were reported in **Table 6-1** while the removal percentage was obtained by solving Equation 6.2:

$$R\% = \frac{C_{in} - C(t)}{C_{in}} \cdot 100 \quad (6.2)$$

Kinetic tests were performed for the solid dosages of 0.187 g/L, 0.350 g/L, 0.875 g/L (the amount of solid and liquid used it is again the one reported in **Table 6-1**) at both 20 ± 0.2 °C and 40 ± 0.2 °C temperatures. Each test lasted 110 minutes and the concentration of MB was measured during time (since the measure was non-destructive the volume of the solution remained constant during the duration of the experiment). Each test was reproduced at least in duplicate. The experimental data were fitted using a mathematical model (discussed in the following section) employing the process simulator gProms (Process System Enterprises, London, UK) to estimate the parameters of the model and detect the controlling resistance of the system.

Table 6-1. Preliminary kinetic tests dosage (g/L) according to the amount of solid and liquid used.

Solid (g)	Liquid (mL)	Dosage (g/L)
0.005	80	0.062
0.010	70	0.142
0.015	80	0.187
0.015	70	0.214
0.015	60	0.250
0.014	40	0.350
0.035	40	0.875

Results and Discussion

6.5 Equilibrium

The isotherms obtained using *Pteris vittata* (PV) at 20°C and 40°C were reported in **Figure 6-3**. Since the experimental data showed a typical saturation behaviour, the Langmuir isotherm was selected to describe the system at equilibrium. The Langmuir equation was given in section 2.1.2 and is reported below in Equation 6.3

$$q_e = q_{max} \frac{bC_e}{1 + bC_e} \quad (6.3)$$

where b (L/mg) is the equilibrium constant of the Langmuir model related to the affinity between MB and the active sites, q_{max} (mg/g) is the maximum adsorption capacity.

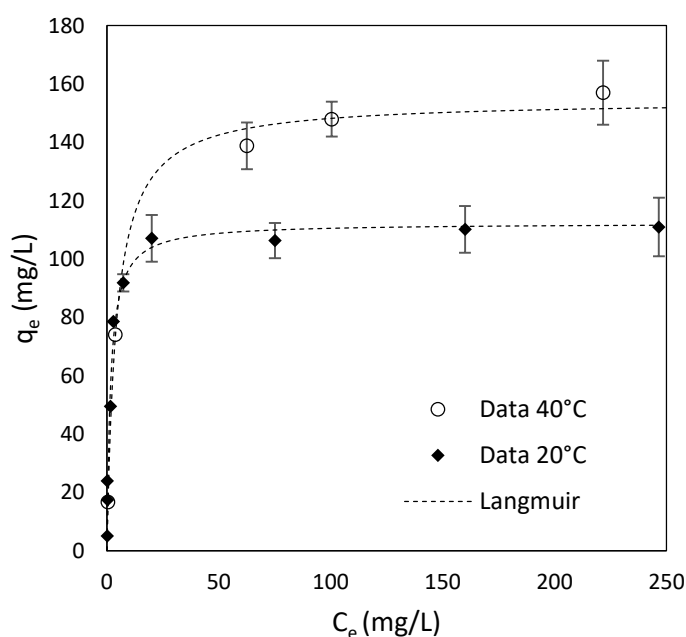


Figure 6-3. Isotherms of *Pteris vittata* (PV) for the adsorption of Methylene Blue at 20°C and 40°C [75].

The Langmuir constants (q_{max} and b) were estimated for each case using the least square non-linear regression method and their values were reported in **Table 6-2**. Langmuir isotherm parameters for PV at 20°C and 40°C, together with their corresponding Root Mean Square Error (RMSE).

Table 6-2. Langmuir isotherm parameters for PV at 20°C and 40°C.

Parameter	20°C	40°C
q_{max} (mg/g)	112.34	154.39
b (L/mg)	0.62	0.24

RMSE (mg/g)	5.71	3.65
-------------	------	------

According to the results of the regression shown in **Table 6-2** a 37% increase of the maximum adsorption capacity q_{max} and a 61% decrease of the Langmuir constant b with respect to the values of the same parameters at 20°C were observed. This because, although at 20°C the material has a higher affinity toward the adsorption of MB, it shows a smaller maximum adsorption capacity due to the thermodynamic condition of the process. It is important to underline that despite the wide usage of the Langmuir model to describe isotherms that present a saturation behaviour, the Langmuir isotherm does not predict the variation of q_{max} with temperature. As happened in this study, several articles in literature observed an increase of the maximum adsorption capacity of MB for different materials [68,94,95,99] and used the Langmuir isotherm to calculate the thermodynamic parameters (ΔG , ΔH , ΔS). In such works it was concluded that the behaviour was due to the endothermic nature of the adsorption mechanism. However, an endothermic behaviour it is always a delicate topic when coupled with adsorption. J. M. Thomas [108] stated that endothermic adsorption exists only for chemisorption and happens in very specific cases such as the dissociative chemisorption of molecular hydrogen which occurs with an increase of entropy. For this reason, in absence of calorimetric data, it was not possible to establish the thermodynamic nature of the adsorption of MB on PV roots (endothermic/exothermic). MB is a non-volatile electrolyte that interacts both with the solvent and the adsorbent material. The formulation of a rigorous explanation for the behaviour of MB adsorption is out of the scope of the present paper, however, it is important to underline the lack of a comprehensive theory that justifies it. Furthermore, in this case, as happened in the work of Xue et al. [109] for the adsorption of MB on activated carbon obtained from waste biomass (ABAC), the Langmuir constant b decreases with temperature even though its adsorption capacity increases. This behaviour could be again attributed to the particular interactions that occur in the system rather than finding explanations in the physical meaning of the Langmuir isotherm. As discussed by Demiral et al. [110] a possible explanation to this result could be an enlargement of the material pores due to the temperature increase which may enhance the number of active sites available.

The Langmuir parameters reported in literature for other agro-waste adsorbents were collected and reported in **Table 6-3** to compare their performances for adsorption of MB with that of *Pteris vittata* (PV). From **Table 6-3** it is possible to observe that there are others waste materials that have a higher adsorption capacity than PV such as papaya seeds, grass waste, rice husk and cotton waste. However, this information is just partial since the Langmuir constant b must be also considered in the comparison between adsorbent materials. As a matter of fact, *Pteris vittata* shows a two orders of magnitude bigger value of b with respect to the aforementioned materials highlighting its great affinity toward MB. This observation is quantified in **Table 6-3** with the product $q_{max}b$ which represents the

angular coefficient of the linear region of the isotherm for low concentrations. It is easy to notice that PV has the second highest $q_{max}b$ value second only to Tea waste. It is clear that the choice of the best adsorbent depends on the initial concentration of MB in the solution to treat, however these results suggest that PV have good performances for MB uptake.

Table 6-3. Langmuir isotherm parameters for agro-waste adsorbents.

Bio-adsorbent	T (°C)	pH	q_{max} (mg/g)	b (L/mg)	$q_{max}b$ (L/g)	Reference
Papaya seeds	30	7	555.5	0.0028	1.55	[71]
Grass waste	30	7	457.6	0.0023	1.05	[72]
AV50 ¹⁸	20	7	346.52	0.018	6.23	[73]
Rice husk	20	7	312.2	0.0171	5.33	[74]
AV25 ¹⁷	20	7	311.81	0.12	37.41	[73]
Cotton waste	20	7	277.7	0.009	2.49	[74]
AV0 ¹⁷	20	7	199.13	0.17	33.85	[73]
Pteris waste roots	20	7	112.3	0.62	69.62	[This study]
Tea waste	25	8	85.1	1.26	107.22	[76]
Peanut hull	20	5	60.05	0.16	9.60	[64]
Yerba Mate	25	6	59.6	0.02	1.19	[90]
Passion fruit waste	25	8	44.70	0.002	0.08	[70]
Apricot shells	25	5	24.31	0.002	0.04	[67]
Banana peel	30	7	20.8	0.06	1.24	[65]
Chaff	25	7	20.03	0.22	4.40	[63]
Spent coffee grounds	25	5	18.72	0.27	5.05	[69]
Orange peel	30	7	18.6	0.05	0.93	[65]
Wheat shells	30	7	16.56	0.02	0.33	[68]

¹⁸ AV stands for Aloe Vera as introduced in Chapter 5.

6.6 Kinetic tests

The results of the preliminary kinetic tests were reported in **Figure 6-4** together with the expected values of q_e and $R\%$ at equilibrium (dotted line). The latter were obtained solving simultaneously Equations 6.1 and 6.3 once estimated q_{max} and b from equilibrium data (see the previous section). Observing **Figure 6-4** it was noticed that only above the solid dosage of 0.25 g/L the experimental points (collected after just 110 minutes) followed the theoretical equilibrium curve. In fact, below such threshold the values obtained for $R\%$ and q were underestimated and overestimated respectively. This behaviour is due to the rate of the process which increases with the solid dosage. Once explored how fast was the process changing the solid dosage it was possible to select the adequate solid-liquid ratios to perform the kinetic tests for 110 min.

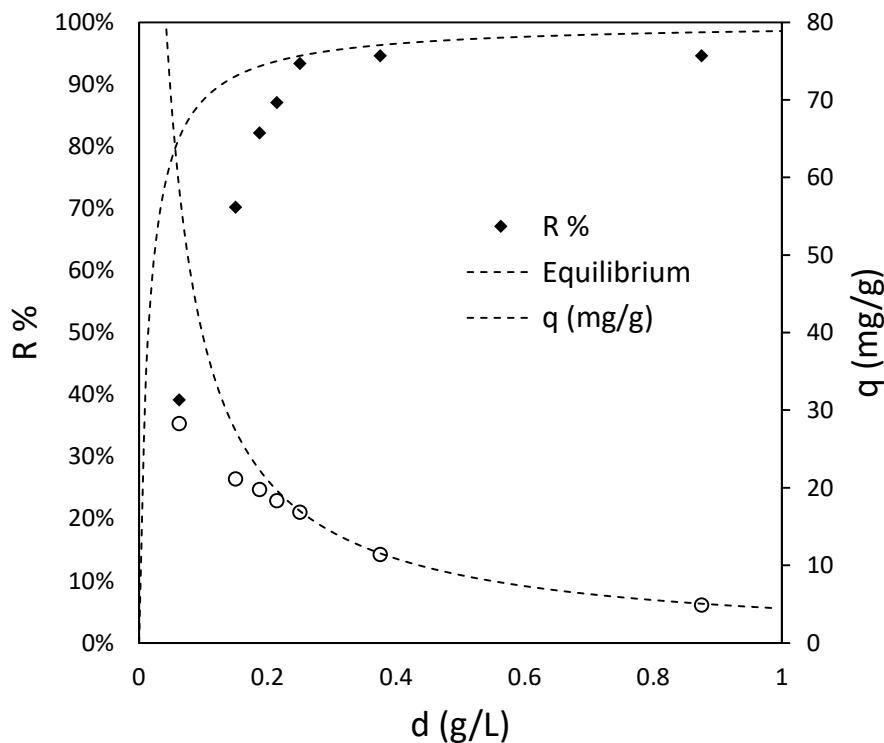
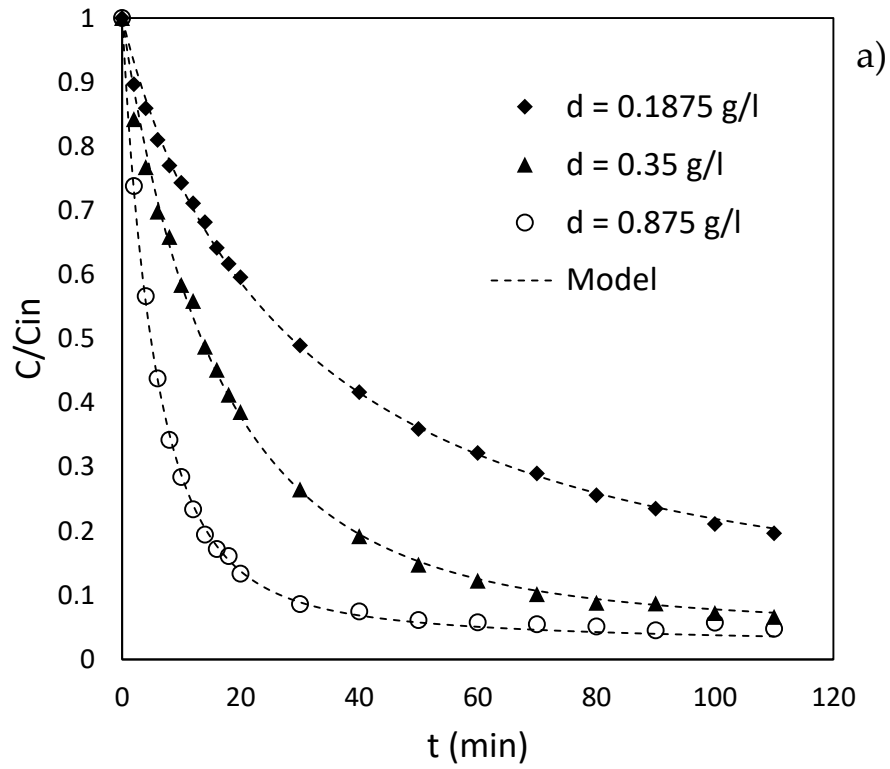


Figure 6-4. Preliminary experimental results (solid concentration q , percentage of MB removed $R\%$) for batch tests at 20°C, initial concentration of MB 4.5 mg/L and duration of the test 110 min for different solid dosages. The dotted lines represent the expected values at equilibrium [75].

The dynamic model used to describe the batch adsorption of Methylene blue on *Pteris vittata* (PV) was described in section 2.1.4 adopting CASE 2 boundary conditions and choosing an initial concentration of 4.5 mg/L of MB which lies in the linear region of the isotherms (as shown in **Figure 6-3**). In such conditions, the diffusivity coefficient is no longer dependent on concentration and it is assumed valid the Equation 2.38. The latter was used in this study to fit the kinetic experimental data and to calculate the values of $k_L a$ and $(\overline{D}_s)_e$ using as

parameter estimation technique the maximum likelihood method. The error variance was considered constant since no dilutions were required in the range of concentrations adopted during the kinetic runs.

The value of the cylindrical diameter used in the model was 216 μm according to SEM analysis as reported in the section 6.2. "Bio-adsorbent preparation".



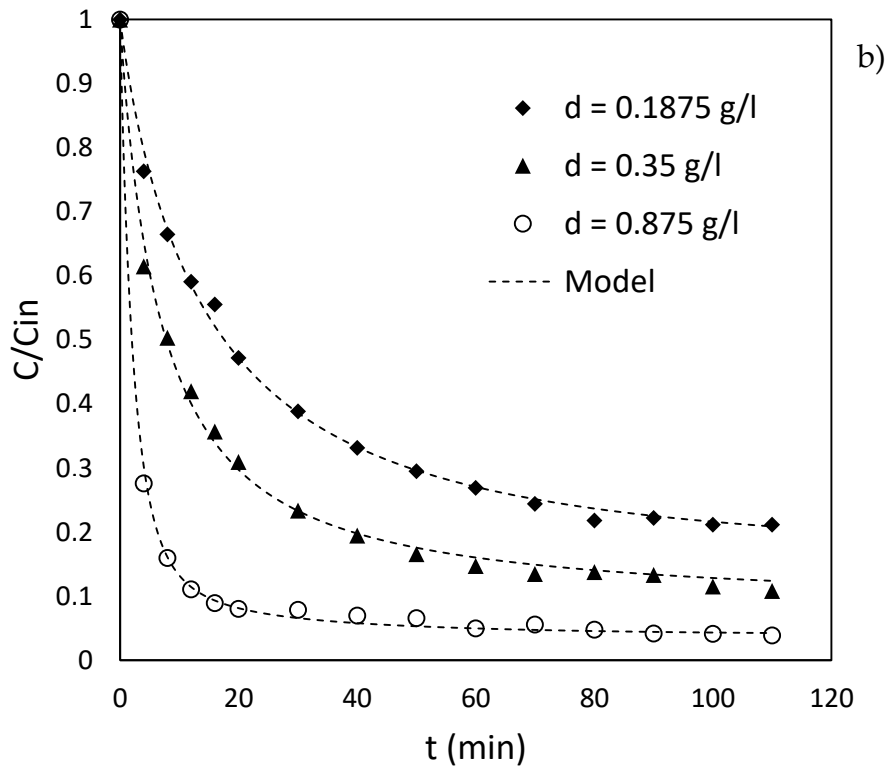


Figure 6-5. Kinetic test results for different solid dosages at 20°C a) and 40°C b). The initial concentration of MB used was 4.5 mg/L [75].

In **Figure 6-5** were reported the kinetic data of the uptake of MB for different solid dosages (solid-liquid ratios) at 20°C (**Figure 6-5 a**) and 40°C (**Figure 6-5 b**). The experimental points were plotted as the ratio between the concentration measured at a certain time of the test and the initial one. It was decided to not report the error bars in the graph because of the very small experimental error observed. As shown in **Figure 6-5** the model well represents the behaviour of the system, moreover the goodness of fit for each estimation was evaluated with the chi-squared test (χ^2) test selecting a significance level of $\alpha = 0.05$ (data not shown).

The values of $k_L a$ estimated were reported together with their standard deviation in **Figure 6-6**. As expected, the mass transfer coefficient $k_L a$ increases with temperature and linearly with the solid dosage. In fact, it is simple to verify that

$$k_L a = k_L \frac{2}{\rho_s R} d \quad (6.4)$$

where d (g/L) is the solid dosage. By means of a linear regression (see **Figure 6-6**) it was then possible to calculate $k_L \frac{2}{\rho_s R}$ which was 0.596 (L g⁻¹ min⁻¹) and 0.199 (L g⁻¹ min⁻¹) at 40°C and 20°C respectively and to detect an increase of the mass transfer coefficient (k_L) of 200% by switching the temperature from 20°C to 40°C. The estimations of the effective diffusivity coefficients were reported in **Table 6-4**. The effective diffusivity obtained at a specific temperature (20°C or 40°C) was then calculated as the average of all the estimated values

for such temperature. As expected, the effective diffusivity increases with temperature. More precisely it rises of 38.5%. The order of magnitude of the effective diffusivity ($\sim 10^{-8}$ cm²/min) suggests solid surface diffusion as the main intra-particle mass transfer mechanism [111].

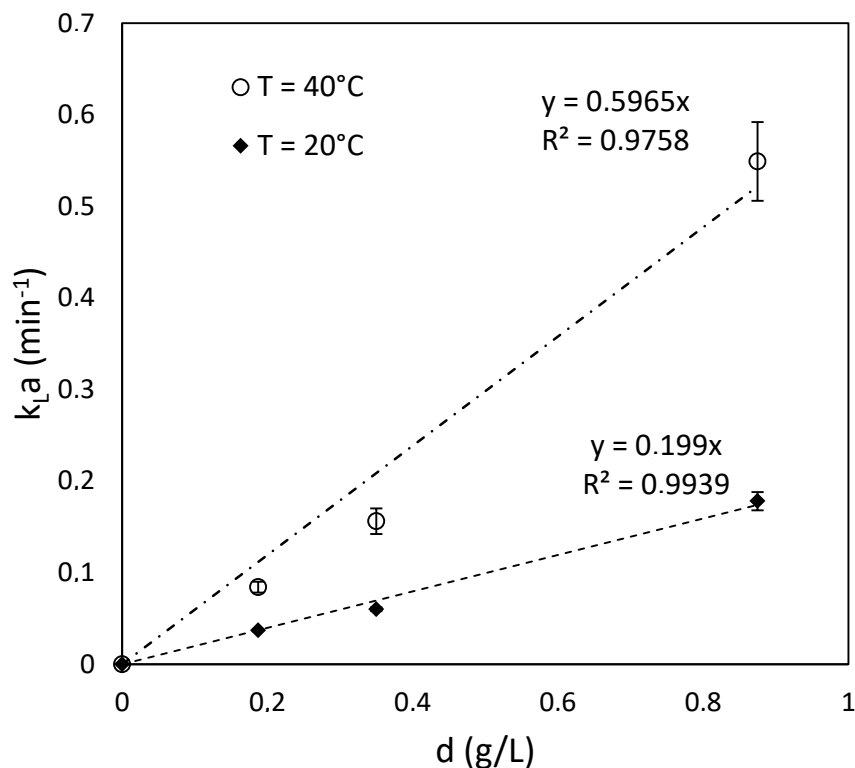


Figure 6-6. Values of $k_L a$ and their standard deviation obtained from each estimation at 20°C and 40°C. The dotted lines represent the result of the linear regression together with the linear expression obtained and the correspondent value of R^2 [75].

Table 6-4. Estimated values for the effective diffusion coefficient at 20°C and 40°C.

Solid dosage (g/L)	$(\widetilde{D}_s)_e, 20^\circ\text{C}$ (cm ² /min)	$(\widetilde{D}_s)_e, 40^\circ\text{C}$ (cm ² /min)
0.187	$5.52 \cdot 10^{-8}$	$10.01 \cdot 10^{-8}$
0.35	$7.34 \cdot 10^{-8}$	$8.93 \cdot 10^{-8}$
0.875	$5.15 \cdot 10^{-8}$	$9.77 \cdot 10^{-8}$
Average ± SD	$5.99 \cdot 10^{-8} \pm 9.6 \cdot 10^{-9}$	$9.56 \cdot 10^{-8} \pm 4.5 \cdot 10^{-9}$

To evaluate the controlling resistance of the adsorption system, the dimensionless number of Biot was calculated. The Biot dimensionless number was theoretically derived from the

flux continuity condition on the boundary of the solid particles [101] and represents the ratio between the characteristic time of solid diffusion (τ_D) respect to the characteristic time of mass transfer (τ_t) across the liquid film around the solid particles. After some manipulations of the standard definition, the following expression was obtained:

$$Bi = \frac{\tau_D}{\tau_t} = \frac{R^2}{(\widetilde{D}_s)_e} k_L a \frac{V_L}{M_S} \frac{C_{in}}{q_e(C_{in})} \quad (6.5)$$

where $q_e(C_{in})$ (mg/g) is the adsorbed phase concentration in equilibrium with the initial bulk concentration C_{in} . In **Table 6-5** were collected all the results of the parameter estimation and the corresponding values of the Biot number (Bi). For both 20°C and 40°C $Bi > 1$ and hence $\tau_D > \tau_t$ which means that the intra-particle mass transfer is the controlling resistance of the adsorption kinetics. However, when $Bi \in [1; 100]$ the external mass transfer resistance plays as well an important role in the process and (under the specific mixing conditions adopted) cannot be neglected [102]. It is important to keep in mind that it is not possible to modify the diameter of the roots and hence the intra-particle resistance which controls the mass transfer rate can't be reduced.

Table 6-5. Estimated values of the dimensionless Biot number (Bi) at 20°C and 40°C.

Parameter	20°C	40°C
k_L/ρ_s (cm L/min g)	$9.95 \cdot 10^{-4}$	$2.98 \cdot 10^{-3}$
$(\widetilde{D}_s)_e$ (cm ² /min)	$5.99 \cdot 10^{-8}$	$9.56 \cdot 10^{-8}$
Bi	18	35

Conclusions

In this chapter the waste roots of the fern *Pteris vittata* were characterized as low-cost adsorbent materials for the uptake of Methylene Blue (MB) from a synthetic water. First of all, the material was washed with demineralized water in order to remove all the impurities due to hydroponic cultivation. A neutral pH condition was selected to perform the adsorption tests. From the equilibrium batch tests it was found out that the Langmuir isotherm well represents the behaviour of the system. Moreover, the adsorption capacity of the material as well as the its Langmuir constant were estimated ($q_{max}=112.34$ mg/g, $b =0.62$ at 20°C and $q_{max}=154.39$ mg/g, $b =0.24$ at 40°C). It was observed how the adsorption capacity increases with temperature while the Langmuir constant b (L/mg) decreases: this phenomenon was attributed to the effect of temperature on the interaction between MB molecule and PV (enlargement of pore sizes). Compared to other agro-waste materials, the *Pteris vittata* waste roots showed good performances and should be considered as promising adsorbent material for MB removal. It was also investigated the kinetic of MB uptake and

in particular it was estimated the effective diffusion coefficient for MB which increased with temperature ($5.99 \cdot 10^{-8}$ at 20°C and $9.56 \cdot 10^{-8}$ at 40°C). From the kinetic results it was then calculated the Biot number which highlighted that both the intra-particle mass transfer as well as the mass transfer across the liquid film are important for the description of the adsorption kinetics.

CHAPTER VII

7. Fixed-bed adsorption of Methylene Blue on *Pteris Vittata* bio-adsorbent

In this chapter continuous operation mode experiments for the uptake of Methylene Blue from water will be provided. It was decided to deeply investigate this topic only for the fern *Pteris Vittata*. The reason why of such choice was made on the following consideration:

- *Aloe Vera*. The rind of aloe Vera was affected by a huge swelling phenomenon. As a matter of fact, it was measured the particle size distribution by means of sieve trays before and after inserting the material in distilled water for 1h and a dramatic increase of the particle diameter was observed. As shown in **Figure 7-1** almost all the material enhanced its dimension above 1mm of diameter. This aspect caused many issues during the column preliminary tests since the high packing of the solid led to liquid losses.

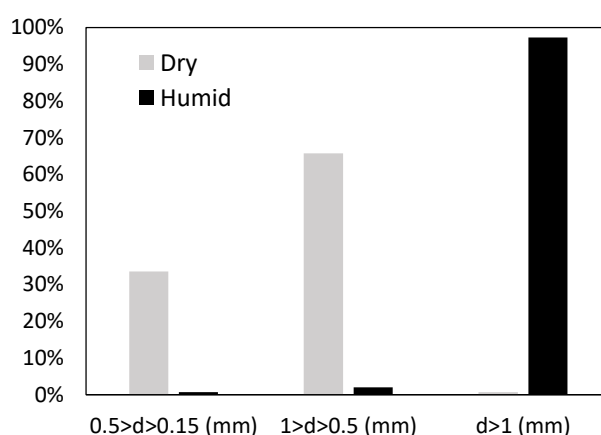


Figure 7-1 Aloe Vera Particle size distribution in dry and wet status.

- *Yerba Mate*. the adsorption capacity of Yerba Mate is almost half with respect to the one of *Pteris Vittata* (see **Table 6-3**).

Materials and methods

7.1 Chemicals

Methylene Blue ($C_{16}H_{18}ClN_3S$; dye content $\geq 82.0\%$) was purchased from Sigma Aldrich (United States) and used without any further purification.

7.2 Bio-adsorbent

Pteris vittata (PV) roots were prepared as described in section 6.2.

7.3 Experimental set-up and column tests

Fixed-bed adsorption runs were carried out in a glass column (1 cm internal diameter). At the bottom of the column was located a porous glass septum used to support the solid adsorbent. The column was filled with 0.232 g of solid in all tests but in T1 and T2 the length of the roots was around 0.8 cm, while in the others it was of 0.4 cm hence the bed height (H) varied accordingly as reported in **Table 7-1**. Liquid inlet solution of Methylene Blue (MB) was continuously fed to the bottom of the column by means of a variable speed peristaltic pump. This configuration was selected to assure a complete wetting of the adsorbent bed since it generates the establishment of a liquid hold-up or, in other words, it fully fills the column of liquid during the adsorption tests. As a matter of fact, it was observed that (in the range of fluid flow rate analyzed 5.9-13.6 ml/min) if the liquid had been fed to the top of the column, droplets of liquid would have been observed wetting the bed without guaranteeing its complete coverage. It is worth noting that upflow promotes the drag of solid particles especially when the intrinsic density of the solid is lower of the liquid one (carbonaceous materials happen to be so respect to water). In order to prevent the movement of particles within the bed it is suggested [112] to set the fluid upflow rate less than about 80% of the minimum fluidization velocity. However, in this study the top of the adsorbent bed was covered by two layers of glass spheres of 1 mm and 50 mm in diameter respectively that avoided solid drag. For this reason, higher velocities than the minimum fluidization one were reached. The column was equipped with a thermostat jacket in order to keep the temperature at 20 ± 0.1 °C. Before the beginning of each test the bed was rinsed with distilled water for 1 h to remove dust or other residues and to reach the complete wetting of the solid surface. A summary of the operating conditions used in the experimental runs was presented in **Table 7-1**. In all the tests the concentration of MB in the liquid solution was calculated by PG Instruments (United States) T80+ UV/Vis spectrophotometer (with glass cells of 1 cm path length) at the wavelength of 664 nm. The experimental data were fitted using a mathematical model (discussed in the following section) employing the process simulator gProms (Process System Enterprises, London, UK) to estimate the parameters of the model and detect the controlling resistance of the system.

Table 7-1 Operating conditions of experimental runs. ($T = 20 \pm 0.1 \text{ }^\circ\text{C}$, $M_s = 0.232 \text{ g}$)

Test	$H \text{ (cm)}$	$Q \text{ (ml/min)}$	$C_{in} \text{ (mg/L)}$
T1	4.5	6.8	6.5
T2	4.5	13.6	7.8
T3	3	5.9	6.1
T4	3	7.7	5.9

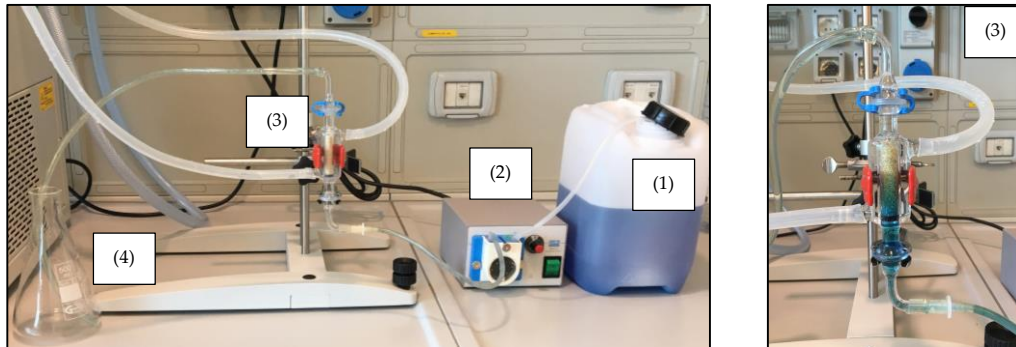


Figure 7-2 Column experimental set-up: (1) Vessel for the storage of the inlet solution; (2) Peristaltic pump; (3) glass column provided of thermostatic jacket; (4) outlet solution drum

7.4 Bed void fraction and solid apparent density estimation

The estimation of the bed void fraction is crucial to avoid mistakes in the comprehension of the mass transfer conditions occurring in the adsorption process. The method developed in this study is based on the measurable time of permanence of the liquid in the column. The interstitial velocity is higher than the superficial one (the definition was given in section 2.1.5) thus the observed residence time in the unit is lower than the one that would exist without packing. According to such consideration, when the packed bed was filled for the first time by distillate water for the rinse, the effective residence time of the liquid was measured (τ^*). Setting the liquid flow rate (Q) and knowing the column height (H) and diameter (R_c), the bed void fraction (ε) was calculated as follows

$$\varepsilon = \frac{Q\tau^*}{H\pi R_c^2} \quad (7.1)$$

Once obtained the value of the bed void fraction it was also possible to evaluate the material apparent density (ρ_s) using Equation 7.2. This step is of fundamental importance when dealing with waste materials since their properties are often unknown.

$$\rho_s = \frac{M_s}{(1 - \varepsilon)H\pi R_c^2} \quad (7.2)$$

For each test performed such method was applied and the results were collected in **Table 7-2**. The validity of the method was verified since the resulting density was almost the same for every test. The average density was calculated to be 299 g/L and this value will be used in the numerical simulation of the continuous kinetic modeling. The test T5 was used just as an additional run for the estimation of the solid density while for all the other tests the kinetic behavior was also investigated.

Table 7-2 Evaluation of the solid intrinsic density of *Pteris Vittata* based on the bed void fraction estimation for each test. ($M_s = 0.232 \text{ g}$)

Test	$H \text{ (cm)}$	$Q \text{ (ml/min)}$	$\tau^* \text{ (s)}$	ε	$\rho_s \text{ (g/L)}$
T1	4.5	6.90	24	0.781	300.3
T2	4.5	7.50	22	0.778	296.5
T3	3	7.07	13.3	0.665	294.4
T4	3	7.95	12	0.675	303.2
T5	3	7.05	13.5	0.674	301.7
Average \pm DS					299.2 \pm 3.6

Results and Discussion

The model used to describe the breakthrough curves of Methylene Blue (MB) during time for all the fixed-bed adsorption tests, was the “real column” model presented in section 2.1.5 by Equations 2.51 and 2.52 based on the Linear Driving Force (LDF) approximation and the presence of longitudinal dispersion (E_z). The latter effect can be calculated from an appropriate dimensionless expression of Peclét number ($Pé$) taken from literature. As a matter of fact, several works dealt with the formulation of a generalized correlation for the prediction of longitudinal dispersion in packed beds. It is worth to mention, for the scope of this study, the works of Chung and Wen [113] and Leitão et al. [114] that developed an empirical correlation of $Pé$ as a function of the Reynolds number (Re) for liquid solutions flowing in fixed packed beds columns. Such expressions were collected in **Table 7-3** together with their range of application. For further information on this topic, a deep review was developed by Delgado [115,116]. The Peclét number ($Pé$) and the Reynolds number (Re) are defined as follows:

$$Pé = \frac{H \langle v \rangle}{E_z}; Re = \frac{\rho_L \langle v \rangle d_p}{\mu_L} \quad (7.3)$$

where $\langle v \rangle$ is the superficial velocity, ρ_L is the liquid density, μ_L is the liquid viscosity and d_p is the diameter for spherical solid particles. In this case the shape of the solid was

assumed cylindrical, hence d_p was substituted by an equivalent diameter (d_e) calculated as shown in Equation 7.4.

$$d_e = 2 \sqrt[3]{\frac{3}{4} R_r^2 L_r} \quad (7.4)$$

where L_r and R_r are the length and the radius of the roots respectively. The equivalent diameter was calculated to be 0.078 cm and 0.062 cm for T1, T2 and T3, T4 respectively. Among the two correlation proposed, it was selected the one of Chung and Wen due to its wider range of validity.

Table 7-3 Empirical expression for the evaluation of $Pé$ in liquid-solid fixed bed columns.

Expression	Range of application	Reference
$Pé = \frac{H}{d_p} 0.508 Re^{0.02}$	$Re \in [1; 50]$ $\varepsilon \in [0.43; 0.56]$	Leitão et al. [114]
$Pé = \frac{H}{d_p} [0.2 + 0.011 Re^{0.48}]$	$Re \in [10^{-3}; 10^3]$	Chung and Wen [113]

At this point, the only unknown parameter of the model is $k_{LDF}a$ that was used as an adjustable parameter to perform data fitting using the maximum likelihood method as estimation technique. The error variance was considered constant since no dilutions were required in the range of concentrations adopted during the kinetic runs. The thermodynamic equilibrium was described using the Langmuir isotherm according to the results obtained in the previous chapter (and the corresponding publication [75]). Thus, the value of the maximum adsorbed capacity for unit mass of adsorbent (q_{max}) and the Langmuir constant b were set as 112.34 mg/g and 0.62 L/mg respectively. A summary of the common parameters to all the kinetic tests and their corresponding values used in the theoretical model were listed in **Table 7-4**

Table 7-4 Values of the common parameters to all the kinetic tests used in theoretical model .

Parameter	Description	Value (UDM)	Reference
ρ_s	Solid apparent density	299.2 g/L	[This work]
q_{max}	Maximum adsorption capacity	112.34 mg/g	[75]
b	Langmuir constant	0.62 L/mg	[75]

The experimental results together with the model predicted MB breakthrough curves were reported in **Figure 7-3 (a)** and **Figure 7-3 (b)** for the roots of length 0.8 cm and 0.4 cm respectively. It was observed that the model well represents the behaviour of the system, moreover the goodness of fit for each estimation was evaluated with the chi-squared test (χ^2) test selecting a significance level of $\alpha = 0.05$ (data not shown). The values of $k_{LDF}a$ estimated were reported in **Figure 7-4** with their corresponding confidence interval versus the Reynolds number. It is immediately noticeable that the estimated parameters seem to lie on a straight line passing from the axis origin. Interestingly, $k_{LDF}a$ seems also not to be affected on the bed void fraction variation nor from the length of the roots. In particular, by means of a linear regression, the relation in Equation (7.5) was obtained showing a $R^2 = 0.989$.

$$k_{LDF}a = 0.45Re \quad (7.5)$$

This result clearly evidences a strong dependence of the LDF mass transfer coefficient from the liquid flow rate, thus proving that the external mass transfer resistance plays a key role in the kinetics of the adsorption process. Moreover, according on such finding, it apparently seems that no mass transfer should occur when $Re \rightarrow 0$ which is obviously not true. In other words, assuming negligible for a moment the intra-particle resistance, the concern regards the possibility that the dimensionless Sherwood number (Sh) (defined as shown in Equation 7.6 where D_m is the molecular diffusion and k_c is the external liquid mass transfer coefficient) goes to zero when $Re \rightarrow 0$.

$$Sh = \frac{k_c d_e}{D_m} \quad (7.6)$$

There are many examples in literature of Sherwood expressions that predict $Sh \rightarrow 0$ when $Re \rightarrow 0$ and some of them were collected in **Table 7-5**. This topic was also deeply discussed by Ruthven in his famous book "*Principle of adsorption and Adsorption processes*" [112]. It concluded that an erroneous underestimation of the axial dispersion coefficient leads to an erroneous low values for the mass transfer coefficient. Then, it is possible that, in this work, the expression of Chung and Wen provides an underestimation of the real effect of longitudinal dispersion. Unfortunately, also the expression of Leitão et al. led to similar results (data not showed).

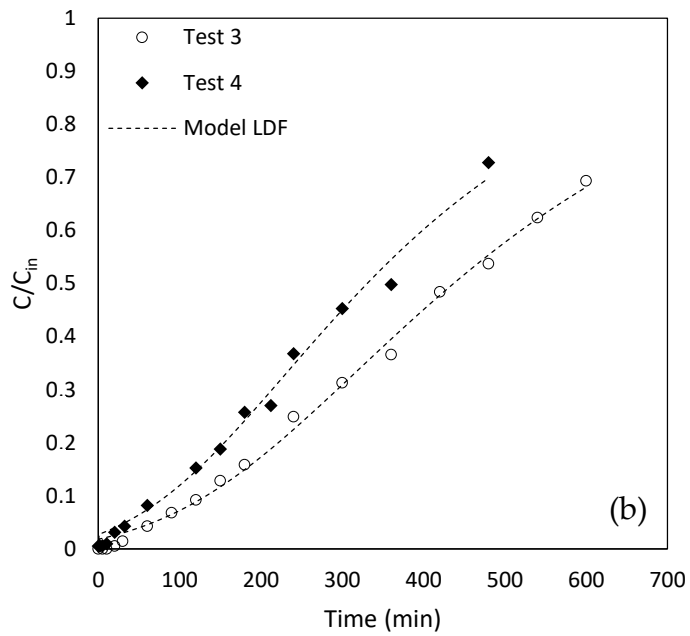
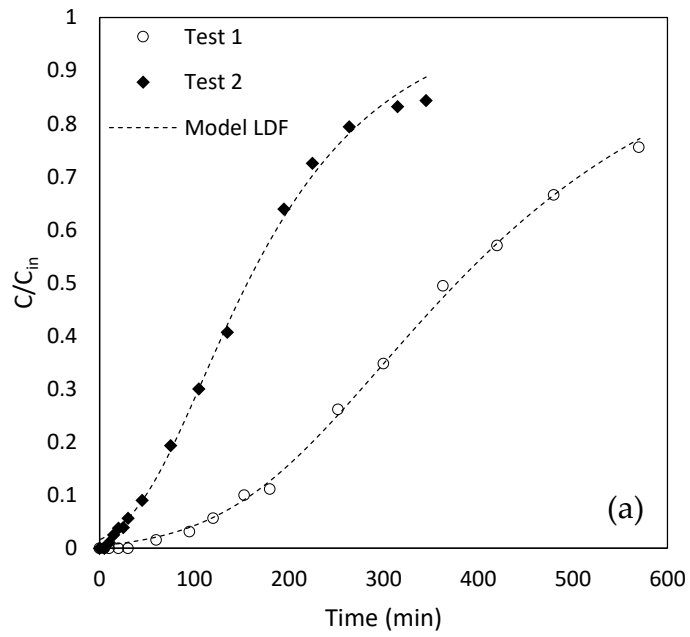


Figure 7-3 MB experimental and predicted breakthrough curves at 20°C for *Pteris Vittata* roots of 0.8 cm (a) and 0.4 cm (b) of length.

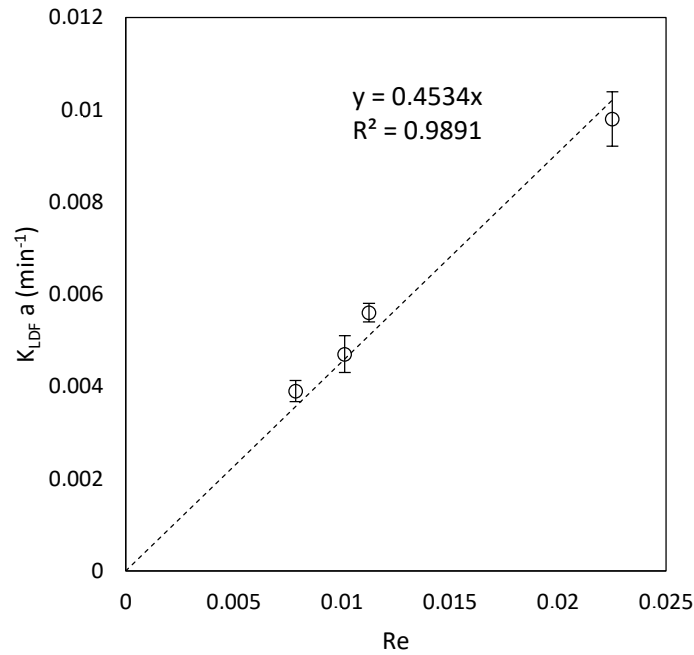


Figure 7-4 Plot of the estimated parameter $k_{LDF} a$ versus the Reynolds number Re . The error bars correspond to the confidence interval with a significance level of $\alpha = 0.02$.

Table 7-5 Empirical expression for the evaluation of Sh in liquid-solid fixed bed columns for low Reynold's numbers¹⁹.

Expression	Range of application	Reference
$Sh = \frac{1.09}{\varepsilon} Re^{0.33} Sc^{0.33}$	$0.0015 < Re < 50$	Wilson and Geankoplis [117]
$Sh = \frac{1.05}{\varepsilon} Re^{0.33} Sc^{0.33}$	$Re < 10$	Kumar et al. [118]
$Sh = \frac{0.18}{(1 - \varepsilon)^{1/3}} \left[\frac{1}{(1 - \varepsilon)^{1/3}} - 1 \right] Re Sc^{2/3}$	$Re \rightarrow 0$	Nelson and Galloway [119]

At this point, in order to verify and validate the expression of Equation 7.6, an additional column run (V1) was performed at $T = 20 \pm 0.1^\circ C$ with the aim of predicting the experimental trend. The particular operating conditions of the test V1 were reported in **Table 7-6** (in the model were also used the values shown in **Table 7-4**). The result was provided in **Figure 7-5** showing a good prediction of the experimental points.

¹⁹ Sc is the Smith number defined as $Sc = \frac{\mu_L}{D_m \rho_L}$.

Table 7-6 Operating conditions of the test V1.

Parameter	Description	Value (UDM)	Notes
M_s	Mass of solid	0.228 g	-
Q	Flow rate	6.3 mL/min	-
C_{in}	Inlet MB concentration	4.1 mg/L	-
H	Bed height	2.7 cm	-
d_e	Equivalent particle diameter	0.078 cm	-
ε	Bed void fraction	0.664	Equation 7.1
Re	Reynolds number	0.0104	Equation 7.3
$k_{LDF}a$	Product of LDF mass transfer coefficient with the specific surface area of PV roots	$4.68 \cdot 10^{-3}$ 1/min	Equation 7.5

It is possible to affirm that in the range of Re explored ($Re < 0.025$) the expression of Equation 7.6 is reliable for the prediction of the system behaviour. It is interesting now to understand also the applicability of this Equation for real wastewater treatment scenarios. According to the book of Cecen and Aktas [31], the range of liquid flow rates in industrial wastewater plants lies between 19-16000 m³/day (Q_{min} and Q_{max} respectively) while typical values of cross sectional areas for adsorption columns are in the range of 5-30 m² (A_{min} and A_{max} respectively). Defining a dimensionless flow rate (\tilde{Q}) and a dimensionless cross sectional area \tilde{A} as shown in Equation 7.9 and 7.10, all the possible combinations of \tilde{Q} and \tilde{A} which resulted in $Re < 0.025$ (considering the length of the roots equal to 1 cm) were calculated with Equation 7.3 and plotted in **Figure 7-6**. The latter constitutes an orientation map for real applications of *Pteris Vittata* as solid adsorbent for MB removal using the expression $k_{LDF}a = 0.45Re$.

$$\tilde{Q} = \frac{Q - Q_{min}}{Q_{max} - Q_{min}} \quad (7.9)$$

$$\tilde{A} = \frac{A - A_{min}}{A_{max} - A_{min}} \quad (7.10)$$

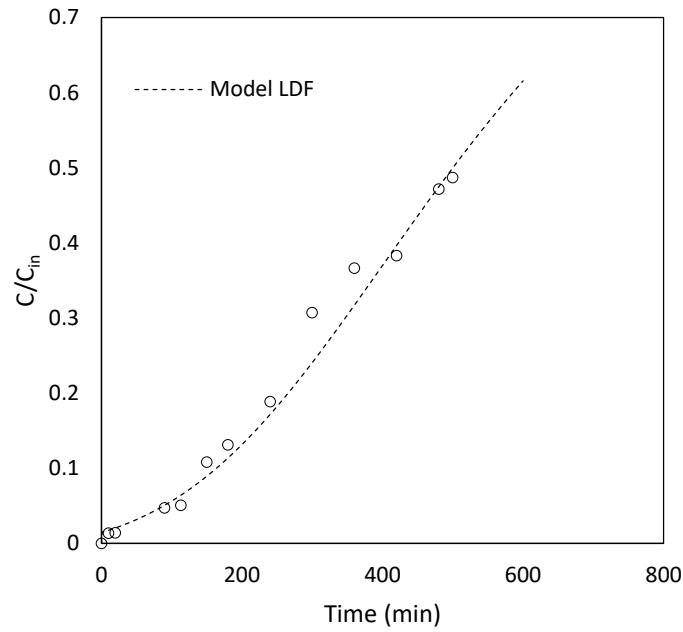


Figure 7-5 MB experimental and predicted breakthrough curve at 20°C for *Pteris Vittata* roots of 0.8 cm of length (test V1).

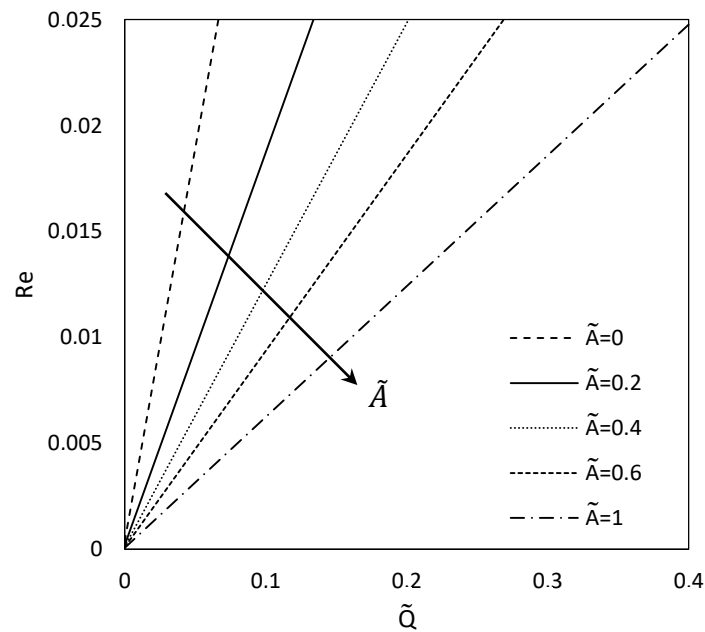


Figure 7-6 Reynolds number vs dimensionless flowrate and column cross sectional area.

Conclusions

In this chapter *Pteris Vittata* was tested as bio-adsorbent in column operation mode for the removal of MB from wastewater. First of all, the bed void fraction of every fixed bed was estimated and later the apparent density of the material was calculated. Then, Column

breakthrough curves were obtained experimentally and fitted using the Linear Driving Force (LDF) mathematical model. It was observed an important contribute of the external liquid film resistance on the mass transfer and an expression for its evaluation was derived accordingly ($k_{LDF}a = 0.45Re$). However, the range of validity of such equation is $Re < 0.025$ and the possible flow rates and cross sectional areas in which it is possible to apply such expression were provided.

Conclusions

The present Ph.D work concerns the study of three different waste materials used as bio-adsorbents for water treatment. In particular, the wastes of *Yerba Mate* tea, *Aloe Vera* and the fern *Pteris Vittata* were tested. All the materials were firstly characterized, secondly their performances toward the uptake of the dye Methylene Blue were evaluated and thirdly an attempt, for *Yerba Mate* tea and *Aloe Vera*, or a deeper investigation, for *Pteris Vittata*, in a fixed-bed adsorption mode was provided. All the materials showed promising performances toward the uptake of the dye Methylene Blue from a thermodynamic and batch tests point of view. However, waste materials present some singular properties that are not tuneable and that should be taken into account when switching from batch to continuous operation mode. The swelling behaviour of *Aloe Vera* caused dramatic decrease of the bed void fraction leading to an excessive pressure loss. The latter induced to not admissible liquid leakage during the LAB-scale runs. Then, despite *Pteris Vittata* was selected with respect to *Yerba Mate* for its higher adsorption capacity, its geometry (cylindrical) and internal diameter were fixed by the nature of the roots. For this reason: the internal mass transfer resistance was not modifiable and resulted negligible; very low Reynolds number occurred during the continuous tests; the liquid flow rate resulted in a fundamental variable for mass transfer control. However, it was provided a relation for the mass transfer coefficient as a function of Reynolds number which is applicable for the design of real operation units.

Next steps will be:

- *Yerba Mate*. Perform experimental column runs to evaluate the feasibility of such material for real applications.
- *Aloe Vera*. Further experimental tests should be conducted to understand how to deal with swelling in column applications.
- *Pteris Vittata*. Further studies should involve higher values of Re in order to extend the reliability of the expression found for the mass transfer coefficient. However, larger scale tests could also be performed based on the results of this work.

References

- [1] UNESCO, *Water reuse: Potential for expanding the Nation's Water Supply through Reuse of Municipal Wastewater*, The National Academies Press, Washington DC, USA, 2015.
- [2] M. Capocelli, M. Prisciandaro, V. Piemonte, D. Barba, A technical-economical approach to promote the water treatment & reuse processes, *J. Clean. Prod.* 207 (2019) 85–96. <https://doi.org/10.1016/j.jclepro.2018.09.135>.
- [3] J. Cheshire, *Making the invisible visible*, 2022. <https://doi.org/10.1111/1740-9713.01654>.
- [4] S. Ahirrao, *Zero Liquid Discharge Solutions*, Elsevier Ltd., 2014. <https://doi.org/10.1016/B978-0-08-099968-5.00013-1>.
- [5] T. Peters, Membrane technology for water treatment, *Chem. Eng. Technol.* 33 (2010) 1233–1240. <https://doi.org/10.1002/ceat.201000139>.
- [6] S. Yoon, *Membrane Bioreactor Processes: principles and applications*, Taylor & Francis, 2016.
- [7] Q. Husain, Potential applications of the oxidoreductive enzymes in the decolorization and detoxification of textile and other synthetic dyes from polluted water: A review, *Crit. Rev. Biotechnol.* 26 (2006) 201–221. <https://doi.org/10.1080/07388550600969936>.
- [8] V.K. Gupta, Suhas, Application of low-cost adsorbents for dye removal - A review, *J. Environ. Manage.* 90 (2009) 2313–2342. <https://doi.org/10.1016/j.jenvman.2008.11.017>.
- [9] A. Malik, E. Grohmann, *Environmental protection strategies for sustainable development*, 2012. <https://doi.org/10.1007/978-94-007-1591-2>.
- [10] K. Piaskowski, R. Świdarska-Dąbrowska, P.K. Zarzycki, Dye removal from water and wastewater using various physical, chemical, and biological processes, *J. AOAC Int.* 101 (2018) 1371–1384. <https://doi.org/10.5740/jaoacint.18-0051>.
- [11] F.I. Hai, K. Yamamoto, K. Fukushi, Hybrid treatment systems for dye wastewater, *Crit. Rev. Environ. Sci. Technol.* 37 (2007) 315–377. <https://doi.org/10.1080/10643380601174723>.
- [12] Y. Anjaneyulu, N. Sreedhara Chary, D. Samuel Suman Raj, Decolourization of industrial effluents - Available methods and emerging technologies - A review, *Rev. Environ. Sci. Biotechnol.* 4 (2005) 245–273. <https://doi.org/10.1007/s11157-005-1246-z>.
- [13] M. Sardar, M. Manna, M. Maharana, S. Sen, Remediation of Dyes from Industrial Wastewater Using Low-Cost Adsorbents, (2021) 377–403. https://doi.org/10.1007/978-3-030-47400-3_15.
- [14] Ş. Taşar, F. Kaya, A. Özer, Biosorption of lead(II) ions from aqueous solution by

- peanut shells: Equilibrium, thermodynamic and kinetic studies, *J. Environ. Chem. Eng.* 2 (2014) 1018–1026. <https://doi.org/10.1016/j.jece.2014.03.015>.
- [15] B. Wang, Z. Bai, H. Jiang, P. Prinsen, R. Luque, S. Zhao, J. Xuan, Selective heavy metal removal and water purification by microfluidically-generated chitosan microspheres: Characteristics, modeling and application, *J. Hazard. Mater.* 364 (2019) 192–205. <https://doi.org/10.1016/j.jhazmat.2018.10.024>.
- [16] A. Bonilla-Petriciolet, D.I. Mendoza-Castillo, H.E. Reynel-Ávila, Adsorption processes for water treatment and purification, 2017. <https://doi.org/10.1007/978-3-319-58136-1>.
- [17] B. Silva, I.C. Neves, T. Tavares, A sustained approach to environmental catalysis: Reutilization of chromium from wastewater, *Crit. Rev. Environ. Sci. Technol.* 46 (2016) 1622–1657. <https://doi.org/10.1080/10643389.2016.1255505>.
- [18] S. Rangabhashiyam, P. Balasubramanian, Adsorption behaviors of hazardous methylene blue and hexavalent chromium on novel materials derived from *Pterospermum acerifolium* shells, *J. Mol. Liq.* 254 (2018) 433–445. <https://doi.org/10.1016/j.molliq.2018.01.131>.
- [19] H. Guo, C. Bi, C. Zeng, W. Ma, L. Yan, K. Li, K. Wei, *Camellia oleifera* seed shell carbon as an efficient renewable bio-adsorbent for the adsorption removal of hexavalent chromium and methylene blue from aqueous solution, *J. Mol. Liq.* 249 (2018) 629–636. <https://doi.org/10.1016/j.molliq.2017.11.096>.
- [20] N. Van Nguyen, J. chun Lee, J. Jeong, B.D. Pandey, Enhancing the adsorption of chromium(VI) from the acidic chloride media using solvent impregnated resin (SIR), *Chem. Eng. J.* 219 (2013) 174–182. <https://doi.org/10.1016/j.cej.2012.12.091>.
- [21] A.C. Mitropoulos, What is a surface excess?, *J. Eng. Sci. Technol. Rev.* 1 (2008) 1–3. <https://doi.org/10.25103/jestr.011.01>.
- [22] S. Carrà, *Termo Dinamica*, Bollati Boringhieri, 1990.
- [23] P.H. Emmett, Adsorption of Gases in Multimolecular Layers, *J. Am. Chem. Soc.* 60 (1938) 309–319.
- [24] S. Brunauer, I. S. Deming, W.E. Deming, E. Teller, On a Theory of the Van Der Waals Adsorption of Gases, *J. Am. Chem. Soc.* 62 (1940) 1723–1732.
- [25] J.M.D. Tascón, One hundred years of the Ostwald – de Izaguirre theory for adsorption from solution. Its connection with carbon adsorbents, *Carbon N. Y.* 196 (2022) 676–682. <https://doi.org/10.1016/j.carbon.2022.05.028>.
- [26] G. McKay, Two-Resistance Mass Transfer Models for the Adsorption of Dyes from Aqueous Solutions Using Activated Carbon., *J. Chem. Technol. Biotechnol. Chem. Technol.* 34 A (1984) 294–310. <https://doi.org/10.1002/jctb.5040340604>.
- [27] G. McKay, Application of Surface Diffusion Model to the Adsorption of Dyes on

- Bagasse Pith, Adsorption. 4 (1998) 361–372. <https://doi.org/10.1023/a:1008854304933>.
- [28] S. Sircar, J.R. Hufton, Intraparticle adsorbate concentration profile for linear driving force model, AIChE J. 46 (2000) 659–660. <https://doi.org/10.1002/aic.690460325>.
- [29] M.C. Annesini, L. Marrelli, V. Piemonte, L. Turchetti, Artificial Organ Engineering, n.d.
- [30] C.K. Zaid, R.S. Summers, G.P. Westerhoff, B.J. Leto, K.O. Nowack, C.J. Corwin, L.B. Passantino, Activated Carbon, 2013.
- [31] O.A. Cecen, Activated Carbon for Water and Wastewater Treatment Integration of Adsorption and Biological Treatment, n.d.
- [32] Z. Hu, M.P. Srinivasan, Y. Ni, Novel activation process for preparing highly microporous and mesoporous activated carbons, Carbon N. Y. 39 (2001) 877–886. [https://doi.org/10.1016/S0008-6223\(00\)00198-6](https://doi.org/10.1016/S0008-6223(00)00198-6).
- [33] L.F. De Magalhães, G.R. Da Silva, A.E.C. Peres, Zeolite Application in Wastewater Treatment, Adsorpt. Sci. Technol. 2022 (2022). <https://doi.org/10.1155/2022/4544104>.
- [34] A. Khaleque, M.M. Alam, M. Hoque, S. Mondal, J. Bin Haider, B. Xu, M.A.H. Johir, A.K. Karmakar, J.L. Zhou, M.B. Ahmed, M.A. Moni, Zeolite synthesis from low-cost materials and environmental applications: A review, Environ. Adv. 2 (2020). <https://doi.org/10.1016/j.envadv.2020.100019>.
- [35] J. Liu, J. Yu, Toward Greener and Designed Synthesis of Zeolite Materials, 2016. <https://doi.org/10.1016/B978-0-444-63506-8.00001-X>.
- [36] M. Cocchi, D. De Angelis, L. Mazzeo, P. Nardozi, V. Piemonte, R. Tuffi, S.V. Cipriotti, Catalytic pyrolysis of a residual plastic waste using zeolites produced by coal fly ash, Catalysts. 10 (2020) 1–17. <https://doi.org/10.3390/catal10101113>.
- [37] C.I. Heck, E.G. De Mejia, Yerba mate tea (*Ilex paraguariensis*): A comprehensive review on chemistry, health implications, and technological considerations, J. Food Sci. 72 (2007) R138–R151. <https://doi.org/10.1111/j.1750-3841.2007.00535.x>.
- [38] R.A. Arreche, G. Montes de Oca-Vásquez, J.R. Vega-Baudrit, P.G. Vázquez, Synthesis of Silver Nanoparticles Using Extracts from Yerba Mate (*Ilex paraguariensis*) Wastes, Waste and Biomass Valorization. (2018) 1–9. <https://doi.org/10.1007/s12649-018-0394-7>.
- [39] M.A. Vieira, M. Maraschin, C.M. Pagliosa, R. Podestá, K.N. de Simas, I.I. Rockenbach, R.D. de M.C. Amboni, E.R. Amante, Phenolic acids and methylxanthines composition and antioxidant properties of mate (*Ilex paraguariensis*) residue, J. Food Sci. 75 (2010) C280–C285. <https://doi.org/10.1111/j.1750-3841.2010.01548.x>.
- [40] C. Anesini, P. López, G. Ferraro, S. Isolabella, L. Cogoi, R. Filip, Study of the bioactive compounds variation during yerba mate (*Ilex paraguariensis*) processing,

Food Chem. 122 (2010) 695–699. <https://doi.org/10.1016/j.foodchem.2010.03.039>.

- [41] L. Lemos da Silva, L. Cristina Nunes Ribeiro, G. Santacruz, S. Arcaro, A. Koop Alves, C. Pérez Bergmann, Glass Foams Produced from Glass and Yerba Mate (*Ilex paraguayensis*) Waste, *FME Trans.* 46 (2018) 70–79. <https://doi.org/10.5937/fmet1801070L>.
- [42] P. Húmpola, H. Odetti, J.C. Moreno-Piraján, L. Giraldo, Activated carbons obtained from agro-industrial waste: textural analysis and adsorption environmental pollutants, *Adsorption.* 22 (2016) 23–31. <https://doi.org/10.1007/s10450-015-9728-y>.
- [43] A.B. Albadarin, S. Solomon, M.A. Daher, G. Walker, Efficient removal of anionic and cationic dyes from aqueous systems using spent Yerba Mate “*Ilex paraguariensis*,” *J. Taiwan Inst. Chem. Eng.* 82 (2018) 144–155. <https://doi.org/10.1016/J.JTICE.2017.11.012>.
- [44] A.A. Maan, A. Nazir, M.K.I. Khan, T. Ahmad, R. Zia, M. Murid, M. Abrar, The therapeutic properties and applications of Aloe vera: A review, *J. Herb. Med.* 12 (2018) 1–10. <https://doi.org/10.1016/j.hermed.2018.01.002>.
- [45] J.H. Hamman, Composition and applications of Aloe vera leaf gel, *Molecules.* 13 (2008) 1599–1616. <https://doi.org/10.3390/molecules13081599>.
- [46] G. Canche-Escamilla, P. Colli-Acevedo, R. Borges-Argaez, P. Quintana-Owen, J.F. May-Crespo, M. Cáceres-Farfan, J.A. Yam Puc, P. Sansores-Peraza, B.M. Vera-Ku, Extraction of phenolic components from an Aloe vera (*Aloe barbadensis* Miller) crop and their potential as antimicrobials and textile dyes, *Sustain. Chem. Pharm.* 14 (2019). <https://doi.org/10.1016/j.scp.2019.100168>.
- [47] L.Q. Ma, K.M. Komar, C. Tu, W. Zhang, Y. Cai, E.D. Kennelley, A fern that hyperaccumulates arsenic, *Nature.* 411 (2001) 438–438. <https://doi.org/10.1038/35078151>.
- [48] N. Singh, L.Q. Ma, Arsenic speciation, and arsenic and phosphate distribution in arsenic hyperaccumulator *Pteris vittata* L. and non-hyperaccumulator *Pteris ensiformis* L., *Environ. Pollut.* 141 (2006) 238–246. <https://doi.org/10.1016/j.envpol.2005.08.050>.
- [49] M.L. Antenzio, G. Giannelli, R. Marabottini, P. Brunetti, E. Allevato, D. Marzi, G. Capobianco, G. Bonifazi, S. Serranti, G. Visioli, S.R. Stazi, M. Cardarelli, Phytoextraction efficiency of *Pteris vittata* grown on a naturally As-rich soil and characterization of As-resistant rhizosphere bacteria, *Sci. Rep.* 11 (2021) 1–11. <https://doi.org/10.1038/s41598-021-86076-7>.
- [50] A.O. Fayiga, L.Q. Ma, J. Santos, B. Rathinasabapathi, B. Stamps, R.C. Littell, Effects of arsenic species and concentrations on arsenic accumulation by different fern species in a hydroponic system, *Int. J. Phytoremediation.* 7 (2005) 231–240. <https://doi.org/10.1080/16226510500215720>.

- [51] Y. Huang, K. Miyauchi, C. Inoze, G. Endo, Development of suitable hydroponics system for phytoremediation of arseniccontaminated water using an arsenic hyperaccumulator plant *Pteris vittata*, *Biosci. Biotechnol. Biochem.* 80 (2016) 614–618. <https://doi.org/10.1080/09168451.2015.1107461>.
- [52] D. Marzi, M.L. Antenzio, S. Vernazzaro, C. Sette, E. Veschetti, L. Lucentini, G. Daniele, P. Brunetti, M. Cardarelli, Advanced drinking groundwater as phytofiltration by the hyperaccumulating fern *pteris vittata*, *Water (Switzerland)*. 13 (2021) 1–10. <https://doi.org/10.3390/w13162187>.
- [53] D. Dollimore, P. Spooner, A. Turner, The bet method of analysis of gas adsorption data and its relevance to the calculation of surface areas, *Surf. Technol.* 4 (1976) 121–160. [https://doi.org/10.1016/0376-4583\(76\)90024-8](https://doi.org/10.1016/0376-4583(76)90024-8).
- [54] L. Mazzeo, I. Bavasso, M.P. Bracciale, M. Cocchi, L. Di Palma, V. Piemonte, Yerba Mate (*Ilex paraguarensis*) as Bio-Adsorbent for the Removal of Methylene Blue , Remazol Brilliant Blue and Chromium Hexavalent : Thermodynamic and Kinetic Studies, (2020).
- [55] O. Afolayan, The Efficacy of Banana Peel Activated Carbon in the Removal of Cyanide and Selected Metals from Cassava Processing Wastewater, (2018). <https://doi.org/10.9734/AIR/2018/43070>.
- [56] R. Bardestani, G.S. Patience, S. Kaliaguine, Experimental methods in chemical engineering: specific surface area and pore size distribution measurements—BET, BJH, DFT, (n.d.). <https://doi.org/10.1002/cjce.23632>.
- [57] S. Selambakkannu, N.A.F. Othman, K.A. Bakar, S.A. Shukor, Z.A. Karim, A kinetic and mechanistic study of adsorptive removal of metal ions by imidazole-functionalized polymer graft banana fiber, *Radiat. Phys. Chem.* 153 (2018) 58–69. <https://doi.org/10.1016/j.radphyschem.2018.09.012>.
- [58] M. US EPA, OSWER, ORCR, SW-846 Test Method 7196A: Chromium, Hexavalent (Colorimetric), (n.d.). <https://www.epa.gov/hw-sw846/sw-846-test-method-7196a-chromium-hexavalent-colorimetric> (accessed February 26, 2019).
- [59] I. Bavasso, M.P. Bracciale, F. Sbardella, J. Tirillò, F. Sarasini, L. Di Palma, Effect of yerba mate (*Ilex paraguariensis*) residue and coupling agent on the mechanical and thermal properties of polyolefin- based composites, (2019) 1–13. <https://doi.org/10.1002/pc.25355>.
- [60] K. Tayebi, A. Ghomari, A. Addou, Removal of methylene blue dye from water by a spent bleaching earth biosorbent Ali Belhaine , Mouffok Redouane Ghezzar , Fatiha Abdelmalek , (2016) 2534–2540. <https://doi.org/10.2166/wst.2016.407>.
- [61] G.D.R. Nogueira, C.R. Duarte, M.A.S. Barrozo, Hydrothermal carbonization of acerola (*Malpighia emarginata* D . C .) wastes and its application as an adsorbent, *Waste Manag.* 95 (2019) 466–475. <https://doi.org/10.1016/j.wasman.2019.06.039>.

- [62] V.K. Gupta, R. Jain, M. Shrivastava, A. Nayak, Equilibrium and Thermodynamic Studies on the Adsorption of the Dye Tartrazine onto Waste “ Coconut Husks ” Carbon and Activated Carbon, (2010) 5083–5090.
- [63] J. Shi, J. Yang, R. Han, Y. Wang, Y. Lu, P. Han, Removal of methylene blue from aqueous solution by chaff in batch mode, *J. Hazard. Mater.* 137 (2006) 550–557. <https://doi.org/10.1016/j.jhazmat.2006.02.029>.
- [64] J. CHEN, C. YANG, M. LI, R. GONG, Y. SUN, Removal of cationic dyes from aqueous solution by adsorption on peanut hull, *J. Hazard. Mater.* 121 (2005) 247–250. <https://doi.org/10.1016/j.jhazmat.2005.01.029>.
- [65] G. Annadurai, R.S. Juang, D.J. Lee, Use of cellulose-based wastes for adsorption of dyes from aqueous solutions, *J. Hazard. Mater.* 92 (2002) 263–274. [https://doi.org/10.1016/S0304-3894\(02\)00017-1](https://doi.org/10.1016/S0304-3894(02)00017-1).
- [66] V. Vadivelan, K.V. Kumar, Equilibrium , kinetics , mechanism , and process design for the sorption of methylene blue onto rice husk, 286 (2005) 90–100. <https://doi.org/10.1016/j.jcis.2005.01.007>.
- [67] T. Sostaric, O. Mineral, R. Materials, J. Milojkovic, BIOSORPTION OF METHYLENE BLUE BY WASTE APRICOT SHELLS FROM, (2018). <https://doi.org/10.7251/JEPMEN1507107S>.
- [68] Y. Bulut, H. Ayd, A kinetics and thermodynamics study of methylene blue adsorption on wheat shells, 194 (2006) 259–267. <https://doi.org/10.1016/j.desal.2005.10.032>.
- [69] A.S. Franca, L.S. Oliveira, M.E. Ferreira, Kinetics and equilibrium studies of methylene blue adsorption by spent coffee grounds, 249 (2009) 267–272. <https://doi.org/10.1016/j.desal.2008.11.017>.
- [70] F.A. Pavan, E.C. Lima, S.L.P. Dias, A.C. Mazzocato, Methylene blue biosorption from aqueous solutions by yellow passion fruit waste, 150 (2008) 703–712. <https://doi.org/10.1016/j.jhazmat.2007.05.023>.
- [71] B.H. Hameed, Evaluation of papaya seeds as a novel non-conventional low-cost adsorbent for removal of methylene blue, *J. Hazard. Mater.* 162 (2009) 939–944. <https://doi.org/10.1016/j.jhazmat.2008.05.120>.
- [72] B.H. Hameed, Grass waste: A novel sorbent for the removal of basic dye from aqueous solution, *J. Hazard. Mater.* 166 (2009) 233–238. <https://doi.org/10.1016/j.jhazmat.2008.11.019>.
- [73] L. Mazzeo, I. Bavasso, M. Spallieri, M.P. Bracciale, V. Piemonte, L. Di Palma, Effect of Water–Ethanol Extraction as Pre-Treatment on the Adsorption Properties of Aloe vera Waste, *Materials (Basel)*. 15 (2022) 1–18. <https://doi.org/10.3390/ma15165566>.
- [74] G. McKay, J.F. Porter, G.R. Prasad, The removal of dye colours from aqueous

solutions by adsorption on low- cost materials, *Water. Air. Soil Pollut.* 114 (1999) 423–438. <https://doi.org/10.1023/A:1005197308228>.

- [75] L. Mazzeo, D. Marzi, B. Irene, M.P. Bracciale, V. Piemonte, L. Di Palma, Characterization of waste roots from the As hyperaccumulator *Pteris vittata* as low-cost adsorbent for Methylene Blue removal, *Chem. Eng. Res. Des.* (2022). <https://doi.org/10.1016/j.cherd.2022.07.025>.
- [76] M.T. Uddin, M.A. Islam, S. Mahmud, M. Rukanuzzaman, Adsorptive removal of methylene blue by tea waste, *J. Hazard. Mater.* 164 (2009) 53–60. <https://doi.org/10.1016/j.jhazmat.2008.07.131>.
- [77] Y. Xie, S. Li, F. Wang, G. Liu, Removal of perchlorate from aqueous solution using protonated cross-linked chitosan, 156 (2010) 56–63. <https://doi.org/10.1016/j.cej.2009.09.033>.
- [78] F. Gode, E. Pehlivan, Removal of Cr(VI) from aqueous solution by two Lewatit-anion exchange resins, *J. Hazard. Mater.* 119 (2005) 175–182. <https://doi.org/10.1016/j.jhazmat.2004.12.004>.
- [79] C. Liu, Y. Cui, F. Pi, Y. Cheng, Y. Guo, H. Qian, Extraction, purification, structural characteristics, biological activities and pharmacological applications of acemannan, a polysaccharide from aloe vera: A review, *Molecules.* 24 (2019). <https://doi.org/10.3390/molecules24081554>.
- [80] Z.J. Tan, F.F. Li, X.L. Xu, Extraction and purification of anthraquinones derivatives from Aloe vera L. using alcohol/salt aqueous two-phase system, *Bioprocess Biosyst. Eng.* 36 (2013) 1105–1113. <https://doi.org/10.1007/s00449-012-0864-4>.
- [81] K.M. Katubi, A. Amari, H.N. Harharah, M.M. Eldirderi, M.A. Tahooun, F. Ben Rebah, Aloe vera as promising material for water treatment: A review, *Processes.* 9 (2021) 1–16. <https://doi.org/10.3390/pr9050782>.
- [82] D.A. Giannakoudakis, A. Hosseini-Bandegharai, P. Tsafraquidou, K.S. Triantafyllidis, M. Kornaros, I. Anastopoulos, Aloe vera waste biomass-based adsorbents for the removal of aquatic pollutants: A review, *J. Environ. Manage.* 227 (2018) 354–364. <https://doi.org/10.1016/j.jenvman.2018.08.064>.
- [83] M.A.K.M. Hanafiah, S.Z. Mohd Jamaludin, K. Khalid, S. Ibrahim, Methylene blue adsorption on aloe vera rind powder: Kinetics, isotherm and mechanisms, *Nat. Environ. Pollut. Technol.* 17 (2018) 1055–1064.
- [84] F. Gironi, V. Piemonte, Temperature and solvent effects on polyphenol extraction process from chestnut tree wood, *Chem. Eng. Res. Des.* 89 (2011) 857–862. <https://doi.org/10.1016/j.cherd.2010.11.003>.
- [85] C. Fanali, V. Gallo, S. Della Posta, L. Dugo, L. Mazzeo, M. Cocchi, V. Piemonte, L. De Gara, Choline chloride–lactic acid-based NADES as an extraction medium in a response surface methodology-optimized method for the extraction of phenolic

compounds from hazelnut skin, *Molecules*. 26 (2021).
<https://doi.org/10.3390/molecules26092652>.

- [86] K. Di Scala, A. Vega-Gálvez, K. Ah-Hen, Y. Nuñez-Mancilla, G. Tabilo-Munizaga, M. Pérez-Won, C. Giovagnoli, Chemical and physical properties of aloe vera (*Aloe barbadensis* Miller) gel stored after high hydrostatic pressure processing, *Food Sci. Technol.* 33 (2013) 52–59. <https://doi.org/10.1590/S0101-20612013005000002>.
- [87] A. Noubigh, C. Jeribi, A. Mgaidi, M. Abderrabba, Solubility of gallic acid in liquid mixtures of (ethanol + water) from (293.15 to 318.15) K, *J. Chem. Thermodyn.* 55 (2012) 75–78. <https://doi.org/10.1016/j.jct.2012.06.022>.
- [88] D. Zanchi, A. Vernhet, C. Poncet-Legrand, D. Cartalade, C. Tribet, R. Schweins, B. Cabane, Colloidal dispersions of tannins in water-ethanol solutions, *Langmuir*. 23 (2007) 9949–9959. <https://doi.org/10.1021/la700694b>.
- [89] G. Perdoncin, G. Scorrano, Protonation Equilibria in Water at Several Temperatures of Alcohols, Ethers, Acetone, Dimethyl Sulfide, and Dimethyl Sulfoxide, *J. Am. Chem. Soc.* 99 (1977) 6983–6986. <https://doi.org/10.1021/ja00463a035>.
- [90] L. Mazzeo, I. Bavasso, M.P. Bracciale, M. Cocchi, L. Di Palma, V. Piemonte, Yerba mate (*Ilex paraguarensis*) as bio-adsorbent for the removal of methylene blue, remazol brilliant blue and chromium hexavalent: Thermodynamic and kinetic studies, *Water (Switzerland)*. 12 (2020). <https://doi.org/10.3390/w12072016>.
- [91] B. Benzidia, M. Barbouchi, H. Hammouch, N. Belahbib, M. Zouarhi, H. Erramli, N. Ait Daoud, N. Badrane, N. Hajjaji, Chemical composition and antioxidant activity of tannins extract from green rind of Aloe vera (*L.*) *Burm. F.*, *J. King Saud Univ. - Sci.* 31 (2019) 1175–1181. <https://doi.org/10.1016/j.jksus.2018.05.022>.
- [92] M. El-Azazy, S.N. Dimassi, A.S. El-Shafie, A.A. Issa, Bio-Waste Aloe vera Leaves as an efficient adsorbent for Titan Yellow from Wastewater: Structuring of a novel adsorbent using Plackett-Burman factorial design, *Appl. Sci.* 9 (2019) 1–20. <https://doi.org/10.3390/app9224856>.
- [93] D.L. Postai, C.A. Demarchi, F. Zanatta, D.C.C. Melo, C.A. Rodrigues, Adsorption of rhodamine B and methylene blue dyes using waste of seeds of *Aleurites Moluccana*, a low cost adsorbent, *Alexandria Eng. J.* 55 (2016) 1713–1723. <https://doi.org/10.1016/j.aej.2016.03.017>.
- [94] S. Hong, C. Wen, J. He, F. Gan, Y.S. Ho, Adsorption thermodynamics of Methylene Blue onto bentonite, *J. Hazard. Mater.* 167 (2009) 630–633. <https://doi.org/10.1016/j.jhazmat.2009.01.014>.
- [95] D. Özer, G. Dursun, A. Özer, Methylene blue adsorption from aqueous solution by dehydrated peanut hull, *J. Hazard. Mater.* 144 (2007) 171–179. <https://doi.org/10.1016/j.jhazmat.2006.09.092>.
- [96] Z. Al-Qodah, W.K. Lafi, Z. Al-Anber, M. Al-Shannag, A. Harahsheh, Adsorption of

- methylene blue by acid and heat treated diatomaceous silica, *Desalination*. 217 (2007) 212–224. <https://doi.org/10.1016/j.desal.2007.03.003>.
- [97] M. Manes, L.J.E. Hofer, Application of the Polanyi Adsorption Potential Theory.pdf, 221 (1966) 584–590.
- [98] *Adsorption: Science and Technology*, 1989. <https://doi.org/10.1007/978-94-009-2263-1>.
- [99] V. Meshko, L. Markovska, M. Mincheva, A.E. Rodrigues, Adsorption of basic dyes on granular activated carbon and natural zeolite, *Water Res.* 35 (2001) 3357–3366. [https://doi.org/10.1016/s0043-1354\(01\)00056-2](https://doi.org/10.1016/s0043-1354(01)00056-2).
- [100] C.A. Sáenz-Alanís, R.B. García-Reyes, E. Soto-Regalado, A. García-González, Phenol and methylene blue adsorption on heat-treated activated carbon: Characterization, kinetics, and equilibrium studies, *Adsorpt. Sci. Technol.* 35 (2017) 789–805. <https://doi.org/10.1177/0263617416684517>.
- [101] C. Yao, C. Zhu, A new method of characterizing mass transfer controlling mechanism in pollutant adsorption from aqueous solutions, *J. Mol. Liq.* 301 (2020) 112455. <https://doi.org/10.1016/j.molliq.2020.112455>.
- [102] S. Baup, C. Jaffre, D. Wolbert, A. Laplanche, Adsorption of pesticides onto granular activated carbon: Determination of surface diffusivities using simple batch experiments, *Adsorption*. 6 (2000) 219–228. <https://doi.org/10.1023/A:1008937210953>.
- [103] X. Wan, M. Lei, T. Chen, Cost–benefit calculation of phytoremediation technology for heavy-metal-contaminated soil, *Sci. Total Environ.* 563–564 (2016) 796–802. <https://doi.org/10.1016/j.scitotenv.2015.12.080>.
- [104] J. Li, J. Chen, S. Chen, Supercritical water treatment of heavy metal and arsenic metalloids-bioaccumulating-biomass, *Ecotoxicol. Environ. Saf.* 157 (2018) 102–110. <https://doi.org/10.1016/j.ecoenv.2018.03.069>.
- [105] J. Chen, Bio-oil production from hydrothermal liquefaction of *Pteris vittata* L.: Effects of operating temperatures and energy recovery, *Bioresour. Technol.* 265 (2018) 320–327. <https://doi.org/10.1016/j.biortech.2018.06.019>.
- [106] Y. Song, J. Liu, F. Evrendilek, J. Kuo, M. Buyukada, Combustion behaviors of *Pteris vittata* using thermogravimetric, kinetic, emission and optimization analyses, *J. Clean. Prod.* 237 (2019) 117772. <https://doi.org/10.1016/j.jclepro.2019.117772>.
- [107] W. Cai, T. Chen, M. Lei, X. Wan, Effective strategy to recycle arsenic-accumulated biomass of *Pteris vittata* with high benefits, *Sci. Total Environ.* 756 (2021) 143890. <https://doi.org/10.1016/j.scitotenv.2020.143890>.
- [108] J.M. Thomas, The existence of endothermic adsorption, *J. Chem. Educ.* 38 (1961) 138. <https://doi.org/10.1021/ed038p138>.
- [109] H. Xue, X. Wang, Q. Xu, F. Dhaouadi, L. Sellaoui, M.K. Seliem, A. Ben Lamine, H.

- Belmabrouk, A. Bajahzar, A. Bonilla-Petriciolet, Z. Li, Q. Li, Adsorption of methylene blue from aqueous solution on activated carbons and composite prepared from an agricultural waste biomass: A comparative study by experimental and advanced modeling analysis, *Chem. Eng. J.* 430 (2022).
<https://doi.org/10.1016/j.cej.2021.132801>.
- [110] H. Demiral, I. Demiral, F. Tımsek, B. Karabacakođlu, Adsorption of chromium(VI) from aqueous solution by activated carbon derived from olive bagasse and applicability of different adsorption models, *Chem. Eng. J.* 144 (2008) 188–196.
<https://doi.org/10.1016/j.cej.2008.01.020>.
- [111] C. Tien, *Introduction to Adsorption*, 2019. <https://doi.org/10.1016/b978-0-12-816446-4.09991-7>.
- [112] D. M. Ruthven, *Principles of adsorption and adsorption processes*, *React. Polym. Ion Exch. Sorbents.* 4 (1985) 62. [https://doi.org/10.1016/0167-6989\(85\)90037-6](https://doi.org/10.1016/0167-6989(85)90037-6).
- [113] S.F. Chung, C.Y. Wen, Longitudinal dispersion of liquid flowing through fixed and fluidized beds, *AIChE J.* 14 (1968) 857–866. <https://doi.org/10.1002/aic.690140608>.
- [114] A. Leitão, P. Carlos, S. Santos, A. Rodrigues, Tracer experiments in fixed beds: effects of flow maldistribution on the estimation of transport kinetic parameters, *Chem. Eng. J. Biochem. Eng. J.* 53 (1994) 193–199. [https://doi.org/10.1016/0923-0467\(93\)02800-C](https://doi.org/10.1016/0923-0467(93)02800-C).
- [115] J.M.P.Q. Delgado, A critical review of dispersion in packed beds, *Heat Mass Transf. Und Stoffuebertragung.* 42 (2006) 279–310. <https://doi.org/10.1007/s00231-005-0019-0>.
- [116] J.M.P.Q. Delgado, Longitudinal and transverse dispersion in porous media, *Chem. Eng. Res. Des.* 85 (2007) 1245–1252. <https://doi.org/10.1205/cherd07017>.
- [117] E.J. Wilson, C.J. Geankoplis, Liquid mass transfer at very low reynolds numbers in packed beds, *Ind. Eng. Chem. Fundam.* 5 (1966) 9–14.
<https://doi.org/10.1021/i160017a002>.
- [118] S. Kumar, S.N. Upadhyay, V.K. Mathur, Low Reynolds Number Mass Transfer in Packed Beds of Cylindrical Particles, *Ind. Eng. Chem. Process Des. Dev.* 16 (1977) 1–8. <https://doi.org/10.1021/i260061a001>.
- [119] P.A. Nelson, T.R. Galloway, Particle-to-fluid heat and mass transfer in dense systems of fine particles, *Chem. Eng. Sci.* 30 (1975) 1–6. [https://doi.org/10.1016/0009-2509\(75\)85109-8](https://doi.org/10.1016/0009-2509(75)85109-8).
- [120] L. Marrelli, *Termodinamica degli equilibri di fasi fluide*, Edizioni Efesto, 2017.
- [121] S. Carrà, L. Forni, *Aspetti cinetici della teoria del reattore chimico*, Tamburini Editore, 1974.
- [122] R. De Santis, *Introduzione al calcolo degli equilibri di fasi fluide*, Editoriale ESA, 1991.